UNIVERSIDADE DE LISBOA
FACULDADE DE CIÊNCIAS
DEPARTAMENTO DE QUÍMICA E BIOQUÍMICA

Synthesis of new 3D-η^5-carboranyl and η^5-methylcyclopentadienyl ruthenium complexes incorporating bipyridine (macro)ligands as promising anticancer agents

Ricardo Jorge Gonçalves Teixeira

Mestrado em Química
Especialização em Química

Dissertação orientada por:
Doutora Andreia Marques Valente
Professora Doutora Clara Viñas i Teixidor

2017

UNIVERSIDADE DE LISBOA
FACULDADE DE CIÊNCIAS
DEPARTAMENTO DE QUÍMICA E BIOQUÍMICA

Synthesis of new 3D-η^5-carboranyl and η^5-methylcyclopentadienyl ruthenium complexes incorporating bipyridine (macro)ligands as promising anticancer agents

Ricardo Jorge Gonçalves Teixeira

Mestrado em Química
Especialização em Química

Dissertação orientada por:
Doutora Andreia Marques Valente
Investigadora FCT, Faculdade de Ciências da Universidade de Lisboa
Professora Doutora Clara Viñas i Teixidor
Research Professor, Institut de Ciència de Materials de Barcelona, CSIC

2017

Para os meus pais e irmã

Acknowledgements

O culminar deste trabalho não poderia ser alcançado sem o contributo de várias pessoas. Assim sendo, e sabendo que para mim, o agradecimento parece ser sempre mais simples de expressar quando escrito, guardei este pequeno espaço para vos dirigir as palavras que se seguem. Obrigado por terem participado ativamente nesta fase de tamanha importância do meu percurso académico e por fazerem, de uma forma ou de outra, parte do meu quotidiano nestes últimos meses.

Em primeiro lugar, tenho a agradecer profundamente à Doutora Andreia Valente por me ter recebido de novo de forma tão entusiasta e calorosa no grupo, e ainda por me ter proposto este trabalho. Obrigado pela amizade e por saberes escutar sempre as minhas ideias e incisivamente criticá-las. To my other supervisor, Professor Clara Viñas i Teixidor, who has supervised this project a few miles away from the *Institut de Ciències de Materials de Barcelona*, and to who I have to express my most sincere gratitude for her critical insight, support and enthusiasm during the development of this project. Às duas, obrigado pela constante motivação, por sempre terem exigido de mim mais e melhor e ainda por me saberem munir de todas as ferramentas que, de certo, irão ser muito úteis no futuro.

À Professora Helena Garcia tenho a agradecer o facto de me ter recebido de novo no seu grupo de investigação e, por toda a sua dedicação, positivismo e transmissão de conhecimentos. O seu sorriso e entusiasmo foram completamente contagiantes.

À Professora Paula Robalo quero agradecer toda a disponibilidade, amabilidade e apoio dado sempre que foi necessário realizar experiências de voltametria cíclica.

Ao Doutor Fernando Avecilla e ao Doutor Xavier Gubau pela resolução das estruturas de raios-X.

À Professora Ana Preto e à sua estudante Ana Rita Brás, da Universidade do Minho, e à Doutora Fernanda Marques do C2TN, pelas colaborações e pela realização de todos os ensaios biológicos.

Obrigado a todos os elementos que constituem o grupo de Química Bioorganometálica da FCUL. Palavras de agradecimento sincero têm de ser dirigidas ao Adhan e à Anabela por sempre me terem acompanhado e pela constante boa disposição, amizade e espírito de entreajuda ao longo dos nossos percursos académicos. À minha querida amiga Patrícia Gírio, a outra estudante de mestrado que seguia na luta ao meu lado, obrigado pelo teu companheirismo e apoio prestado nestes últimos meses. Um obrigado especial à aspirante a doutora, Leonor Côrte-Real, por desde o início do projecto, sempre me ter acompanhado, partilhado as suas experiências e ainda por ter estado sempre disponível para me ajudar e aconselhar. E ainda uma palavra às restantes membros do grupo: à Doutora Ana Isabel Tomaz pelo seu extraordinário e oportuno sentido crítico; à Doutora Tânia Morais por todo o apoio e companheirismo no laboratório; à Professora Maria José Brito pela sua simpatia e ajuda no passo "crítico" da síntese e ainda, à (quase doutora) Cristina Matos, pela companhia e tranquilidade que sempre proporcionou no laboratório.

To Professor Francesc Teixidor, Doctor José Ginger Planas and Doctor Rosario Núñez for their sincere warm welcome. I will not forget your support and kind hospitality during my stay in Barcelona. Along with them, I want to thank Arpita, Abhishek, Bego, Flavia, Isabel, Mahdi and Xavier at ICMAB for

being such nice people to work with. Thank you for the excellent working atmosphere which always make me feel like home. Elena Oleskevich deserves special attention not only for being such a good friend at ICMAB but also for all the time she spent helping me in the laboratory. Thank you all for your support.

Aos meus pais e irmã, obrigado pelo amor, carinho e apoio incondicional que sempre me fizeram chegar. Se hoje estou onde estou, a vocês o devo. Obrigado por me ensinarem a lutar todos os dias e por nunca me terem deixado baixar os braços, mesmo quando o mais fácil era fazê-lo. A mensagem que me fizeram chegar à mais ou menos dois anos, "Há um tempo em que é preciso abandonar as roupas usadas, que já têm a forma do nosso corpo, e esquecer os nossos caminhos, que nos levam sempre aos mesmos lugares. É o tempo da travessia: e, se não ousarmos fazê-la, teremos ficado, para sempre, à margem de nós mesmos», toma cada vez mais sentido hoje. ∞ Um agradecimento ainda aos meus avós, que fizeram sempre por estar por perto e ainda por me ajudarem sempre naquilo que mais precisava. ∞

À Vanessa por ter feito esta caminhada comigo. Um obrigado incalculável por sempre teres estado a meu lado, por teres acreditado sempre e por todas as palavras que me fizeste chegar, mesmo quando os momentos eram os mais delicados. A ti, ficam a faltar muitas mais palavras. ∞

One last acknowledgement to the COST action CM1302 (SIPs) for financial support in the displacement to the ICMAB-CSIC facilities.

Espero, um dia, conseguir retribuir-vos todo o carinho, amor e amizade que têm depositado em mim.

A todos, o meu mais profundo obrigado!

Ricardo Teixeira

Abstract

Cancer is considered one of the leading causes of death worldwide. Therefore, the search for potential anticancer drugs is nowadays a mandatory topic and many research groups focus their interests and efforts in this area. About 50-70 % of all tumors are treated with platinum based compounds (cisplatin, carboplatin and oxaliplatin) but due to several and severe side effects caused by these metallodrugs and to the resistance phenomena (acquired or intrinsic), complexes with metal ions other than platinum, have been widely investigated for their anticancer properties. In this frame, ruthenium appears as a strong candidate for drug development showing low toxicity, selectivity for tumors, inhibition of metastasis progression and antiangiogenic properties.

Within this project, seven new organometallic compounds were synthesized and characterized. The successful formulation of these complexes, with general formula [Ru(η^5-MeCp)(PPh_3)(4,4'-R_2-2,2'-bipy)]][CF_3SO_3] (**1a**, R = -CH_3; **1b**, R = -CH_2OH; **1c**, R = -$O(CH_2)_3(CF_2)_7CF_3$; **1d**, R = -CH_2OPLA) or [3-CO-3,3-{k^2-4,4'-R_2-2,2'-bipy}-*closo*-3,1,2-$RuC_2B_9H_{11}$] (**2a**, R = -CH_3; **2b**, R = -CH_2OH; **2c**, R = -CH_2OPLA) was supported by spectroscopic (NMR, UV-Vis, FTIR), electrochemical (cyclic voltammetry) and structural (single crystal X-ray diffraction) data. When applicable, the purity was evaluated through elemental analysis. The stability of all compounds was tested by electronic spectroscopy using DMSO/DMEM as solvents, over a period of 24 hours. All complexes displayed an adequate stability (average of less than 6 % variation over a 24 hours period) which proved to be adequate to proceed to the *in vitro* biological screening assays. The partition coefficient in *n*-octanol/water, P_{ow}, was also determined when the solubility of the compounds allowed it, showing that, generally, these compounds are lipophilic.

The cytotoxicity of the complexes was evaluated *in vitro* in a panel of human cancer cell lines namely A2780 (human ovary adenocarcinoma), A375 (human melanoma), and RKO and SW480 (human colon adenocarcinoma), within a 24 h or 48 h incubation time. The results obtained for all the cell lines tested confirm the potential of these two families of compounds as anticancer agents in traditional chemotherapy (compounds **1a**-**1d**) or in Boron Neutron Capture Therapy (BNCT, compounds **2a**-**2c**).

Keywords

Ruthenium(II) complexes

η^5-Methylcylopentadienyl

3D-η^5-Carboranyl

Polymer-metal conjugates

Anticancer agents

Resumo

Considerado como uma das principais causas de morte no mundo inteiro, o cancro é visto como um conjunto de doenças genericamente caracterizado pelo crescimento descontrolado de células anormais que têm a capacidade de invadir regiões circundantes ao espaço onde se encontram e se espalhar pelo organismo. Apesar de, até à data, cerca de 50-70 % do tratamento de tumores se basear em fármacos de platina (cisplatina, oxaliplatina e carboplatina), a ocorrência de múltiplos e fortes efeitos secundários adversos e de processos de resistência (intrínseca ou adquirida) implica que se invista no desenvolvimento de novos agentes quimioterapêuticos.

É neste sentido que alguns compostos organometálicos têm aparecido como alternativas bastante promissoras. Tem sido desenvolvida uma vasta linha de investigação em torno de outros iões metálicos e é neste contexto que surge o ruténio. Este metal é um potencial candidato para o desenvolvimento de novos fármacos a utilizar em quimioterapia, uma vez que apresenta baixa toxicidade, seletividade para os tumores, inibição da progressão de metástases e propriedades anti-angiogénicas.

A conjugação da química de coordenação com a polimerização controlada tem vindo a dar resultados promissores na terapia do cancro. Esta é conseguida pela conjugação de centros metálicos com cadeias poliméricas, dando origem a potenciais fármacos macromoleculares, os PMCs ou *polymer-metal conjugates*. O design racional para o desenvolvimento destes compostos é baseado na capacidade que as macromoléculas têm para uma melhor permeação e retenção nos tumores (efeito EPR – *Enhanced permeation and retention effect*) relativamente às moléculas com baixo peso molecular. Para além disso, tem vindo a ser descrito que a conjugação de ligandos poliméricos aos compostos de platina já existentes comercialmente provoca um efeito sinérgico que induz a uma maior estabilidade do composto, o que pode levar a uma libertação mais controlada do centro metálico e, desta forma, diminuir a intensidade dos efeitos secundários inerentes ao fármaco sem o polímero. Foi neste âmbito que o Laboratório de Química Bio-organometálica da Faculdade de Ciências da Universidade de Lisboa, onde este trabalho foi realizado, desenvolveu uma nova geração de compostos organometálicos de ruténio à qual foi conjugada uma cadeia polimérica de polilactídeo (PLA, considerado um dos biopolímeros mais promissores hoje em dia, devido, em grande parte, à sua biodegradabilidade e biocompatibilidade), os RuPMCs. Verificou-se que a internalização do metal em células tumorais nos ensaios *in vitro* é superior quando comparada com a do seu análogo de baixo molecular não polimérico, o que permite concluir que o mecanismo de internalização é, provavelmente, diferente e pode estar eventualmente relacionado com a presença da cadeia polimérica. É então a partir dos promissores resultados obtidos que o desenvolvimento de fármacos macromoleculares ganha especial atenção.

A terapia de captura de neutrões pelo boro (BNCT, do inglês *Boron Neutron Capture Therapy*) é um instrumento terapêutico atualmente em ensaios clínicos que pode ser utilizado no tratamento de diversos tumores. Baseia-se na administração de um composto que contenha o isótopo 10 do elemento boro (^{10}B), seguido de irradiação local com neutrões térmicos, com consequente reação nuclear e libertação de alta transferência, através da libertação de partículas α e núcleos de lítio (^{7}Li). Os produtos formados pela reação têm curto alcance e conseguem, desta forma, atingir apenas as células que incorporam o

composto com boro. A grande vantagem associada à BNCT é o facto de se tratar de uma terapia localizada, a qual tem associada a si um número reduzido de efeitos colaterais. Porém, a necessidade de compostos com boro seletivos para as células tumorais deverá ser um dos requisitos prévios. Atualmente têm vindo a ser desenvolvidos e estudados vários compostos para aumentar a seletividade para as células cancerígenas.

É então neste contexto que surge a concretização deste trabalho de mestrado que pretende conjugar o conhecimento de dois grupos de investigação especializados em síntese organometálica e inorgânica. O trabalho desenvolvido no âmbito desta tese baseou-se na síntese e caracterização de 7 novos compostos organometálicos de ruténio(II), baseados no fragmento η^5-metilciclopentadienilo (MeCp) e η^5-carboranil, contendo na sua estrutura derivados do ligando bidentado 2,2'-bipiridina.

O desenvolvimento de duas novas famílias de compostos foi então conseguida com sucesso. A primeira, (Ru-MeCp), que deu origem a quatro complexos de fórmula geral [Ru(η^5-MeCp)(PPh_3)(4,4'-R_2-2,2'-bipy)]][CF_3SO_3] (**1a**, R = -CH_3; **1b**, R = -CH_2OH; **1c**, R = -$O(CH_2)_3(CF_2)_7CF_3$; **1d**, R = -CH_2OPLA) foi conseguida através da abstração de halogeneto com trifluorofosfato de prata ($AgCF_3SO_3$) no fragmento [Ru(η^5-MeCp)(PPh_3)$_2$Cl]. A segunda, (Ru-carboranil), deu origem a três complexos estruturalmente semelhantes com fórmula geral [3-CO-3,3-{k^2-4,4'-R_2-2,2'-bipy}-*closo*-3,1,2-$RuC_2B_9H_{11}$] (**2a**, R = -CH_3; **2b**, R = -CH_2OH; **2c**, R = -CH_2OPLA). Estes compostos foram obtidos através da substituição de dois ligandos carbonilo presentes no percursor [3,3,3-$(CO)_3$-*closo*-3,1,2-$RuC_2B_9H_{11}$] através da adição do sal de óxido de trimetilamónio (Me_3NO).

Todos os compostos sintetizados foram caraterizados através da combinação de várias técnicas espetroscópicas, nomeadamente ressonância magnética nuclear uni- e bidimensionais (^{1}H, ^{11}B, ^{13}C, ^{19}F, ^{31}P, COSY, HMBC e HMQC), UV-Vis e FTIR e, eletroquímicas (voltametria cíclica). Quando possível, uma caracterização mais completa foi conseguida graças à obtenção de monocristais adequados à técnica de difração de raios-X. O grau de pureza dos compostos foi determinado, quando adequado, através de análise elementar.

A estabilidade em meio aquoso (fazendo uso do meio celular DMEM) e os valores do coeficiente de partição no sistema *n*-octanol/água (P_{ow}) foram determinados para todos os compostos por espectroscopia eletrónica. No geral, verificou-se que os compostos apresentaram estabilidade adequada para prosseguir nos ensaios biológicos preliminares (regra geral, variações menores que 6 % ao final de 24 horas) e um carácter lipofílico.

A citoxicidade dos complexos foi avaliada através de ensaios celulares *in vitro* nas linhas celulares A2780 (adenocarcinoma do ovário humano), A375 (melanoma humano), RKO e SW480 (adenocarcinoma do colon humano), durante um período de incubação de 24 horas ou 48 horas. Os valores de IC_{50} encontrados mostraram ser bastante promissores para todos os compostos podendo ser dada especial atenção a: o complexo **1a,** que nesse período, mostrou ser duas vezes mais ativo que a cisplatina, nas mesmas condições experimentais; o complexo **1c** mostrou preferencial seletividade para as linhas tumorais do cancro do cólon relativamente à linha celular normal da mucosa do colon humano, NCM460; e aos complexos **2a** e **2c** que mostraram ser pouco citotóxicos na linha celular onde foram estudados, comprovando assim a sua adequabilidade para o uso na terapia alternativa BNCT.

No capítulo 3 são ainda descritas, de forma resumida, todas as tentativas de síntese que não levaram à obtenção do composto desejado. Todo o processo de otimização desbravado na síntese dos compostos possuidores do fragmento {Ru-$C_2B_9H_{11}$} pode ser considerado como um bom ponto de partida para trabalhos futuros.

Palavras-chave

Complexos de ruténio(II)

η^5-Metilciclopentadienilo

3D-η^5-Carboranil

Complexos de metal-polímero

Compostos antitumorais

Contents

List of figures

Introduction

Organometallic ruthenium-methylcyclopentadienyl complexes incorporating 2,2'-bipyridine derivatives

Organometallic ruthenium-carboranyl complexes incorporating 2,2'-bipyridine derivatives

Annexes

List of schemes

List of tables

Organometallic ruthenium-methylcyclopentadienyl complexes incorporating 2,2'-bipyridine derivatives

Organometallic ruthenium-carboranyl complexes incorporating 2,2'-bipyridine derivatives

List of symbols and abbreviations

Bipy	Bipyridine
Bipy(CH_2OH)$_2$	4,4'-Bis(hydroxymethyl)-2,2´-bipyridine
Bipy(CH_2OPLA)$_2$	4,4'-Bis-polylactide-2,2'-bipyridine
br	Broad signal
BNCT	Boron Neutron Capture Therapy
COSY	Correlation Spectroscopy
CDDP	*Cis*-dichlorodiammineplatinum
CT	Charge transfer
CV	Cyclic voltammetry
d	Doublet
dd	Doublet of doublet
DMSO	Dimethylsulfoxide
DMAP	4-dimethylaminopyridine
DP	Degree of Polymerization
et al.	*et alii*
EPR	Enhanced Permeability and Retention
FDA	Food and Drug Administration
GPC	Gel Permeation Chromatography
HMBC	Heteronuclear Multiple Bond Correlation
HMQC	Heteronuclear Multiple Quantum Coherence
HMW	High Molecular Weight
IC_{50}	Half maximal inhibitory concentration
ILCT	Intra-Ligand charge transfer
KP1019	Indazolium [*trans*-[tetrachlorobis(1H-indazole)ruthenate(III)]
LMCT	Ligand-Metal Charge Transfer
LMW	Low Molecular Weight
m	Multiplet
mL	Milliliter
M	Molar (moles per liter)
Me	Methyl
MeCp	Methylcyclopentadienyl

MALDI-ToF	Matrix Assisted Laser Desorption/Ionization – Time of Flight
MLCT	Metal-Ligand Charge Transfer
MTT	3-(4,5-dimethylthiazol-2-yl)-2,5-diphenyltetrazolium bromide
µL	Microlitre
NAMI-A	Imadozolium *trans*-[tetrachloro(dimethylsulfoxide)(imidazole)ruthenate(III)]
PLA	Polylactide
PMC	Polymer-metal conjugate
ppm	Part per million (NMR)
NMR	Nuclear Magnetic Resonance
^{1}H NMR	Proton Nuclear Magnetic Resonance
^{11}B NMR	Boron-11 Nuclear Magnetic Resonance
^{13}C NMR	Carbon-13 Nuclear Magnetic Resonance
^{31}P NMR	Phosphorus-31 Nuclear Magnetic Resonance
^{19}F NMR	Fluorine-19 Nuclear Magnetic Resonance
$^{n}J_{AB}$	Coupling constant (in Hz) between the atoms A and B separated by n bonds
ROP	Ring-Opening Polymerization
s	Singlet
Sh	Shoulder
SCE	Saturated calomel electrode
SRB	Sulforhodamine B
t	Triplet
THF	Tetrahydrofuran
TLC	Thin-layer chromatography
TMS	Tetramethylsilane
UV-Vis	Ultraviolet-Visible spectroscopy
WHO	World Health Organization
δ / ppm	Chemical shift in ppm (NMR)
ε / M^{-1}cm^{-1}	Molar extinction coefficient (UV-Vis)
λ / nm	Wavelength (UV-Vis)
υ / cm^{-1}	Wavenumber (FTIR)

List of compounds

Precursors

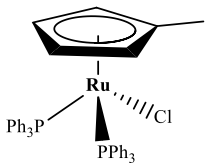

1

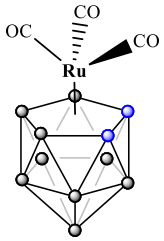

2

Organometallic complexes incorporating bipyridyl derivatives

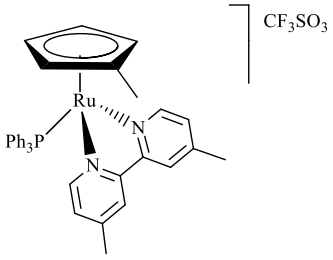

1a

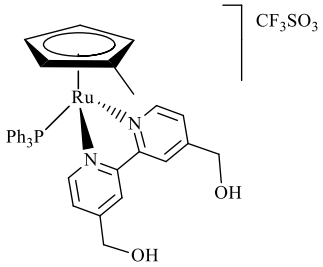

1b

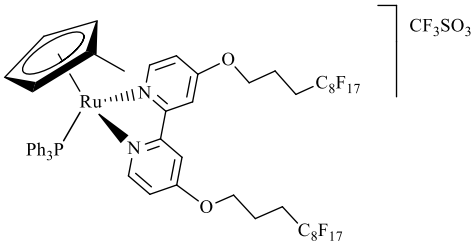

1c

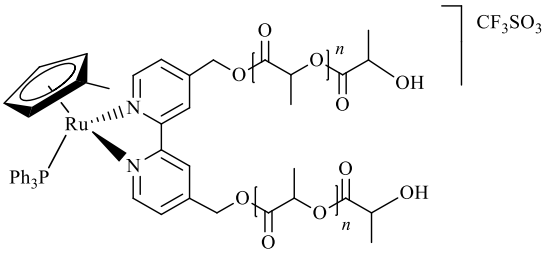

1d

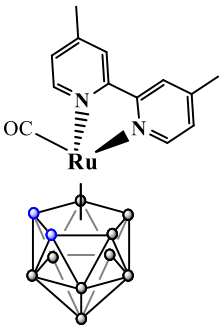

2a

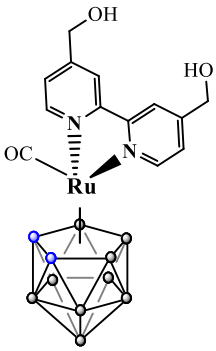

2b

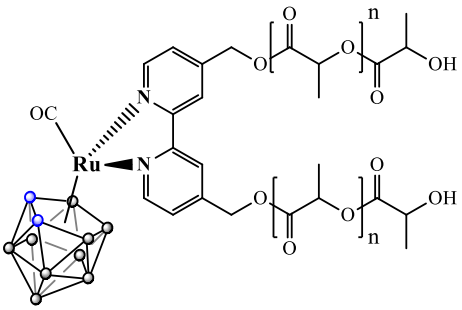

2c

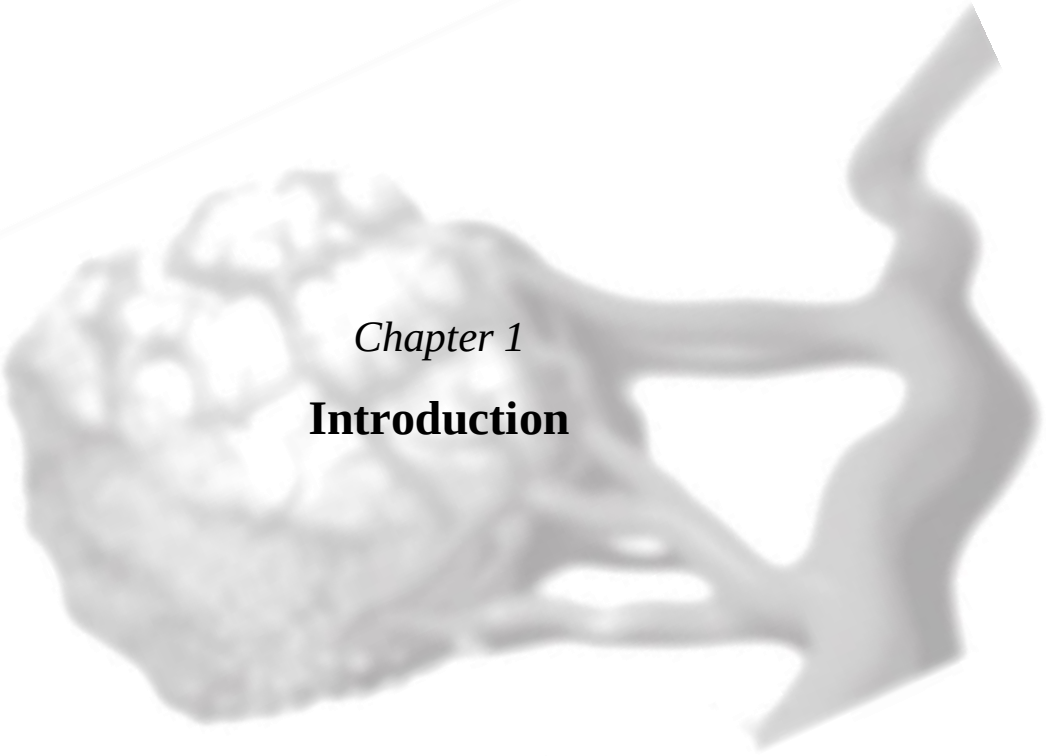

Chapter 1

Introduction

Introduction

1.1 Cancer

Cancer is defined as a collection of life-threatening diseases. This condition, characterized by the uncontrolled division of abnormal cells,[1] is a consequence of several disturbances of the most fundamental rules of behavior of the cells in a multicellular organism. Because of the failure of growth or division regulatory systems, the affected cells can proliferate boundlessly, and colonize tissues normally reserved for other cells.[1] Statistical data, from the World Health Organization (WHO), points to nearly 14 million new cases and 8.8 million deaths worldwide in 2012 and 2015, respectively[2] which put cancer at the top of the leading causes of morbidity and mortality, along with other major diseases, such as heart disease and infections.[3] In fact, WHO estimates an increase of about 70 % on the incidence of cancer. Recent research has shown that 50 % of cancers could be prevented by lifestyle changes such as smoking cessation, sensible eating and drinking, and increased exercise.[2]

The traditional methods of cancer treatment include surgery, radiotherapy, chemotherapy, and immunotherapy. The choice of the therapeutic option depends upon the cancer type and the stage of the disease, as well as the general condition of the patient. Complete removal of the affected tissue with least harm to the rest of the body is the treatment goal. The surgery alone is effective mainly in the cases of benign tumors (their cells do not have the ability to invade the surrounding tissue, and stay clustered together in a single mass). In contrast, the malignant tumors have the tendency to invade adjacent tissues or to spread through the bloodstream and lymphatic vessels to form metastasis at other sites of the body, which often limits surgery effectiveness. In such cases, the combination of treatments for cancer therapy (usually surgery combined with chemotherapy) has become an increasingly common practice once synergistic actions can be selected as, for example, targeting different points in the cell cycle, or blocking different growth factor receptors.

Conventional chemotherapy is usually based on a series of injections of highly cytotoxic drugs, which are small enough to leave the vascular system by passing through pores in the blood vessel walls. Therefore, they are distributed throughout the body. These drugs owe low selectivity for cancer cells and this fact can lead to increased toxicities against normal tissues that also show enhanced proliferative rates, such as the marrow bone, gastrointestinal tract and hair follicles. The resulting severe side effects often restrict the frequency and size of dosages, much to the detriment of tumor inhibition.[4]

1.2 The usage of metal ions in cancer therapy

1.2.1 Platinum compounds

Accidentally discovered as an anticancer agent in 1968 by Rosenberg,[5] cisplatin (*cis*-dichlorodiamineplatinum(II), **Figure 1.1**, left) has been in clinical use since 1971, when studies first demonstrated its efficacy.[6] By that time, anticancer compounds' screening was mainly focused on small organic molecules, thus the discovery of the anticancer properties of cisplatin surely marked the entry of inorganic compounds into the arena. Cisplatin is especially effective against solid tumors, such as

testicular, ovarian, head and neck, and small-cell lung cancer.[7,8] For testicular cancer, when recognized in an early stage, curing rates exceed 90 %. As a result, the intense research that preceded cisplatin's discover shifted focus to include inorganic complexes with objective of both widening the spectrum of chemotherapy of cisplatin and improving its clinical profile by decreasing toxicity and overcome some acquired mechanisms developed in some cancer cell lines.[9]

The replacement of the two chloride groups by two oxalate type of ligand in the [*cis*-$Pt(NH_3)_2$] fragment gave origin to carboplatin and oxaliplatin, *cis*-diamminecyclobutane-dicarboxylatoplatinum(II) and *R*,*R*-cyclohexane-1,2-diamineoxalatoplatinum(II), respectively (**Figure 1.1**, center and right). These two compounds were thought to operate by a mechanism of action similar to that observed for cisplatin however, the presence of the bidentate dicarboxylate seems to reduce the activity of the agent. Although less effective, carboplatin is also less toxic than cisplatin, which allow the use of higher doses to achieve a comparable level of treatment efficacy.

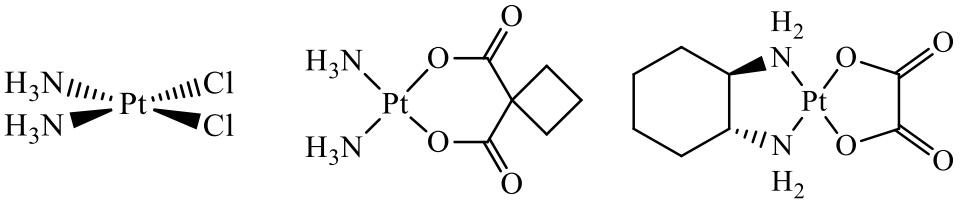

Figure 1.1 – Platinum base chemotherapeutics used in 50-70 % of cancer treatments. Cisplatin (left), carboplatin (center) and oxaliplatin (right) molecular structure.

Cisplatin and its derivatives still representing 50-70 % of all cancer treatment regimens nowadays. This line of platinum-based chemotherapeutic agents is not used in all cancer treatments due to some tumor types of resistance at the maximum tolerable dose. Dosage is limited by general toxicity, which manifests as severe side effects, including nausea, vomiting, loss of sensation in the extremities and nephrotoxicity. Some relevant types of cancer that are resistant to cisplatin include types of breast cancer, the most common cancer among woman in Europe, and prostate cancer, which is the most common cancer among men in the United States and in Europe.[2] Additionally, cisplatin showed to be largely ineffective and also unresponsive on some types of cancer (notably on colorectal cancers, which have increasing incidences in many countries),[2] and which effectiveness can be related to resistance mechanisms acquired during treatment.

Despite the success of these platinum anticancer agents, further research on other metallic cytotoxic compounds with equal or greater antitumor activity and lower toxicity is envisaged. This had led to an ongoing quest for the discovery of non-platinum metals that may extend the spectrum of activity of metal-based drugs.[10] Among these, organoruthenium compounds appear to be the most promising.[11]

1.2.2 Ruthenium compounds

Over the past four decades, many ruthenium-containing agents have been prepared and screened for their potential antitumor activity.[12] Ruthenium, a transition metal of the platinum group, was first hypothesized to exert its anticancer effects by direct interaction with DNA as observed with platinum. However, it is now known that ruthenium metallodrugs show a number of differences with platinum

based compounds.[13] First, ruthenium appears to accumulate preferentially in neoplastic masses rather than normal tissues, possibly by using transferrin to enter in tumor.[14] It has been proposed that transferrin-ruthenium complexes are actively transported into neoplastic tissues containing high transferrin receptor densities. Once bound by the transferrin receptor, it is assumed that the complex releases ruthenium that is then internalized by the tumor.[14] Moreover, is important to enhance that, in the case of Ru(III) complexes, they can stay in its relatively inactive oxidative state until they reach the tumor site. Once there, and because the cancerous environment has a lower oxygen level content and higher acidity compared to normal tissues, reduction to the more reactive Ru(II) might occur.[15] This reaction, termed activation-by-reduction, not only results in selective tumor targeting but may also direct cytotoxicity activity toward hypoxic tumors that are more likely to be resistant to chemotherapy and radiation. Finally, some ruthenium agents demonstrate greater efficacy against cancer metastases than against primary tumors.[16] This antimetastatic effect is likely mediated by inhibition of tumor cell detachment, invasion/migration, and re-adhesion to a new growth substrate.[17] In view of these properties, ruthenium is predicted to show patterns of antitumor activity and clinical toxicity that are distinct from those of platinum.

1.2.2.1 NAMI-A and KP1019

The first ruthenium agent to enter clinical trials was NAMI-A, imadozolium *trans*-[tetrachloro(dimethylsulfoxide)(imidazole)ruthenate(III)] (**Figure 1.2**). The drug, developed by Alessio and Sava,[18] is an anionic complex which contains an octahedral ruthenium(III) center bound to one imidazole ligand, with a *S*-coordinated dimethylsulfoxide ligand *trans* to the imidazole and four chlorides completing the coordination sphere. The results from the clinical trials of this drug were quite remarkable: despite its lack of activity against primary tumors, the drug is, however, a potent agent against metastasis. This is potentially very important because, although great leaps have been made in treating primary cancers (by surgery, chemotherapy and radiotherapy) secondary metastases represent a major clinical challenge.

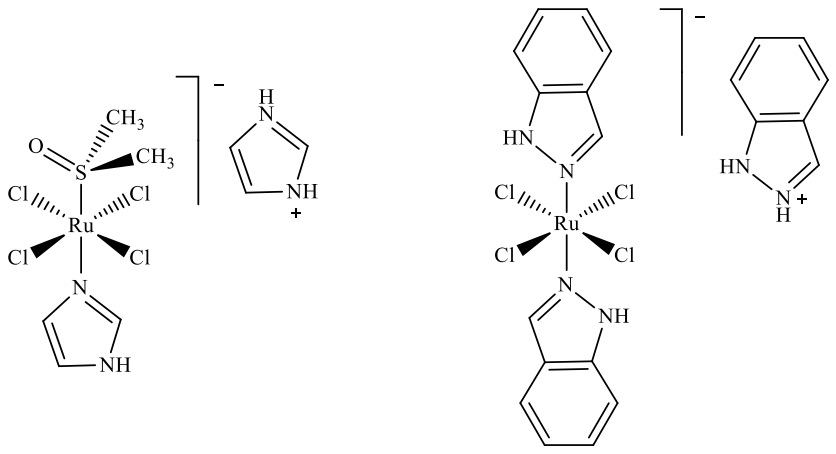

Figure 1.2 – First ruthenium containing complexes entering clinical trials: NAMI-A (left) and KP1019 (right).

Along with NAMI-A, a second ruthenium agent entered clinical trials. Indazolium [*trans*-[tetrachlorobis(1H-indazole)ruthenate(III)] or KP1019 (**Figure 1.2**) was developed by Keppler[19] and

despite their structural resemblances with NAMI-A, this cytotoxic agent has shown to be very active against primary tumors. Nevertheless, many aspects about the tumor-inhibitory effects of these ruthenium drugs are not still completely understood.

1.2.2.2 Ruthenium-arene compounds as promising anticancer agents

More recently, two other classes of ruthenium anticancer agents have been developed, based on ruthenium arene compounds. Strikingly parallel to NAMI-A and KP1019, two sets of agents that are structurally very similar have been described, and while one shows good cytotoxicity against primary tumors, the other is an antimetastactic agent with low toxicity.

The first class has been developed by Sadler and consists of an aryl ruthenium with "piano-stool" type of conformation, with a bidentate ethylenediamine and a chloride occupying the three remaining coordination sites (**Figure 1.3**, left). These water-soluble stable organometallic agents are as potent as the platinum drugs cisplatin and carboplatin in some primary cell lines, and *in vivo* activity has also been demonstrated.[20] They exhibit a wide spectrum of activity and are also active against some tumors which have become resistant to cisplatin. The level of anticancer activity is dependent on the aryl unit with more extended aryls, such as biphenyl or tetrahydroanthracene, showing higher activity. Replacing the ethylenediamine with bulkier *N*-donor ligands such as bipyridine or *N*,*N*,*N*',*N*'-tetramethylethylediamine reduces the activity, although with 1,2-diaminobenzene the activity is retained.[20] While these compounds can interact with a variety of different biomolecules, the biomolecular target might be the DNA,[21] since the chloride can be replaced by a water ligand in aqueous solution, and the complex can coordinate to DNA base at this position.

The second class of compounds are the ruthenium arene 1,3,5-triaza-7-phosphaadamantane (RAPTA) agents developed by Dyson which are similar aryl ruthenium piano-stool complexes, but in which the three remaining coordination sites are occupied by two chlorides and a monodentate 1,3,5-triaza-7-phosphatricyclo[3.3.1.1]decane[22] (**Figure 1.3**, right). The compounds were developed out to create pH-dependent DNA-binding agents, but were shown very low toxicity towards cancer cell lines. Like NAMI-A, these agents are inactive against primary tumors but found *in vivo* to have activity against metastases. The RAPTA complexes are slightly less potent antimetastic agents than NAMI-A, but less toxic (in mice) and thus can be administered at higher doses.

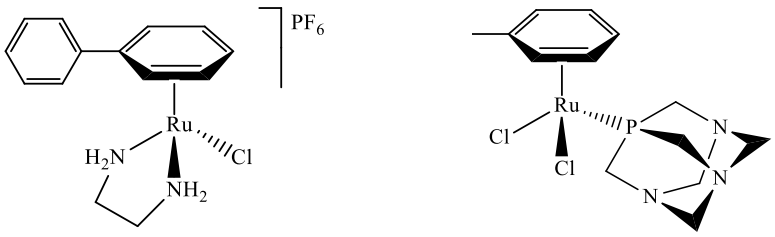

Figure 1.3 – "Piano-stool" organoruthenium anticancer RAED agent of Sadler (left) and the antimetastatic RAPTA agent of Dyson (right).

1.2.2.3 Ruthenium-cyclopentadienyl complexes

During the last years, our research group has been exploring the half-sandwich compounds based on the "Ru(η^5-Cp)" fragment (Cp = cyclopentadienyl) for their potential as chemotherapeutics. These

compounds with the general formula [Ru(η^5-Cp)(PP)(L)][X] (PP = mono- or bidentate phosphane ligand; L = *N*-donor ligand; X = counter-ion)[23-26] and [Ru(η^5-Cp)(P)(N-N)][X] (P = phosphane ligand; N-N = bidentate ligand; X = counter-ion) have been showing significant cytotoxicity against a considerable panel of human cancer cell lines.[27] [Ru(η^5-Cp)(PPh_3)(bipy)][CF_3SO_3] (PPh_3 = triphenylphosphane; bipy = 2,2'-bipyridine; **Figure 1.4** TM34, at left)[28-30] is an extraordinary example of our investigation line.[31]

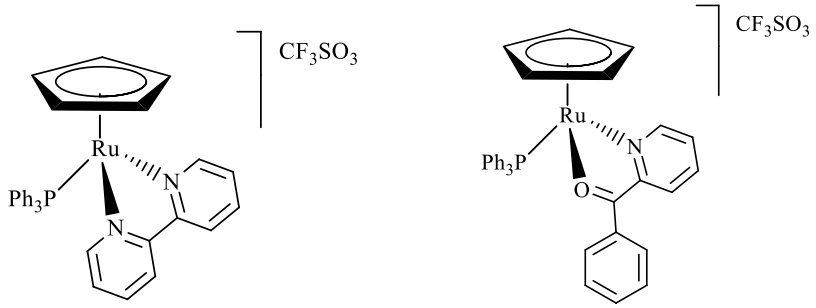

Figure 1.4 – Organometallic ruthenium-cyclopentadienyl complexes bearing efficient anticancer properties.

TM34 showed good stability under air and aqueous solutions and high cytotoxicity in the low micromolar range in a wide range of cell lines, namely, A2780 and A2780cisR (ovarian and ovarian resistant to cisplatin treatment), MCF7 (breast), PC3 (prostate) and HT29 (colorectal) human cancer cell lines. TM34 showed to be 17-fold more active at A2780 cell line and 200-fold more cytotoxic in the A2780cisR cell line, when compared to the control cisplatin.[31]

The coordination of other heteroaromatic molecules to the "Ru(η^5-C_5H_5)" fragment have been equally explored in our group. The complex showed in **Figure 1.4** (right), TM90, is one example of this type of compounds. Similarly to TM34, TM90 showed to have very low values of IC_{50} when compared to the control drug used (cisplatin) in the same tested cell lines.[31a] Preliminary *in vivo* studies on N:NIH(S)II-nu/nu nude female mice[31b] bearing triple negative breast cancer (TNBC) orthotopic tumors, showed remarkable results supporting the effectiveness and potential of this drug: treatment of the malignant tissue with TM90 allowed suppression of *ca*. 50 % of the primary tumor growth tissue along with inhibition of its metastatic behavior.[31b]

To sum up, ruthenium compounds have the ability of mimicking iron in the binding to biomolecules, strong affinity to tumor masses and, moreover, are generally less toxic than the commercial available platinum-based drugs, which make can point them out as good candidates to potential chemotherapeutics.

1.3 Enhancement of selectivity towards tumors

1.3.1 Passive targeting

The selective cytotoxicity of an anticancer drug can be increased by either increasing the dose of the drug that reaches the diseased tissue or by decreasing the dose that reaches normal tissues. Several

approaches for improving the selective toxicity of anticancer therapeutics are being pursued at present, one of them being the conjugation of anticancer-drugs to macromolecular carrier systems.

When combined to polymers, drugs are limited to the vascular system, which prevent them from distributing throughout the body and causing side effects. The conjugated drugs can be transported directly to the area of drug effect. Passive targeting by polymers is possible because macromolecular systems accumulate in tumor tissue due to the so called "enhanced permeability and retention effect" (EPR-effect), first described and investigated by Maeda *et al.*[32] Like normal tissues, tumors require sustenance in the form of nutrients and oxygen. Tumors that reach a size of about 2 millimeters in diameter, however, need to be supplied by active transport of oxygen and nutrients for further growth. To that end, they induce pathological neoangiogenesis by releasing vascular endothelial growth factors (VEGFs) into the extracellular space. VEGFs bind to and activate receptors located on the membrane of endothelial cells, triggering the corresponding intracellular pathways which leads to the transcription of angiogenesis-related genes, resulting in the growth of blood vessels that interpenetrate the tumor tissue (**Figure 1.5**).

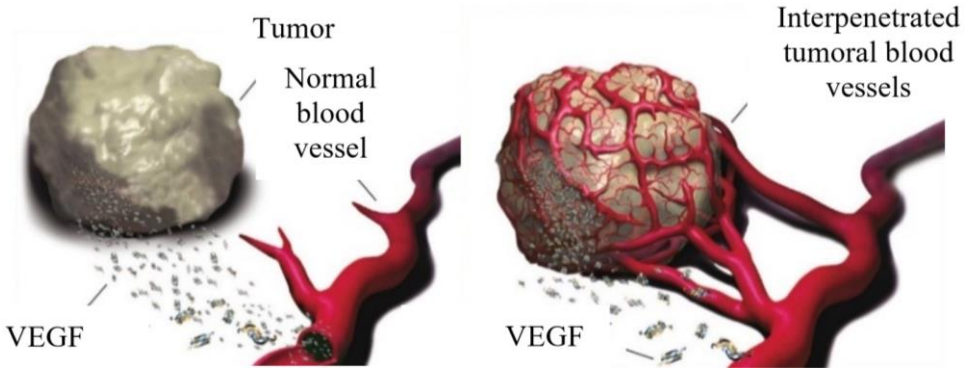

Figure 1.5 – Angiogenesis process. Adapted from [1b].

The resulting new blood vessels are lacking the tight junctions that are normally present between adjacent vascular endothelial cells, which leaves holes of greater magnitude than normal vascular pores (healthy tissues has pores of 5-8 nm whereas tumors can have pores of about 50 nm). These defects allow for the extravasation of macromolecules into the tumor interstitium (**Figure 1.6**). Since tumors are not part of the lymphatic system, the polymer that is present extracellularly cannot be removed and returned to the blood compartment, which explains why polymers accumulate in tumor tissue. This significantly increases the amount of drug delivered to solid tumors relative to the free drug. At the same time, peak drug levels and distribution of the drugs to normal tissue is decreased, leading to fewer side effects.

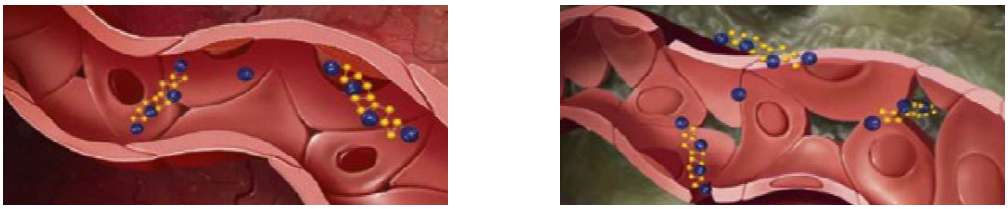

Figure 1.6 – Comparison between normal blood vessels (left) and abnormal blood vessels (right) interpenetrated at the tumor surface. The suitable structural defects for polymer-metal conjugates accumulation.

1.3.2 Active targeting

Passive targeting limitations can be overcome by attaching affinity ligands (for example, antibodies, peptides or even small molecules[33]) to the surface of the nanocarriers that can only bind to specific receptors on the cell surface. Nanocarriers will recognize and bind to target cells through ligand–receptor interactions by the expression of receptors or epitopes on the cell surface. In order to achieve high specificity, those receptors should be highly expressed on tumor cells, but not on normal cells. Ideally, these receptors should be homogeneously express and should not be shed into the blood circulation. Internalization of targeting conjugates can also occur by receptor-mediated endocytosis after binding to target cells, facilitating drug release inside the cells (**Figure 1.7**). Based on the receptor-mediated endocytosis mechanism, targeting conjugates bind with their receptors first, followed by plasma membrane enclosure around the ligand–receptor complex to form an endosome. The newly formed endosome is transferred to specific organelles, and drugs could be released by acidic pH or enzymes.

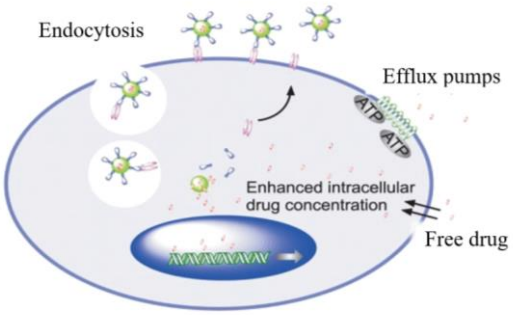

Figure 1.7 – Active targeting strategy for controlled drug delivery. Adapted from [1].

1.3.3 Polymer-metal conjugates

The development of macromolecular drugs by conjugation of low molecular metallodrugs with polymers is now a well-established field. Several reports show the improvement of stability, release control and the decrease of side effects of several platinum compounds already in clinical use, such as oxaliplatin.[33]

As described earlier, the EPR-effect virtually states that all macromolecules can selectively be accumulated in tumors rather than in healthy tissues, due to their defective vessel vascular structure and decreased lymphatic drainage however, this passive targeting results suffers from some limitations, once certain tumors do not exhibit the EPR-effect, and the permeability of vessels may not be the same

throughout a single tumor. In addition, nanodrugs currently under clinical development lack of specific targeting.[34] One way to overcome these limitations is to attach affinity ligands to the nanocarriers that interacts with specific receptors overexpressed on cancer cells (active targeting), increasing the drugs internalization in the cancer cell.[34,35]

ProLindac (diaminocyclohexane, DACH or also known as AP5346, **Figure 1.8**) is a platinum based polymer prodrug currently in phase II clinical development.[36] It uses a 25 kDa polymer delivery vehicle based on hydroxypropylmethacrylamide (HPMA) to target the active form of the approved drug oxaliplatin to tumors. The pH-sensitive linker that binds platinum to the polymer releases platinum more rapidly at low pH environments, as found typically in many tumors. Both preclinical and clinical study data indicate that ProLindac exhibits efficacy at least equal to, and likely superior to oxaliplatin, while demonstrating excellent tolerability. Additional clinical studies of ProLindac used in combination with other chemotherapeutic agents are at the moment a possibility.

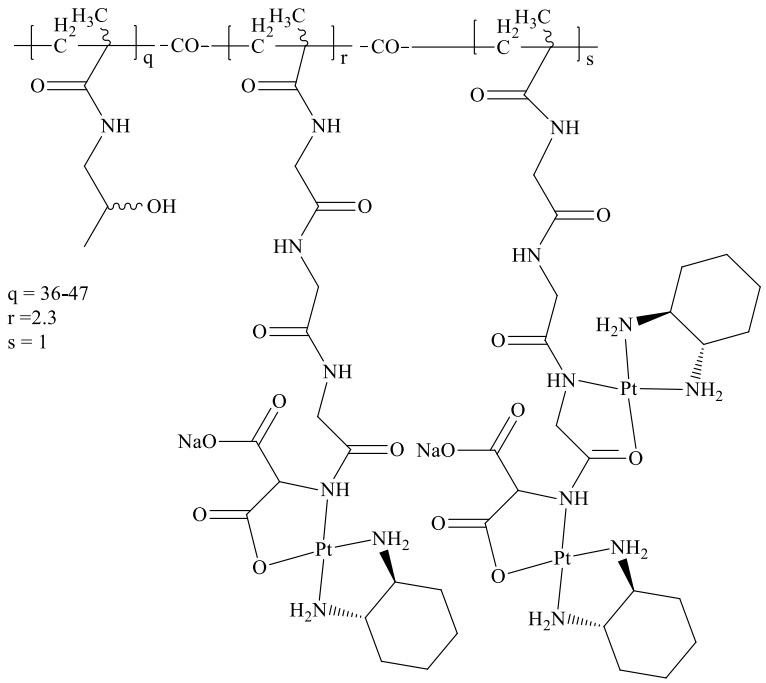

Figure 1.8 – Partial structure of AP5346 (or *ProLindac*).

In this context, our group has recently published the first ruthenium polymer conjugate, based in the low molecular weight ruthenium precursor, TM34. This macromolecule (RuPMC, **Figure 1.9**) takes advantage from passive targeting (EPR effect) given by the biodegradable and biocompatible polylactide chain (approved by the Food and Drug Administration, FDA) and from active targeting given by the glucose derivatized molecule present in the chain end, due to the higher demand of sugar from the cancer cells compared to the normal cells.[37] In fact, the RuPMC has shown to enter the MCF7 cancer cells and is retained *ca.* 50 % in the nucleus fraction, while TM34 is mainly found in the membrane (*ca*. 80 %), forecasting different mechanisms of cellular uptake and of cell death for these two compounds bearing the same cytotoxic fragment. The introduction of the biofunctionalized polymeric chains also provided a significant increase in the cellular uptake showing that macromolecules can own a different cellular internalization mechanism that, in this case, does not affect the general cytotoxicity of the compound.

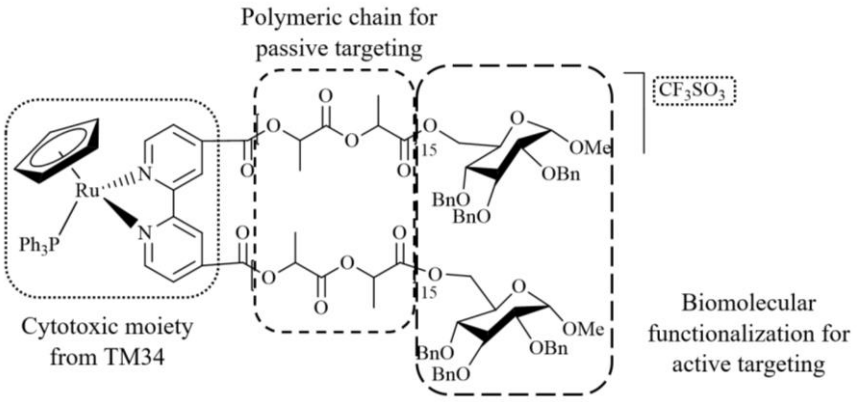

Figure 1.9 – First ruthenium-cyclopentadienyl polymer conjugate incorporating a D-glucose end-capped polylactide macroligand.

1.4 Boranes and carboranes

Boron hydrides (also called boranes) are composed of boron and hydrogen and are the simplest compounds of boron. In the periodic table, boron and carbon form the most molecular hydrides.

Additionally, carbon is the only element beside boron that has a capacity to catenate and to form selfbonded complex molecular networks.[38] Boranes, the binary compounds of boron and hydrogen, posed serious problems of structure and bonding from the very beginning. Boron is in the Group 13 of the periodic table and thus has only three valence electrons. The simplest boron hydride is not BH_3 because it has two electrons fewer than required to satisfy the octet rule.

In 1954, Lipscomb and co-workers,[39] introduced the idea of three-center two-electron (*3c-2e*) bonding; when electrons are in short supply, a pair of electrons can bond three atoms in a triangular array. Thus, the boranes are described as electron deficient. The simplest boron hydride, diborane B_2H_6 (**Figure 1.10**), has the same stoichiometry of ethane, C_2H_6, but two electrons fewer.

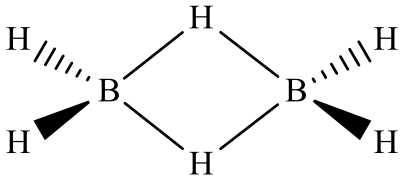

Figure 1.10 – B_2H_6 and chemical structure.

Carboranes, known since the 1960's, are boron clusters compounds with one or more carbon(s) incorporated into the structural framework.[40] The first carboranes discovered were $C_2B_3H_5$, $C_2B_4H_6$ and $C_2B_5H_7$.[38] The synthesis and properties of the three isomers of dicarba-*closo*-dodecaborane, $C_2B_{10}H_{12}$, were reported in 1963 both in the United States and USSR.[41]

In dicarba-*closo*-dodecarboranes, hexacoordinated carbon and boron atoms adopt the regular icosahedral geometry. Dicarba-*closo*-dodecarborane has three isomers (**Figure 1.11**): 1,2-, 1,7- and 1,12- dicarba-*closo*-dodecarborane, i.e. *o*-, *m*-, *p*-carborane, respectively. The respective numbering is

also depicted in the figure; the lines of the skeleton are not electron-pair bonds but merely clarifying the cluster geometry.[42] However, the exopolyhedral C-H and B-H are electron pair bonds.

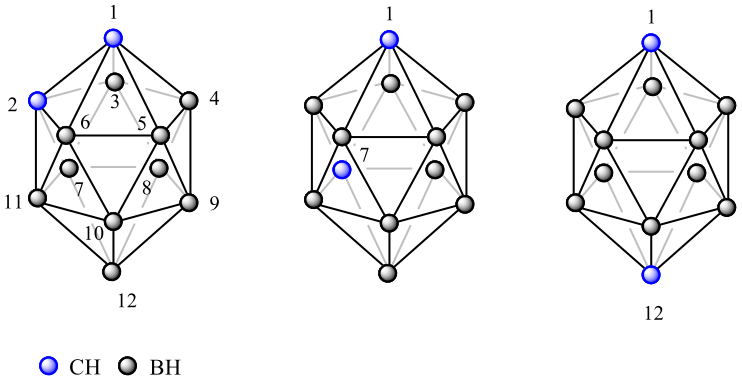

Figure 1.11 – The isomers of dicarba-*closo*-dodecarborane showing the numbering of the cage. Carbon-hydrogen and boron-hydrogen bonds are omitted for clarity.

The two carbons vertices in dicarba-*closo*-dodecarboranes bear relatively acidic hydrogen atoms, which are readily replaced by metals or organic groups.[43] Substituents can also be introduced with good control to at least a certain number of boron vertices. Carborane compounds with M-C and M-B σ bonds are known for most transition and non-transition metals and for some lanthanides.[41] The first organometallic derivatives of carboranes were obtained from the reaction of lithiocarborane with compounds with metal-halogen bond. Carboranes with open polyhedral structures are the basis of metallocarborane chemistry as they can form stable sandwich-type complexes with transition metals.[40,44]

Even though the very important advantage of dicarba-*closo*-dodecaboranes is their unique thermal and chemical stability to most organic and organometallic compounds, they do have one very important degradation reaction. Carboranes are unstable in alkaline media, where they are susceptible to nucleophilic attack by Lewis bases and undergo partial degradation (or decapitation). The degradation of the icosahedral *ortho*-carborane, 1,2-*closo*-$C_2B_{10}H_{12}$, by KOH in MeOH (**Figure 1.12**) was first reported by Hawthorne and co-workers in 1964.[45] This treatment leads to the selective removal of a single boron atom producing, upon work up, a 11-vertex *nido* carborane anion, [7,8-*nido*-$C_2B_9H_{12}]^-$, which contains an *endo* proton associated with the open face of the *nido* cage. Aside from KOH, decapitation can be performed with methanolic piperidine,[46] "wet" fluoride ion solutions ($[Bu_4N]F.xH_20$),[47] pyrrolyl,[48] dimethylpyrrollyl[49] and $HNP(NMe_2)$.[50]

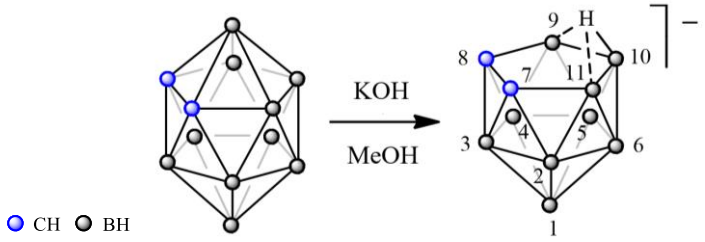

Figure 1.12 – Deboronation of the closo cluster. The bridging hydrogen in the 7,8-dicarba-*nido*-undecaborate(-1) is shown in both equivalent bridged positions.

1.4.1 Boron Neutron Capture Therapy (BNCT) as an alternative therapy

Applications associated with the properties of boron as the element within the deltahedral species primarily exploit the unusually high cross section of the ^{10}B isotope for neutron capture (20 % natural abundance). This led to the development of light weight neutron shields and, in particular, to the Boron Neutron Capture Therapy (BNCT) of tumors. From all boron cluster applications in medicine and pharmacology, the greatest number of publications refer to cancer treatment using BNCT.[51] This technique, discovered by Locher in 1936,[52] is currently in clinical trials in the U.S.A, Japan and some European countries.

BNCT is a binary treatment modality (**Figure 1.13**) that combines irradiation with a thermal or epithermal neutron beam with tumor-seeking, boron-containing drugs that are taken up preferentially by neoplastic cells to produce selective irradiation of tumor tissue. The high linear energy transfer (LET) alpha particles and recoiling ^{7}Li nuclei emitted during the ^{10}B reaction in tissue are known to have a high relative biological effectiveness (RBE – the relative amount of damage that a fixed amount of ionizing radiation of a given type can inflict on biological tissues).[53] Their short path length in tissues (up to 10 μm) limits their effect mostly to cells containing ^{10}B atoms, providing a strategy to damage the majority of tumor cells, protecting the healthy tissue.

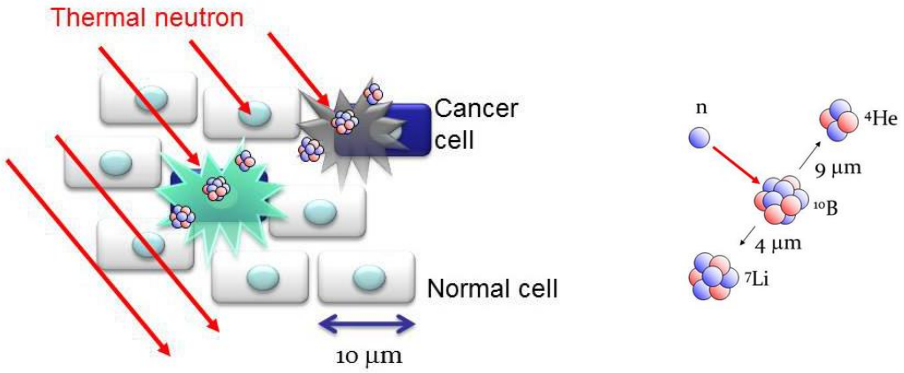

Figure 1.13 – Boron neutron capture reaction: Non-radioactive isotope, ^{10}B atoms, absorb low energy neutrons (< 0.5 eV) and desintegrates into an alpha (^{4}He) particle and a recoiling lithium nucleus (^{7}Li). These particles deposit large energy along their very short path (less than 10 μm).

For BNCT to be successful, an effective boron delivery agent must possess the following basic requirements: (i) overall low toxicity; (ii) exhibit good tumor-cell selectivity; (iii) persist intracellularly at constant concentrations during neutron radiation; (iv) be deliverable at constant 20-35 μg ^{10}B per gram of tumor; (v) have the capacity to reach the target site through the blood stream by penetrating biological barriers, such as the blood-brain barrier (BBB). Early-molecular design approaches were guided by the observation that BBB is more permeable in the diseased state than it is in the healthy state, but therapeutics strategies that emerged from these approaches did not prove successful, mainly because isolated clusters of tumor cells protected by the normal BBB, retain the potential to become the center for tumor resistance.

BNCT has been applied clinically for the treatment of patients with malignant brain tumors and malignant melanoma, using sodium mercaptoundecahydrododecaborate ($Na_2[^{10}B_{12}H_{11}SH]$; $Na_2{}^{10}BSH$)[54] and L-p-(dihydroxyboryl)phenylalanine (L-^{10}BPA)[55] respectively. In 1998, positron emission tomography (PET) using ^{18}F-BPA has been developed. Some structures of boron compounds which

have already been used for clinical treatment of BNCT are show in **Figure 1.14**. The achievement of ^{18}F-BPA PET imaging allowed the prediction of tumor/blood and tumor/normal tissues ratios of L-^{10}BPA before neutron irradiation. This PET technology also displayed selective accumulation of ^{18}F-BPA in various tumors. Thus, BNCT has been applied for various cancers including head and neck cancer, lung cancer and hepatoma.[56a,b]

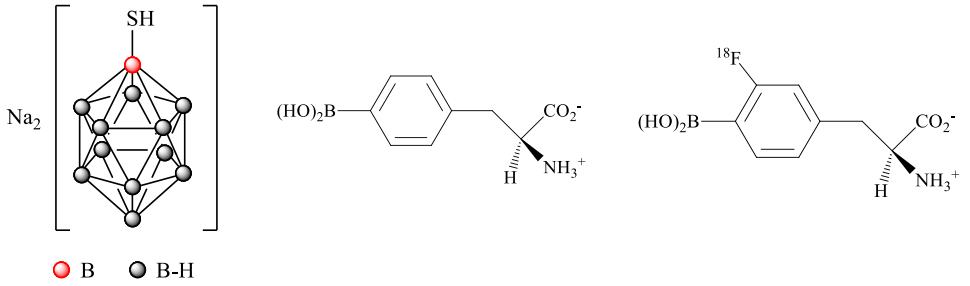

Figure 1.14 – Boron containing compounds used in BNCT: Na_2 ^{10}BSH (left), L-^{10}BPA (center) and ^{18}F-BPA (right). The two first are effective boron delivery agents whereas the third one is a used as imaging agent.

Although several efforts have been performed, the development of new ^{10}B-carriers that deliver an adequate concentration of ^{10}B atoms to the malignant masses is still an important requirement for effective and extensive cancer therapy in BNCT. Recent promising approaches that meet the requirement involve the use of small boron molecules[57] such as porphyrins, nucleosides, aminoacids, peptides, and boron-conjugated biological complexes, such as monoclonal antibodies, epidermal growth factors, carborane oligomers, micelles and dendrimers.[58]

In a study by Trivillin and coworkers on hamster cheek pouch oral cancer model, it was observed that low-dose BNCT using BPA and $Na_2{}^{10}B_{10}H_{10}$ (GB-10) administered jointly induced significant tumor control with no radiotoxic effect on normal tissue and precancerous tissue (tissues with potentially malignant disorders, from which tumors may arise)[59]. Boric acid [$B(OH)_3$] and borane clusters (*closo*-$B_{12}H_{12}^{2-}$ or $C_2B_{10}H_{12}$) are the two main types of boron entities used so far in the synthesis of carrier molecules for BNCT.

Besides that, the synthesis of boron-rich drugs is of upmost importance because it is extremely important to increase the efficiency of generating highly energy particles. The rationale design of therapeutic agents that incorporate polyhedral borane ligands[60] (for instance, the carborane $C_2B_{10}H_{12}$ moiety) can be seen as a sophisticated strategy to the synthesis of appropriate boron carrying therapeutic agents due to their stability, versatility and very high boron content useful for specific use.[61-63] In addition, their low toxicity and ability to be quickly excreted from the body apply further merits to their use in BNCT.

Boron-containing porphyrin compounds, and derivatives, have been extensively investigated due to their usually low toxicity and natural affinity for tumors.[64, 65] Examples of such compounds are BOPP (**Annex A1**)[66], CuTCPH (**Annex A2**),[67] and H_2OCP (**Annex A3**)[68]. Porphyrin derivatives have been shown to deliver therapeutic amounts of boron to tumor bearing mice and rats. They attained high tumor:brain and tumor:blood boron concentration ratios, and longer retention times in tumors than BSH and BPA. In addition, these types of boron-containing materials show to be promising dual agents for both BNCT and photodynamic therapy (PDT) of tumors, due to the strong absorptions of these macrocycles in the red and near-infrared regions of the optical spectrum along with their unique photosensitizing properties.[64]

1.5 Scope of the current work

Despite the great advances achieved in cancer therapy, cancer still one of the leading causes of death worldwide. Several cytotoxic agents have been found to surpass the worldwide cisplatin drug activity but the lack of selectivity in chemotherapy could be one of the major causes of failure in their progress into clinical trials. The introduction of macromolecules, particularly as polymer-metal conjugates, may endow the compounds with some advantages when compared to their parental Low Molecular Weight complexes (**LMW**), namely: a) passive tumor targeting, b) lower toxicity and c) stabilization and prolongation of the half-life of the LMW parents, among others.

This thesis appears as a conjugation of knowledge from two research groups, namely the *Group of Bioinorganic Chemistry and Drug Development* (at FCUL), specialized in organometallic chemistry mainly focused in cancer therapy, and the *Inorganic Materials and Catalyst Laboratory* (at ICMAB-CSIC) specialized in boron chemistry. In particular, this work is based on the development of two new families of organoruthenium compounds bearing different η^5 coordination motifs: the 3D-carboranyl motif and the 2D-methylcyclopentadienyl one.

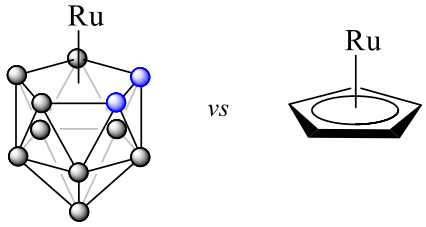

Figure 1.15 – Comparison between the two η^5-coordination motifs used in this thesis: the ruthenium-carboranyl (left) and the ruthenium-cyclopentadienyl (right).

In this frame, and due to their geometrical resemblance, we chose the dianion [*nido*-7,8-$C_2B_9H_{11}]^{2-}$ as an alternative 3D-motif to substitute the cyclopentadienyl ligand $[C_5H_5]^-$ (widely present in our ruthenium polymer-metal conjugate's family, PMCs). This structural substitution can lead to (chemically and biologically) interesting compounds once the carboranyl ligand can be seen as an efficient ^{10}B source, adequate for application of this type of compounds in BNCT.

The rationale design of the new potential chemotherapeutics was based in previous results obtained in our group and follow the next steps:

(i) synthesis of new organometallic compounds based on the "Ru(η^5-methylcyclopentadienyl)" fragment to be studied in the frame of traditional chemotherapy;
(ii) synthesis of new organometallic compounds based on the "Ru(η^5-carboranyl)" fragment to be studied in the frame of BNCT;
(iii) preparation of PMCs analogues to (i) and (ii) defined as High Molecular Weight compounds (**HMW**);
(iv) complete characterization of all the new compounds by spectroscopic, analytic and electrochemical techniques;
(v) assessment of the new compounds stability;
(vi) and, finally, preliminary *in vitro* evaluation of the anticancer properties of these new complexes by means of determination of their IC_{50} values.

Chapter 2

Organometallic ruthenium-methylcyclopentadienyl complexes incorporating 2,2'-bipyridine derivatives

Organometallic ruthenium-methylcyclopentadienyl complexes incorporating 2,2'-bipyridine derivatives

2.1 Introduction

During the last years, the *Group of Bioinorganic Chemistry and Drug Development* has focus much attention on the development of new families of piano-stool-structured complexes based on the 'M(η^5-Cp)' skeleton (where M = Ru(II), Fe(II) and Cp = C_5H_5). As described in the general introduction, this type of compounds exhibited important cytotoxic properties against several cancer cell lines. The presence of a π-bonded cyclopentadienyl ring to the metal center has shown great interest due to their ability to act as donor and electron acceptor group.

The strategy undertaken envisages the development of new complexes that might present alternative modes of action to overcome the limitations presented by the platinum drugs used in clinical use. Our ruthenium and iron complexes have a pseudo octahedral geometry (piano-stool) in which the cyclopentadienyl ring occupies three coordination positions and the other three coordination positions are completed (in most of the cases) with heteroaromatic bidentate ligands (with N, O or S donors), and phosphane ligands.

The 'Ru(η^5-C_5H_5)' unit has revealed to be a very attractive and convenient scaffold to build new molecules due to its high stability, confirmed by ESI–MS studies carried out with several complexes of the family [M(η^5-Cp)(P)(N,X)][CF_3SO_3] (where P = phosphane; N,X = heteroaromatic ligand, with X = N,S,O).[27] The fragments obtained belong always to the 'Ru(η^5-C_5H_5)' as the final species, impossible to dissociate even at very high values of energy.[27]

In this frame, the 'Ru(η^5-C_5H_5)' core seems to be a very attractive building block for the design of new molecules in view to cancer treatment. With the purpose of expanding our families of compounds, the introduction of an electron donating group in the cyclopentadienyl ring, such as a methyl group, in the ruthenium complexes was proposed in order to get a more stabilized metal-ligand system and to infer about the influence of this group on the overall electronic flow of the complexes and on their cytotoxicity.

2.2 Results and discussion

2.2.1 Synthesis of the ruthenium-methylcyclopentadienyl complexes

A new family of ruthenium-methylcyclopentadienyl complexes incorporating bipyridyl derivatives was isolated as triflate salts for the first time. [Ru(η^5-MeCp)(PPh_3)(4,4'-R_2-2,2'-bipy)]$^+$ complexes (**1a**, R = -CH_3; **1b**, R = -CH_2OH; **1c**, R = -$O(CH_2)_3(CF_2)_7CF_3$; **1d**, R = -CH_2OPLA) were synthesized in good yields by σ coordination of bidentate *N,N* chelating ligands. Coordination of these ligands was achieved by prior halide abstraction from the starting material [Ru(η^5-MeCp)(PPh_3)$_2$Cl] with silver triflate ($AgCF_3SO_3$), as **Scheme 2.1** suggests.

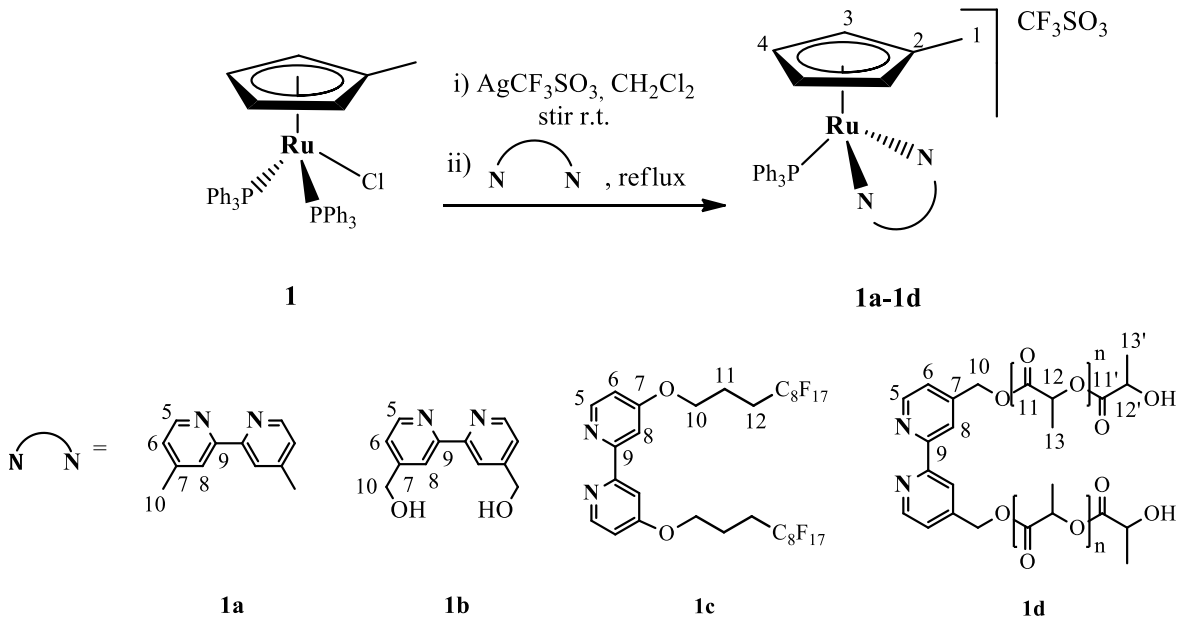

Scheme 2.1 – General synthetic route of complexes **1a-1d**; ligands are numbered for NMR spectral assignments.

After AgCl precipitation, the hypothetical intermediate $[Ru(\eta^5\text{-MeCp})(PPh_3)_2(CH_2Cl_2)]^+$ is formed by the introduction of one molecule of solvent in the coordination sphere of the metal. The presence, in slight excess, of the intended bipyridyl derivative facilitate the exchange of the CH_2Cl_2 in the intermediate promoting, the formulation of the series of compounds **1a-1d**. The coordination of the bipyridyl ligands was accompanied by gradual darkening of the solution color in all cases, obtaining, at the end of the reaction, a dark orange to light brown solution.

The purification methodology used to isolate the compounds passed by slow diffusion recrystallizations (**LMW** complexes **1a** and **1b)**, and forced precipitations (**HMW** complexes **1c** and **1d**) using, normally, *n*-hexane as precipitating agent and dichloromethane to dissolve the compounds. When necessary, dissolution of complexes in acetonitrile was performed to remove any residual traces of the free ligand.

2.2.2 Characterization of the ruthenium-cyclopentadienyl complexes

2.2.2.1 NMR spectroscopy

The full ^{1}H NMR and ^{31}P NMR spectral data for all complexes are given in **Figure 2.1**, whereas **Table 2.1** summarizes the ^{13}C NMR data for all compounds along with specific ^{19}F NMR resonances obtained for complex **1c**. When possible, resonances were attributed using 1D and 2D NMR experiments (^{1}H, ^{13}C, COSY, HMQC and HMBC) and follows the atom labelling presented in **Scheme 2.1**.

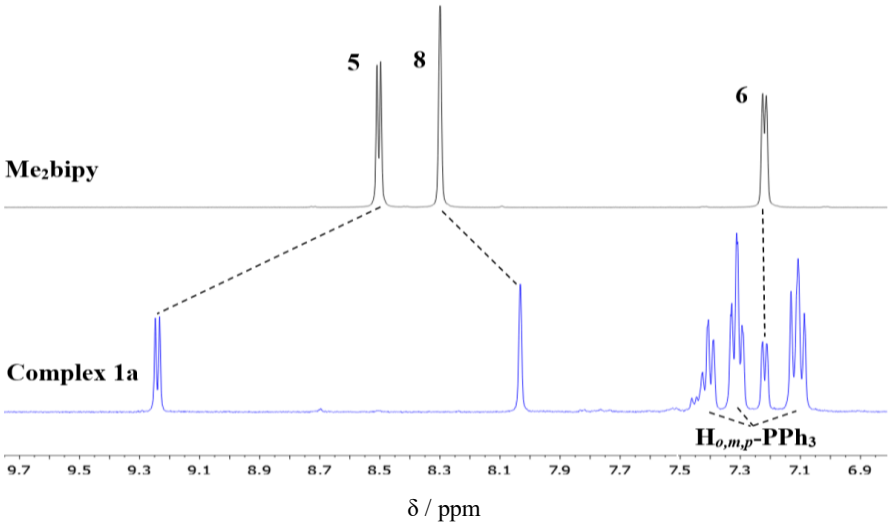

Figure 2.1 – Comparison of ^{1}H NMR spectra of free **Me$_2$bipy** ligand (up) and complex **1a** (down). In the picture, only the aromatic resonances are presented.

The two low **LMW** ruthenium-cyclopentadienyl complexes showed three different resonances in their ^{1}H NMR spectra that were ascribed to the three nonequivalent protons of the substituted cyclopentadienyl unit. These resonances appeared at δ 4.68 ppm, 4.57 ppm and 1.65 ppm (**1a**) and δ 4.60 ppm, 4.71 ppm and 1.66 ppm (**1b**) and revealed, for both cases, an appropriate 1:1 proportion between the η^5-MeCp unit and the respective 2,2'-bipyridyl derivative. In both complexes, the non-equivalent bipyridyl aromatic protons resonate at different chemical shift values when compared to the corresponding resonances of the free ligand (for complex **1a,** $\Delta H_5 \approx +0.53$ ppm, $\Delta H_8 \approx -0.26$ ppm and H_6 remains at their chemical shift, as

Figure 2.*1* suggests). The evident deshielding on the H_5 protons, adjacent to the nitrogen of the bipyridine ring, and a shielding on the H_8 protons ligand (**Table 2.1**), observed in both complexes **1a** and **1b**, is a clear evidence of successful coordination of the bipyridyl derivative to the metal. This type of effect has been already observed for related compounds where the bipyridine is substituted at the *para*-position (relatively to the nitrogen).[69] The protons of the substituent groups located at the later positions of the aromatic ring, also tend to subtly shift to low field upon coordination to the metal or maintain their resonance position (in the case of the geminal protons of the hydroxymethyl group in **1b**). Additionally, three resonances appear as triplet signals in the ^{1}H NMR (7.41 ppm < δ < 7.11 ppm) in both complexes and are readily attributed to the protons of the carbon skeleton of the single triphenylphosphane co-ligand that is still coordinated to the ruthenium center.

Characterization of these complexes was completed with ^{13}C-APT NMR measurements. The results are in accordance with the previous discussed effects in the ^{1}H NMR analysis. All the detailed spectroscopic data concerning the ^{13}C NMR experiments are in the due experimental section (**Chapter 5**). In the ^{13}C{^{1}H} NMR spectra of complexes **1a** and **1b**, contrary to the parental [RuCp(PPh$_3$)(4,4'-R$_2$-2,2'-bipy)]$^+$ analogues, the substituted cyclopentadienyl unit of complexes **1-1d** does not exhibit only one equivalent single resonance, but four different resonances in the ^{13}C NMR experiments. These non-equivalent carbon atoms appear as singlets (and one of them as doublet, **C$_3$**) in the same chemical rage as its precursor [Ru(η^5-MeCp)(PPh$_3$)$_2$Cl]. The resonances for the remaining carbons of the bipyridyl ligand appear along with the carbon signals for the triphenylphosphane co-ligand. The resonances of the latter were easily identified since they are the only resonances that appear as doublets in the ^{13}C{^{1}H}, consequence of the phosphorous-carbon coupling. Carbon-phosphorous coupling constants give also

important information in the attribution of all signals and the values obtained are in agreement with the expected (2 Hz < $^{n}J_{CP}$ < 40 Hz).

The ^{31}P NMR spectra as itself, show, for all compounds, a unique sharp singlet resonance that was easily attributed to the coordinated triphenylphosphane co-ligand (δ 51.83 ppm and δ 51.85 ppm, respectively for **1a** and **1b**) and are in good agreement with all ^{1}H NMR and ^{13}C NMR collected data.

Table 2.1 – ^{1}H NMR and ^{31}P NMR data collected from the spectra of complexes **1-1d**, in deuterated acetone.

	^{1}H NMR δ / ppm [a]									**^{31}P NMR δ / ppm** [a]
Compound	**H_1**	**H_3**	**H_4**	**H_5**	**H_6**	**H_8**	**H_{10}**	**H_{11} / $H_{11'}$**	**H_{12} / $H_{12'}$**	**PPh_3**
Me_2bipy	-	-		8.51	7.22	8.30	2.43	-	-	-
bipy$(CH_2OH)_2$ ¥	-	-		8.60	7.39	8.50	4.79	-	-	-
***per*F-bipy**	-	-		8.38	6.88	7.84	4.36	2.35 / -	2.51 / -	-
bipy$(CH_2OPLA)_2$	-	-		8.71	7.45	8.49	5.39	5.20 / 4.31	1.55 / 1.39	-
Complex 1	1.87	3.88	3.33	-	-	-	-	-	-	40.01
Complex 1a	1.65 (-0.22)	4.57 (0.69)	4.68 (1.35)	9.24 (0.73)	7.22 (0.00)	8.04 (-0.26)	2.46 (0.03)	-	-	51.83 (11.82)
Complex 1b	1.66 (-0.21)	4.71 (0.83)	4.60 (1.27)	9.34 (0.74)	7.36 (-0.03)	8.10 (-0.40)	4.79 (0.00)	-	-	51.85 (11.84)
Complex 1c	1.66 (-0.21)	4.51 (0.63)	4.63 (1.30)	9.16 (0.78)	7.03 (0.15)	7.82 (-0.02)	4.39 (0.03)	2.15 / - (-0.20 / -)	2.47 / - (-0.04 / -)	51.50 (11.49)
Complex 1d	1.68 (-0.19)	4.67 (0.79)	4.78 (1.45)	9.47 (0.76)	7.55 (-0.10)	8.11 (-0.41)	5.36 (-0.03)	5.20 / 4.31 (0.00 / 0.00)	1.55 / 1.39 (0.00 / 0.00)	51.63 (11.62)

[a] In parenthesis the difference between the coordinated and free ligand resonances (δ_{coord} - δ_{free}). *under the solvent signal. ¥ OH resonance for **$(CH_2OH)_2$bipy** is observed at 4.59 pp**m.**

Table 2.2 – Selected ^{13}C NMR and ^{19}F NMR data collected from the spectra of complexes **1-1d**, in deuterated acetone.

	^{13}C NMR δ / ppm													**^{19}F NMR δ / ppm** [b]
Compound	**C_1**	**C_2**	**C_3**	**C_4**	**C_5**	**C_6**	**C_7**	**C_8**	**C_9**	**C_{10}**	**C_{11} / $C_{11'}$**	**C_{12} / $C_{12'}$**	**C_{13} / $C_{13'}$**	
Complex 1[a]	12.0	104.9	81.0	76.7	-	-	-	-	-	-	-	-	-	-
Complex 1a[b]	11.7	103.0	76.4	76.5	155.9	127.3	149.2	124.6	156.3	20.8	-	-	-	-
Complex 1b[b]	11.7	103.0	76.6	76.7	156.1	123.6	153.7	120.8	156.3	62.5	-	-	-	-
Complex 1c[b]	11.8	102.5	75.8	76.0	157.2	114.3	166.3	110.2	158.1	68.6	20.9 / -	28.0 / -	-	-78.83, -81.65, -114.77, -122.24/-122,44, -123.27, -123.93, -126.73
Complex 1d[b]	11.7	103.4	77.0		156.3	124.4	146.5	121.9	156.5	65.0	170.2 / 175.0	69.8 / 67.1	17.1 / 20.8	-

[a] Recorded in deuterated chloroform. [b] Recorded in deuterated acetone.

In addition to the presence of the aromatic protons resonances of the bipyridyl rings, the **HMW** complexes display at their ^{1}H NMR spectra the expected signals of the η^5-MeCp moiety at δ 4.63 ppm, 4.51 ppm and 1.66 ppm (**1c**) and δ 4.67 ppm, 4.78 ppm and 1.68 ppm (**1d**) revealing the same behavior as its **LMW** relatives by clearly shifting upon σ-coordination of the macromolecular *N*,*N*' ligands.

Figure 2.2 shows the shift observed for the nonequivalent hydrogen atoms of the methylcyclopentadienyl for complex **1c**, and along with these, the three signals for the -CH_2- groups in the perfluorinated alkylic chain that resonate at δ 4.39 as a triplet (for the -CH_2- group of atoms directly attached to the oxygen atom) and other two consecutive -CH_2- hydrogen groups that appear as multiplets at δ 2.47 and 2.15, respectively. ^{1}H NMR spectrum of complex **1d** shows that, upon coordination of the macromolecular ligand, the shift of the Cp signals ($\Delta H_1 \approx$ -0.19 ppm, $\Delta H_3 \approx$ +0.79 ppm and $\Delta H_4 \approx$ +1.45 ppm) accompanies the shift of the aromatic protons of the bipyridyl rings ($\Delta H_5 \approx$ +0.76 ppm, $\Delta H_6 \approx$ -0.10 ppm and $\Delta H_8 \approx$ -0.41 ppm, as **Figure 2.3** shows). The resonances of the polymeric chains (-CH- and -CH_3 groups) do not change after reaction with the parental complex **1**, confirming that, as expected, this fragment remains intact after the reaction takes place.

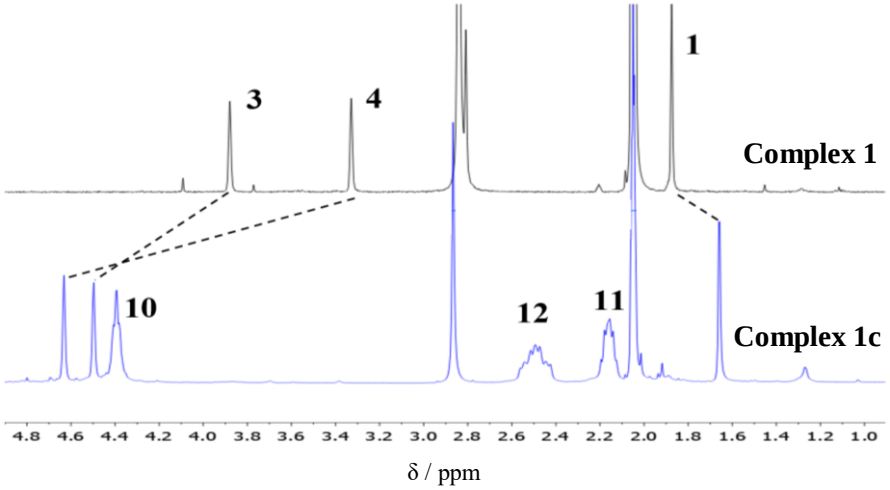

Figure 2.2 – Comparison of ^{1}H NMR spectra of the precursor complex **1** (up) and complex **1c** (down). In the picture, only the resonances from the methylcyclopentadienyl unit (and the -CH_2- resonances of the fluorinated chains) are presented.

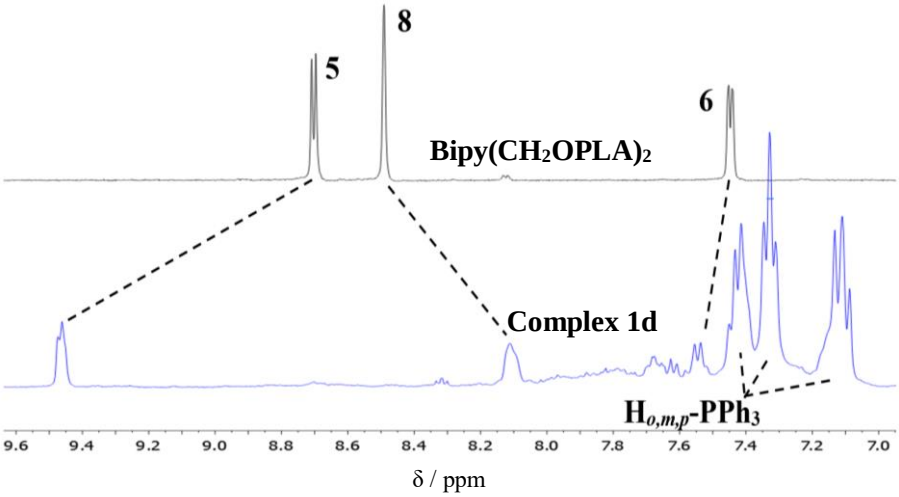

Figure 2.3 – Comparison of ^{1}H NMR spectra of free macromolecular ligand (up) and complex **1d** (down). In the picture, only the aromatic resonances are presented.

The ^{13}C NMR spectroscopic data obtained for complexes **1c** and **1d** is also in agreement with the previously observed for the **LMW** analogues. The peaks correspondent to the cyclopentadienyl motif appears, for instance for complex **1c**, as singlets at δ 76.0 ppm, 75.8 ppm and 11.8 ppm and, although a direct comparison could not be assessed, they seem to be more shielded than its precursor, complex **1** (δ 81.0 ppm, 76.7 ppm and 12.0 ppm). This shielding effect could be strongly correlated to the fact that, upon coordination of the macroligand, a prominent electronic donation is generated towards the metal center by the strong donors as the bipyridyl derivative.

Once again, the confirmed displacement of the aromatic protons of the η^5-coordinated cyclopentadienyl ring and the shift of the bipyridyl protons revealed that the syntheses were successful and the results are coherent with a formulation of cationic compounds. It is also very clear that the presence of a more donating group at the Cp unit, influences the π-backdonation on the Cp ring, that is proved by the bigger deshielding effect observed in the aromatic Cp protons relatively to its analogues [$RuCp(PPh_3)$(4,4'-R_2-2,2'-bipy)][CF_3SO_3] (δ ~ 4.8 ppm).

2.2.2.2 Elemental analysis

Elemental analysis was performed to conclude about the purity of the new compounds and the obtained results are shown in **Table 2.3**. The purity level of complex **1d** was not assessed by elemental analysis due to the high molecular weight of this compound. In this case, gel permeation chromatography and Maldi-ToF mass spectrometry analysis are preferred and are undergoing.

Table 2.3 – Analytical data for the series of complexes **1-1c**.

	Analyses [a] / %			
Compound	**C**	**H**	**N**	**S**
Complex **1**	67.8 (68.1)	5.4 (5.0)	-	-
Complex **1a** • ⅓ CH_2Cl_2	55.5 (55.7)	4.2 (4.3)	3.4 (3.4)	4.2 (4.0)
Complex **1b** • ½ CH_2Cl_2	53.0 (53.0)	4.0 (4.2)	3.3 (3.3)	4.0 (3.8)
Complex **1c** • ¼ C_6H_{14}	41.0 (41.2)	2.6 (2.6)	1.2 (1.6)	2.0 (1.9)

[a]Calculated values are given in parenthesis

Despite the possible contamination by residual solvents that probably were not eliminated in the overnight drying process, the results obtained by this analytical technique give a reasonable correlation between the calculated and experimental values. These results agree well with the NMR data and indicate a good level of purity for all compounds.

2.2.2.3 UV-vis spectroscopy

The optical absorption spectra of all ruthenium-cyclopentadienyl complexes were recorded using $1.0x10^{-4}$ to $1.0x10^{-5}$ M solutions in dichloromethane and dimethylsulfoxide. The characterization of these new compounds by UV-Vis spectroscopy allow, not only the evaluation of possible solvatochroism effects, but also charge transfer phenomena. **Table 2.4** presents all the values obtained for the molar absorptivity coefficient and the correspondent wavelength, whereas **Figure 2.4** and **Figure 2.5** show the behavior of the **LMW** and **HMW** complexes **1a** and **1d**, respectively, in both solvents.

The general effect observed in the electronic absorption spectra of this series of compounds follows the trend observed in the presented figures and is representative of their behavior.

In addition to the strong absorption bands, characteristic of each bipyridyl derivative and the {[Ru(MeCp)(PPh_3]$^+$} organometallic fragment (appearing below 300 nm), typical electronic spectra of this series of compounds are characterized essentially by one broad, medium-strength, absorption band appearing in the range of 420-450 nm.

Table 2.4 – Optical spectral data for complexes **1** – **1d** in different solvents. Measurements were performed at room temperature using 10^{-4}-10^{-5} M solutions. (*Sh* = Shoulder).

	λ_{max}/nm (ε x 10^3 / $M^{-1}cm^{-1}$)	
Compound	**Dichloromethane**	**Dimethylsulfoxide**
Complex **1**	289 (*Sh*), 336 (*Sh*), 386 (*Sh*), 448 (*Sh*)	-
Complex **1a**	288 (24.8), 323 (*Sh*), 423 (4.6), 478 (*Sh*)	291 (26.7), 333 (*Sh*), 418 (4.8), 479 (*Sh*)
Complex **1b**	292 (20.8), 354 (*Sh*), 424 (3.6), 472 (*Sh*)	290 (54.0), 350 (*Sh*), 422 (6.8), 480 (*Sh*)
Complex **1c**	270 (22.6), 294 (*Sh*), 348 (*Sh*), 419 (4.2), 476 (*Sh*)	273 (27.1), 297 (*Sh*), 355 (*Sh*), 414 (4.6), 473 (*Sh*)
Complex **1d**	294 (29.7), 329 (*Sh*), 438 (4.8), 507 (*Sh*)	295 (23.5), 332 (*Sh*), 430 (4.2), 503 (*Sh*)

Similarly, and as it can be seen in **Figure 2.4** and **Figure 2.5**, below 300 nm, there can be found two strong absorptions transitions with high intensity and energy: the first one (near 240 nm) is attributed to the electronic transitions that occur in the organometallic fragment by resemblance with the precursor complex [Ru(η^5-MeCp)(PPh_3)$_2$Cl], and the second one is attributed to the $\pi \rightarrow \pi^*$ transitions that take place in the coordinated chromophores.

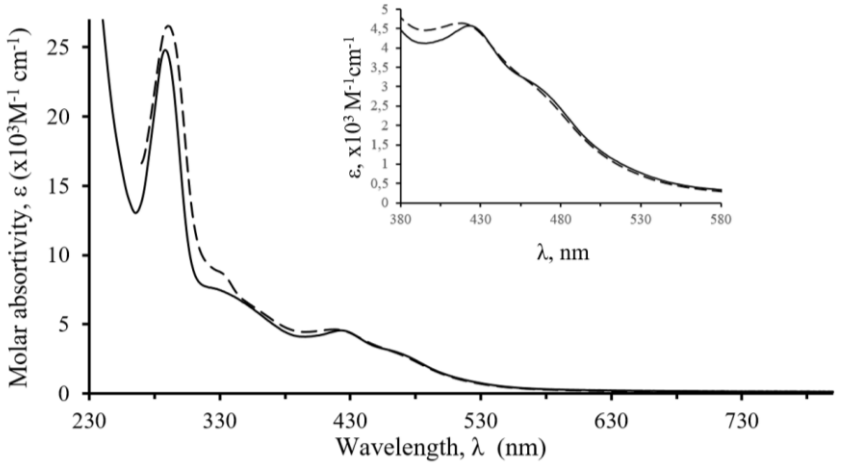

Figure 2.4 – Electronic spectra of complex **1a** in dichloromethane (———) and dimethylsulfoxide (– – – – – –). Expansion of the spectra to better seeing the identified CT transition.

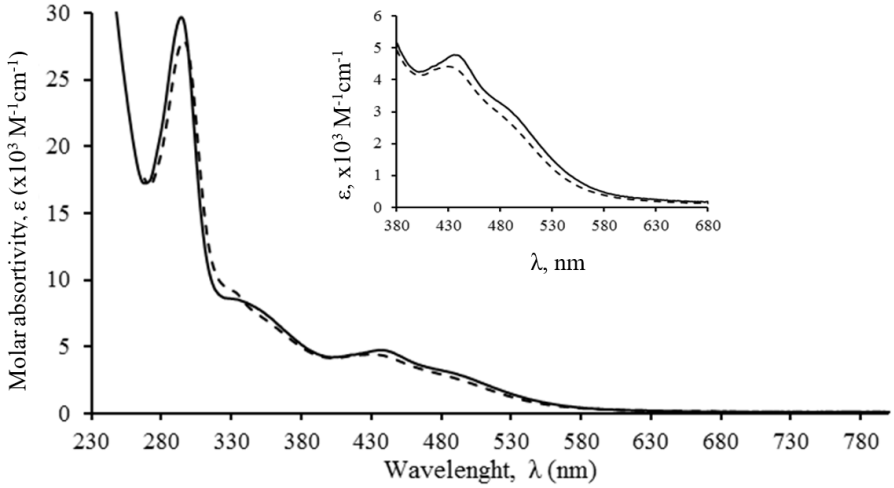

Figure 2.5 – Electronic spectra of complex **1d** in dichloromethane (———) and dimethylsulfoxide (– – – – – –). Expansion of the spectra to better seeing the identified CT transition.

The other band of much less intensity observed at 423 nm ($4.6x10^3$ $M^{-1}cm^{-1}$) for complex **1a** and 438 nm ($4.8x10^3$ $M^{-1}cm^{-1}$) for complex **1d**, for example, shows to be slightly blue-shifted with the increase of the polarity of the solvent: 423 nm in CH_2Cl_2 vs. 418 nm in DMSO for complex **1a** and 438 nm in CH_2Cl_2 vs. 430 nm in DMSO for complex **1d**. Based in their positions, intensity and similar behavior in related compounds, we can affirm that they are indicative of a charge transfer processes involving the metal and ligand(s).

2.2.2.4 IR spectroscopy

Based on a qualitative analysis of the vibrational spectra, it is possible to identify the presence of specific functional groups that are expected to be found at the molecular structure of each compound of this ruthenium-cyclopentadienyl series.

The analysis of the solid-state FTIR spectra of the organometallic ruthenium-methylcyclopentadienyl derivatives **1a-1d** confirms the presence of the cyclopentadienyl and the bipyridyl ligands in the 3000-2850 cm^{-1} range for all complexes. The presence of the triflate counter-ion was also found in the typical region for this group (ca. 1260 cm^{-1}) on FTIR spectra of complexes **1a-1d** (and it is clearly absent in the neutral precursor complex **1**), which agrees with the cationic character of this type of compounds. Despite the presence of the aforesaid stretching bands, specific groups as the hydroxyl groups present at the bipy$(CH_2OH)_2$ and the CF_2 of complex **1b** and **1c**, were also found at its typical frequency range.

In addition to the previously presented vibrational bands, complex **1d** also present the characteristic stretching frequencies for the υ(C=O) and υ(C-O) as strong and medium-strength bands at 1757 cm^{-1} and 1220 cm^{-1}, respectively, and a broad band in the range of 3450-3410 cm^{-1}, which can possibly be attributed to the stretching frequencies of the terminal hydroxyl group υ(O-H) located at the end of the polymeric chain.

2.2.2.5 Electrochemical studies

The electrochemical behavior of organometallic ruthenium-methylcyclopentadienyl complexes was studied by cyclic voltammetry in acetonitrile and dichloromethane. The potentials were measured using a platinum disk as working electrode and a silver wire pseudo-reference electrode, ferrocene as internal reference and ammonium hexafluorophosphate as supporting electrolyte.

Table 2.5 summarizes all the electrochemical data for complexes bearing bipyridyl derivatives in acetonitrile and dichloromethane, at room temperature.

Table 2.5 – Electrochemical data for complexes **1**-**1d** (all values *vs.* SCE, v = 100 mVs^{-1}).

Compound	Acetonitrile					Dichloromethane				
	E_{pa} (V)	E_{pc} (V)	$E_{1/2}$ (V)	$E_{pa} - E_{pc}$ (mV)	I_c/I_a	E_{pa} (V)	E_{pc} (V)	$E_{1/2}$ (V)	$E_{pa} - E_{pc}$ (mV)	I_c/I_a
Complex **1**	0.54	0.46	0.50	80	1.0	1.67 1.41 0.51	-- -- 0.43	-- -- 0.47	-- -- 80	-- -- 1.0
Complex **1a**	0.93 -1.60	0.85 -1.68	0.89 -1.64	80 80	0.9 0.9[a]	1.61 1.40 0.96	-- -- 0.88	-- -- 0.92	-- -- 80	-- -- 0.8
Complex **1b**	0.94 --	0.87 -1.58	0.905 --	70 --	0.7 --	1.63 1.30 0.95	-- -- 0.85	-- -- 0.90	-- -- 100	-- -- 0.9
Complex **1c**	0.87 -1.59	0.79 -1.69	0.83 --	80 100	1.0 --	0.90	0.81	0.85(5)	90	1.0
Complex **1d**	1.01 -- --	0.91 -1.49 -1.70	0.96 -- --	100 -- --	0.8 -- --	1.07	0.99	1.03	80	0.9
$[RuCp(Me_2bipy)(PPh_3)]^+$	0.97	0.87	0.92	100	0.9	1.62 1.33 1.01	-- -- 0.91	-- -- 0.96	-- -- 100	-- -- 0.9

[a] I_a/I_c

The typical electrochemical behaviour observed is similar and, in fact, all complexes were electroactive in the sweep range used (± 1.8 V), displaying one-electron quasi-reversible coupled redox wave in both solvents used.

The precursor, complex **1**, showed to be redox-active in both solvents, with ruthenium oxidation processes at 0.54 V (acetonitrile) and 0.51 V (dichloromethane) with I_c/I_a ratios of 0.7, suggesting some instability of the oxidized ruthenium species at the electrode surface. However, when the scan direction is immediately reverted after the oxidation potential, the processes turn quasi-reversible ($E_{1/2}$ = 0.50 V and $E_{1/2}$ = 0.47V

for acetonitrile and dichloromethane, respectively). In dichloromethane, this ruthenium centred process is followed by two other irreversible oxidative processes.

In acetonitrile (**Figure 2.6**), complex **1c** is characterized by a quasi-reversible ruthenium centred process at $E_{1/2}$ = 0.83 V and an irreversible redox process at E_{pc} = -1.69 V, which can be addressed to a bipyridyl-based process. The electrochemical response of **1c** in dichloromethane is coherent with the behaviour observed in acetonitrile, with a quasi-reversible redox process at $E_{1/2}$ = 0.855 V, found when the scan direction is reverted after the oxidation potential and attributed to the Ru^{II}/Ru^{III} redox couple.

Similarly, complexes **1a**, **1b** and **1d** presented a quasi-reversible process in acetonitrile at $E_{1/2}$ = 0.89 V, 0.905 V and 0.96 V, respectively, which can be attributed to the Ru^{II}/Ru^{III} redox process, in accordance with our earlier results in some ruthenium-cyclopentadienyl analogous.

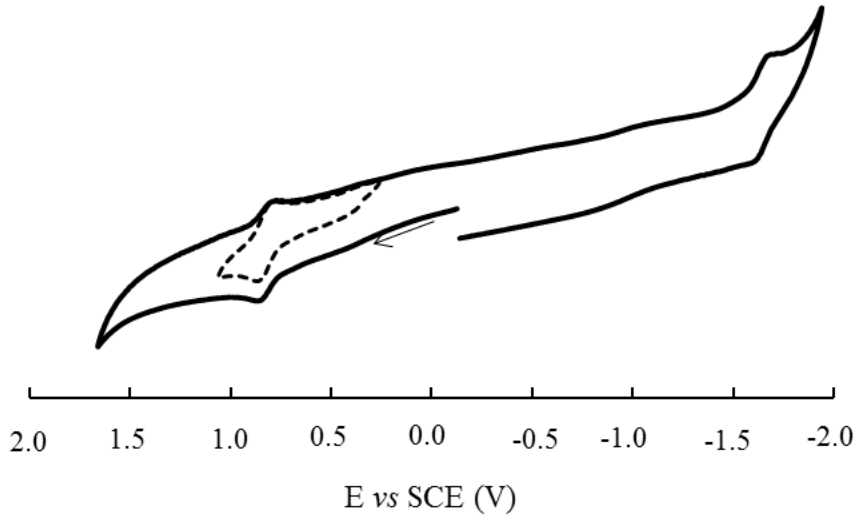

Figure 2.6 – Cyclic voltammogram of complex **1c** in acetonitrile, at 100 mVs^{-1}, showing the reversibility of the isolated oxidative process (dashed line).

Concerning the complex **1a**, the redox potential found for the Ru^{II}/Ru^{III} redox pair is lower than the one found for the related $[Ru(\eta^5\text{-}C_5H_5)(PPh_3)(Me_2bipy)][CF_3SO_3]$ complex ($E_{1/2}$ = 0.92 V in acetonitrile)[69] in the same experimental conditions, indicating that the introduction of the electron donor methyl group in the cyclopentadienyl ring influences the electronic capability of the ruthenium(II) centre, making the oxidation process easier.

Comparison of complexes **1a**, **1b** and **1c** showed that the presence of different substituents on the *para*-position of the bipyridine rings did not influence significantly the ruthenium centred processes.

2.2.2.6 Single crystal X-ray diffraction of complex 1a

Structural determination of complex **1a** (**Figure 2.7**) was performed and information about some of the interatomic distances of these complexes are presented in **Table 2.6**. Single orange crystals for **1a** were grown at room temperature by slow diffusion recrystallization from *n*-hexane in dichloromethane, under nitrogen atmosphere.

Efforts to get good single crystals of **1b** and **1c** were performed but were not successful due to insufficient crystal's sizes.

Complex **1a** crystallizes in triclinic system, space group $P\bar{1}$. Crystallographic data revealed that the basic structural motif of complex **1a** is the proposed three-legged piano stool structure, with the molecular architecture composed by the planar bipyridyl ligand and the triphenylphosphane co-ligand coordinated to the ruthenium-cyclopentadienyl unit, as **Figure 2.7** shows. **Table 2.6** summarizes some selected interatomic distances of complex **1a**.

As expected, upon coordination of the heteroaromatic ligand, the π-bonded cyclopentadienyl moiety keeps fully engaged to the metallic center**.** In addition, there is the fully coordinated planar and bidentate ligand (Ru-N1 2.092 Å, Ru-N2 2.092 Å) and the triphenylphosphane co-ligand (Ru-P 2.3062 Å).

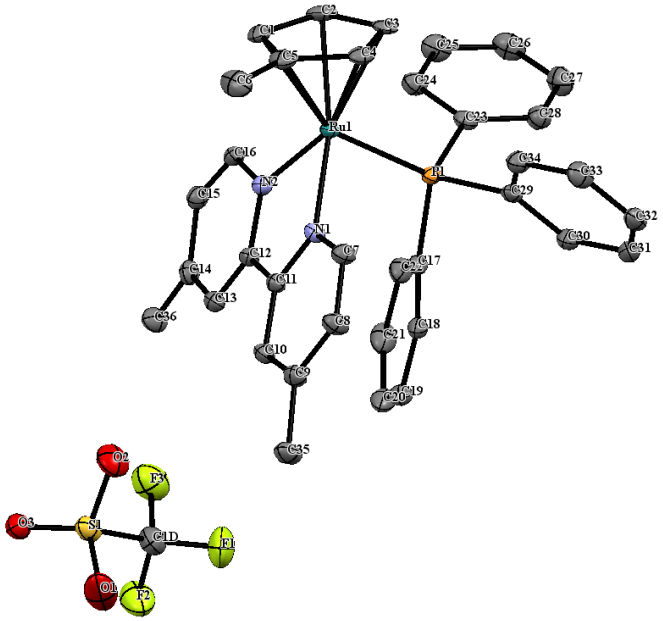

Figure 2.7 – Molecular structure of complex 1**a**. All the non-hydrogen atoms are presented by their 50 % probability ellipsoids. Hydrogen atoms are omitted for clarity.

Table 2.6 – Selected distances and angles from molecular structures of complex **1** and **1a**, obtained by single crystal X-ray diffraction analysis.

Distances (Å)	Complex 1a
Ru(1)-N(1)	2.092(2)
Ru(1)-N(2)	2.092(2)
Ru(1)-C(3)	2.170(3)
Ru(1)-C(2)	2.185(3)
Ru(1)-C(4)	2.194(3)
Ru(1)-C(1)	2.208(3)
Ru(1)-C(5)	2.224(3)
Ru(1)-P(1)	2.3062(7)
P(1)-C(29)	1.826(3)
P(1)-C(23)	1.830(3)
P(1)-C(17)	1.832(3)
N(1)-C(7)	1.354(3)
N(1)-C(11)	1.355(3)
C(1)-C(5)	1.414(4)
C(1)-C(2)	1.427(4)
S(1)-O(1)	1.429(2)
S(1)-O(2)	1.436(2)
S(1)-O(3)	1.443(2)
S(1)-C(1D)	1.834(4)
C(1D)- F(1)	1.332(4)
C(1D)-F(2)	1.322(4)
C(1D)-F(3)	1.342(4)

Angles (Degree)	Complex 1a
N(1)-Ru(1)-N(2)	76.23(9)
N(1)-Ru(1)-C(3)	140.34(10)
N(2)-Ru(1)-C(3)	143.43(10)
N(1)-Ru(1)-C(2)	162.66(10)
N(2)-Ru(1)-C(2)	107.68(10)
N(1)-Ru(1)-C(4)	106.41(10)
N(1)-Ru(1)-C(1)	125.54(10)
N(1)-Ru(1)-C(5)	100.00(10)
N(1)-Ru(1)-P(1)	88.63(6)
N(2)-Ru(1)-P(1)	89.98(6)
C(3)-Ru(1)-P(1)	90.91(8)
C(2)-Ru(1)-P(1)	108.04(8)
C(4)-Ru(1)-P(1)	110.72(8)
C(1)-Ru(1)-P(1)	145.83(8)
C(5)-Ru(1)-P(1)	148.56(8)
C(29)-P(1)-C(23)	104.76(13)
C(29)-P(1)-C(17)	101.20(12)
C(23)-P(1)-C(17)	101.87(13)
C(29)-P(1)-Ru(1)	116.85(9)
C(23)-P(1)-Ru(1)	115.52(9)
O(1)-S(1)-O(2)	115.45(17)
O(1)-S(1)-O(3)	115.25(15)
O(2)-S(1)-O(3)	115.04(14)

2.2.3 Stability and biological studies

2.2.3.1 Stability studies in aqueous media

Stability is a major key issue when assessing the biological activity of any metallodrug and it is often overlooked in biological assays. In this context, it is important to evaluate the stability of the complexes in aqueous media. All complexes presented in this chapter were tested for their aqueous stability over time using DMSO and culture cellular media DMEM by UV–Vis spectroscopy. DMSO was used to dissolve the compounds since they are not completely soluble in the DMEM media.

The UV-Vis absorption spectra of complexes **1**, **1a**, **1b**, **1c** and **1d** in cellular media exhibit one strong absorption band in the UV range and a broad medium absorption in the visible range, quite similarly to the correspondent behavior observed in the electronic absorption studies presented in section **2.2.2.3**. The samples used in the measurements were protected from light sources and were stored at room temperature between measurements. Only small variations (lower than 6% over the first 6 hours) were observed for all complexes with the bipyridyl derivatives, keeping the sample variation percentage until the last measurement at 24 h, supporting that the complexes are quite stable over the period tested (**Figure 2.8**). Complex **1** is the only complex that show a slight spectral change over the 24 h challenge. This fact could be addressed as a consequence of hydrolysis of the Ru-Cl bond,[70] common in this type of complexes.

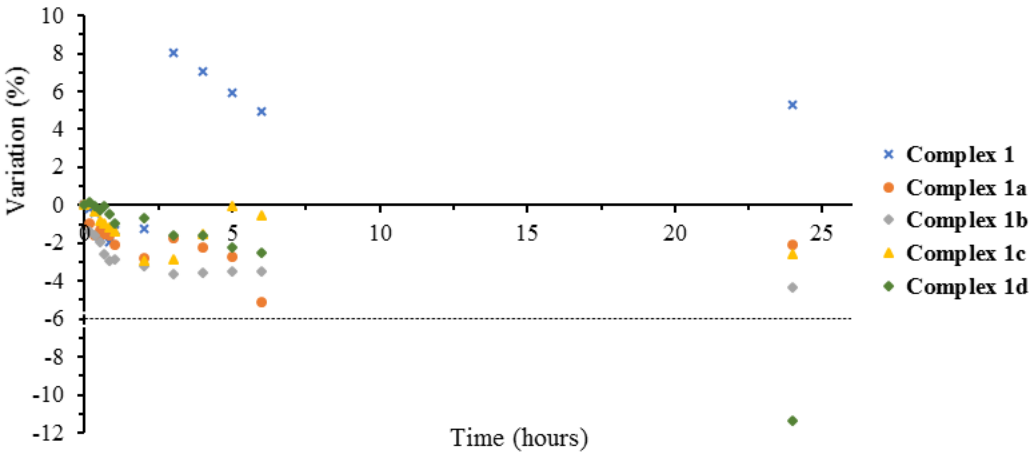

Figure 2.8 – Stability studies in cellular media DMEM and DMSO (98 % / 2 %).

Altogether, these results indicate that the compounds are stable when dissolved and the original solid-state three-legged piano stool molecular architecture, bearing the bipyridyl and the phosphane co-ligands, is kept as such in solution during this period.

2.2.3.2 *n*-Octanol/Water partition coefficient determination

The *n*-octanol/water partition coefficient, P_{ow}, is frequently a key feature in the development of new drugs since the hydrophobic/lipophilic character of the new compounds can affect their tissue permeability and their binding to biomolecules, for instance. Measured values of $\log P_{ow}$ for organic compounds have been found as low as -3 and as high as 7. Values of $\log P_{ow}$ can be considered to have some meaning in themselves since they represent the tendency of the compound to partition itself between and organic phase and an aqueous phase. Compounds with low $\log P_{ow}$ (e.g., less than -1) may be considered hydrophilic (they tend to have high water solubility) whereas compounds with high $\log P_{ow}$ values (e.g., greater than 4) may be considered hydrophobic (they have bigger tendency to solubilize in the organic phase).[71]

The rationale design of drugs tries to achieve an equilibrate model where the proposed synthesized drug is sufficiently lipophilic that is able to enter the lipid core of a cell membrane, but not so lipophilic that it is held in that core and does not move into the cell. In this frame, the assessment of the hydrophobic/lipophilic character of the compounds synthesized was determined using the shake-flask method, at room temperature, and it is of upmost importance as the compounds are expected to be used in medicinal purposes.

The *n*-octanol/water partition coefficient is a measure of how the new drug will partition in a solution of a polar (water) and a non-polar (*n*-octanol) solvent and is then determined by using the concentrations of the new drug in each phase, as shown by **Equation 2.1**:

$$log\ P_{ow} = log\ \frac{c_{ow}}{c_{wo}} \qquad \textbf{(2.1)}$$

where P_{ow} is the octanol-water partitioning coefficient, c_{ow} is the concentration of solute in the octanol phase, and c_{wo} is the concentration of solute in the water phase.

The *n*-octanol and the aqueous phases were mutually saturated before the experiments, using analytical grade octanol and double distilled water. The samples were dissolved in octanol (stock solution: ~1.0×10^{-4} M) and aliquots of the stock solution were equilibrated with water for 4 h in a mechanical shaker using a phase ratio of 2 mL *n*-octanol / 2 mL water. After separation of the equilibrated phases (by centrifugation at 5000 rpm for 10 min) the absorbance in the *n*-octanol phase was measured by UV-Vis spectrophotometry. Triplicate experiments have been performed for each complex. The concentration for each sample was determined using the calibration curve previously prepared (shown in **Figure 2.9**, for complex **1a)**. The values obtained for this series of compounds are summarized in **Table 2.7**.

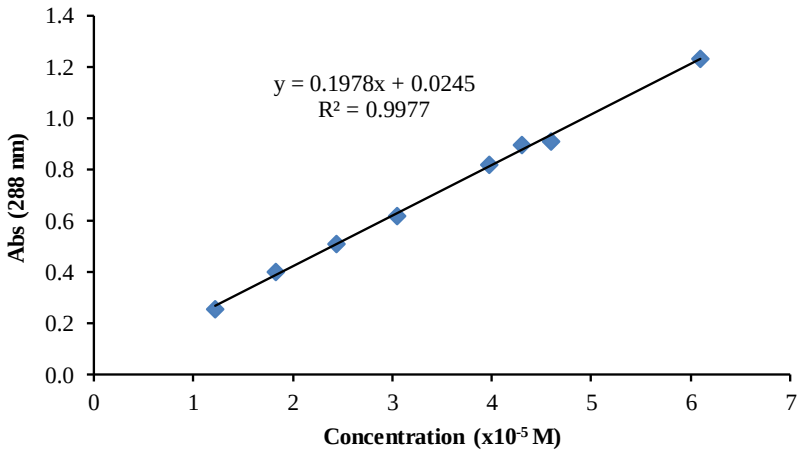

Figure 2.9 – Calibration curve obtained for complex **1a**.

Table 2.7 – Partition coefficients obtained by the shake flask method for complexes **1-1d**.

Compound	**logP_{ow}**
Complex **1**	*
Complex **1a**	1.85
Complex **1b**	1.06
Complex **1c**	0.25
Complex **1d**	0.64

*It was not possible to calculate an exact value for this compound.

Although an exact value could not be obtained for complex **1** (due to spectral changes), the set of experiments performed for this series of compounds has shown that they possess a more lipophilic character since all the compounds mostly remained in the organic fraction. This is an important property for a drug development once it can influence the passive transport across the cell membranes.

2.2.3.3 Cell viability assay

The cell viability assays were performed in collaboration with two Portuguese institutes on behalf of a collaboration with Dr. Fernanda Marques (Centre for Nuclear Sciences and Technologies, University of Lisboa) and Professor Ana Preto (Centre of Molecular and Environmental Biology, University of Minho).

The cytotoxicity of the ruthenium-cyclopentadienyl complexes **1-1d** was studied on three human cancer cell lines and one noncancerous cell line, using two different colorimetric methods (the MTT assay for the A2780 cancer cell line and the SRB assay for the SW480, RKO cancer cell lines and NCM460, a normal human colon mucosal epithelial cell line). Low IC_{50} values (the concentration needed to induce 50 % cell death) are indicative of cytotoxicity or antiproliferative activity at low drug concentrations.

Cells were incubated with each compound, in a concentration range of 1 μM to 200 μM, for a period of 24 hours (or 48 for the colorectal cell lines). After the incubation period, cells were assayed with one of the mentioned colorimetric methodology. **Table 2.8** summarizes the IC_{50} values obtained in the biological assays and can be compared with the IC_{50} value for metallodrug used as reference, cisplatin (CDDP).

Table 2.8 – *In vitro* cytotoxicity measured as half-inhibitory concentration (IC_{50}) for the **LMW 1**, **1a** and **1b** and **HML** complexes **1c** and **1d** on human A2780 human ovarian adenocarcinoma cell line and SW480, RKO and NCM460 colorectal cell lines. IC_{50} values are reported in μM (± SD) for a 24 h period of incubation.

	IC_{50} (μM) [a]			
Compound	**A2780[b]**	**SW480[c]**	**RKO[c]**	**NCM460[c]**
Complex **1**	15.60 ± 5.50	NT	NT	NT
Complex **1a**	1.67 ± 0.27	NT	NT	NT
Complex **1b**	2.26 ± 0.60	NT	NT	NT
Complex **1c**	NT	1.50 ± 0.30	2.00 ± 0.20	8.70 ± 0.90
Complex **1d**	2.53 ± 0.55	NT	NT	NT
CDDP	36.00	7.00	12.50	NT

[a] Measured after 24 h of incubation. [b] Cell line used for evaluation of the cytotoxicity effect of complexes **1a**, **1b** and **1d**. [c] Cell lines used for the cytotoxicity effect of complexes **1c**. **NT** means that for that cell line, the compound was not tested.

All compounds exhibited high cytotoxicity against the tested cell lines. The dose-response profiles of cell-viability obtained for complexes **1-1b** and **1d** are also shown in Annex. Neither the free ligands (Me_2bipy, bipy$(CH_2OH)_2$, or bipy$(CH_2OPLA)_2$) shown cytotoxicity against the tested cell lines, within the concentration range used. The best IC_{50} value obtained in the A2780 cancer cell line was observed for complex **1a** (1.67 ± 0.27 μM at 24 hours), which possess approximately 22-fold higher cytotoxicity than the commercially available metallodrug cisplatin.

Altogether, the compounds of this series showed to be potential cytotoxic agents as they show a high cytotoxic profile in the human cancer cell line tested with IC_{50} values much lower than cisplatin, under the same experimental conditions. When (indirectly) compared to previous compounds synthesized in our group, namely the compounds with general formula $[Ru(\eta^5\text{-}C_5H_5)(4,4'\text{-}R_2\text{-}2,2'\text{-bipy})(PPh_3)]^+$, with R = CH_3 (IC_{50} A2780 (72 h) = 0.1 μM), R = CH_2OH (pmc79, IC_{50} A2780 (72 h) = 3.9 μM), or R = CH_2OPLA (RuPMC, IC_{50} A2780 (72 h) = 3.4 μM), we can state that the new analogues with the methyl group in the Cp ring (**1a**, **1b** and **1c** respectively) have, apparently, enhanced activity for shorter periods

of incubation since smaller IC_{50} values are obtained (for complex **1b** and **1d** *vs.* pmc79 and RuPMC, respectively). The polymeric compound **1d** showed to be as much more cytotoxicity than cisplatin and due to the high molecular of the first, it is expected that the secondary effects observed in cisplatin might be reduced.

2.3 Conclusions

This chapter dealt with the synthesis, characterization and preliminary cytotoxic evaluation of new Ru^{II}-η^5-methylcyclopentadienyl complexes containing 2,2'-bipyridine derivatives as ligands. Four new complexes of general formula $[Ru(\eta^5\text{-MeCp})(PPh_3)(4,4'\text{-}R_2\text{-}2,2'\text{-bipy})]^+$, with R = $-CH_3$ (**1a**), R = $-CH_2OH$ (**1b**), R = $-O(CH_2)_3C_8F_{17}$ (**1c**) and R = $-CH_2OPLA$ (**1d**), have been isolated as triflate salts from their neutral parental complex, $[Ru(\eta^5\text{-MeCp})(PPh_3)_2Cl]$, in good yields. They were fully characterized by spectroscopic, electrochemical and analytical techniques. The screening of their anticancer properties was also assessed by preliminary *in vitro* studies.

A structural image was also obtained for complex **1a** since appropriate crystals for single crystal X-ray diffraction were obtained. The molecular structure of compound **1a** is the expected three-legged piano stool geometry.

The overall NMR data collected from the ^1H and ^{13}C measurements confirms the σ dative contribution of the derivatized bipyridine (and the phosphane) and the effect of the electron donor methyl group on the cyclopentadienyl ring, which revealed to be coherent with the previous results obtained for "RuCp" analogues. The presence of a single sharp resonance in the ^{31}P NMR spectra belonging to the phosphane co-ligand was located at the typical chemical shift range of the coordinated ligand (~ 50 ppm).

The coordination of the bipyridyl derivatives was also confirmed by UV-vis spectroscopic data. The electronic spectra of all compounds presented, along with the transitions observed for the coordinated ligands ($\pi \rightarrow \pi^*$), the transitions observed in the $\{[Ru(\eta^5\text{-MeCp})(PPh_3)]^+\}$ organometallic fragment, a new transition located in the 420-450 nm range, with medium-strength intensity and broad character region could be addressed to charge transfer transitions.

The electrochemical behavior of the compounds **1**-**1d** was studied by cyclic voltammetry in acetonitrile and dichloromethane. All compounds showed to be electroactive and their behavior was mainly characterized by one quasi-reversible oxidation process at positive potentials ascribe to the ruthenium metal followed by other two irreversible reductive processes at negative potentials, which were addressed to the to the bipyridyl ligands.

The preliminary biological assays performed to infer about the cytotoxic potential of this series of compounds were determined *in vitro* and were extremely promising. The panel of cells where the compounds were screened was carefully selected taking in account the aggressiveness and the incidence of these type of cancers (ovarian adenocarcinoma, A2780, and colon carcinoma RKO and SW480). Exceptional cytotoxicity against A2780 cell line must be reported for the LMW complex **1a** that showed to be, at 24 hours challenge, two-fold more cytotoxic than cisplatin. Special attention goes also to complex **1c,** since it shows selectivity onto cancer cells lines rather than healthy cells. The remaining results were in the range of the IC_{50} found for cisplatin at the same experimental conditions. The great overall results of this first screen are encouraging since the IC_{50} values were similar for a shorter time of incubation (24 hours incubation *vs* 72 hours) for our previous "Ru-Cp" analogues.[27] Moreover, the high molecular weight compounds **1c** and **1d**, besides their high cytotoxicity, might show a better accumulation in tumours and thus, should be further explored.

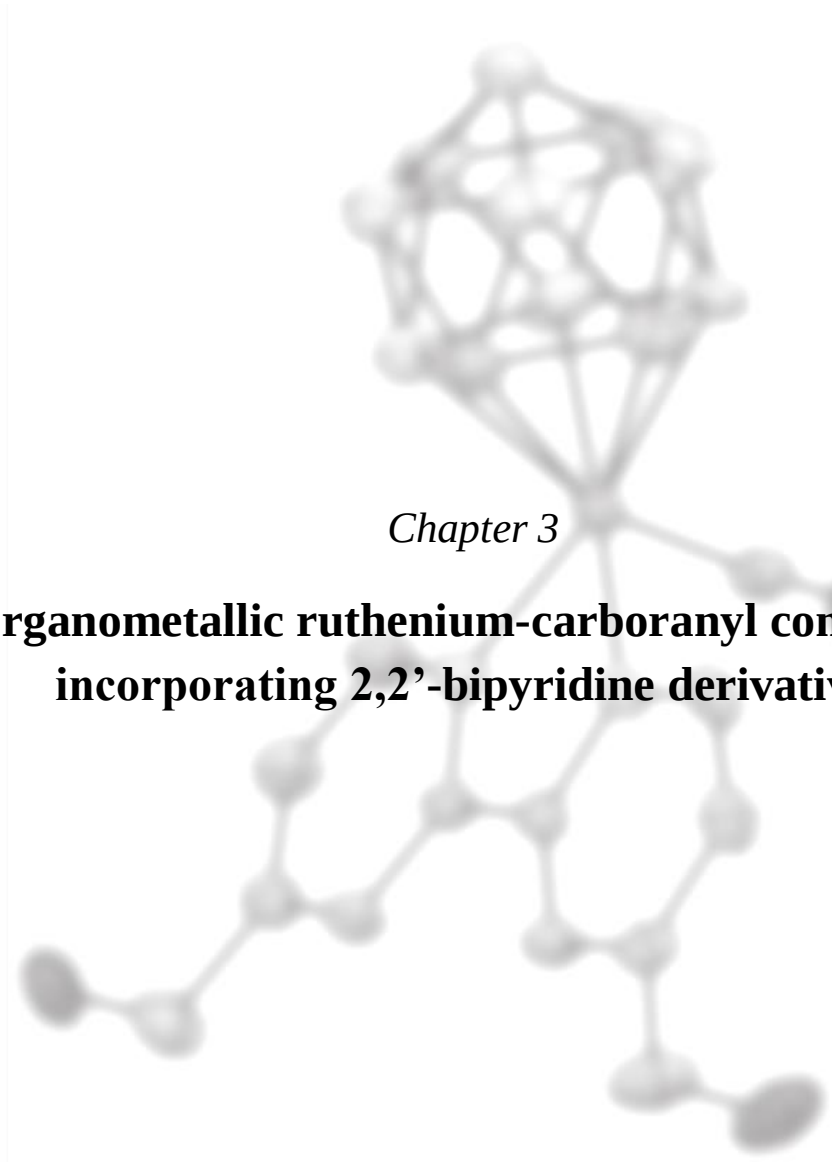

Chapter 3

Organometallic ruthenium-carboranyl complexes incorporating 2,2'-bipyridine derivatives

Organometallic ruthenium-carboranyl complexes incorporating 2,2'-bipyridyl derivatives

3.1 Introduction

As previously reported in **Chapter 2**, the strategy to overcome some limitations presented by the platinum drugs is to the development new complexes that might present alternative modes of action. An alternative way to overcome these issues can pass by the conjugation of our ruthenium-bipyridyl based core to the *nido*-carborane structural motif. This can be a good exploratory field because, as fair as we know, this type of complexes has never been applied in cancer therapy, neither as possible chemotherapeutics neither as high boron containing molecules for BNCT.

In this frame, a collaboration between our research group with a highly specialized group, as Professor's Clara Viñas i Teixidor at *Institut de Ciència de Materials de Barcelona*, in boron based chemistry allow the design of a new family of compounds that might possess adequate characteristics to be applied as alternative chemotherapeutics and/or agents for the BNCT.

We proposed to maintain the same pseudo octahedral (piano-stool) geometry, where the carboranyl ($[C_2B_9H_{11}]^{2-}$) occupies three coordination positions (similarly to the Cp moiety) and the other three coordination positions are completed by the correspondent bidentate bipyridyl derivative and a carbonyl as co-ligand. The [*nido*-$C_2B_9H_{12}]^-$ carboranyl ligand is already well characterized and was a kind offer from Professor's Clara Viñas research group. This motif was used to substitute the Cp ring in the previous presented complexes at **Chapter 2** keeping up with the ruthenium-bipyridyl derivative fragment. The rationale choice of the carbonyl instead of the triphenylphosphane co-ligand was based in our previous results. To be applied in BNCT, the compounds should not be active until activated by radiation. In this frame, CO was chosen over PPh_3 since within our family of $[Ru(\eta^5\text{-Cp})(bipy)(L)]^+$ compounds we have observed that when L was PPh_3, highly cytotoxic compounds were obtained; when L was CO, only moderate activity was achieved.[27]

3.2 Results and discussion

The presence of relatively electronegative carbon atoms in 1,2-*closo*-$C_2B_{10}H_{12}$ induces a slight positive charge on the boron atoms adjacent to both carbon atoms within the cluster which makes them open to nucleophilic attack. The addition of a strong base such as KOH/MeOH affords decapitation at the B3/B6 position (**Figure 3.1**) since these are the most electron deficient boron atoms in the carborane cage.

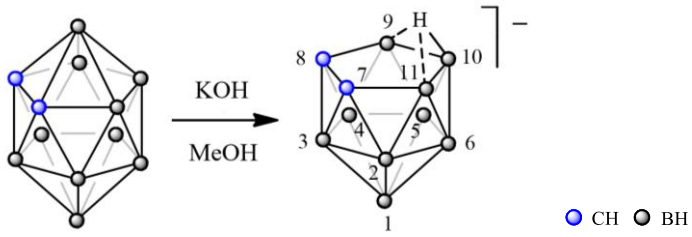

Figure 3.1 – Decapitation at B3/B6 position.

The degradation of the icosahedral ortho-carborane, 1,2-*closo*-$C_2B_{10}H_{12}$, by KOH in MeOH was first reported by Hawthorne and co-workers in 1964.[72] The decapitation produced, on work up, a 11-vertex *nido* carborane anion, [7,8-*nido*-$C_2B_9H_{12}]^-$ which contains an *endo* proton associated with the open face of the *nido* cage. The *endo* proton is relatively acidic compared to the other protons so we can easily remove it by adding *n*-butyllithium to produce the dicarbollide anion $[C_2B_9H_{11}]^{2-}$, which can be used as starting material for the synthesis of a wide range of 12-vertex metallacarboranes. Reaction with {M-L} fragments can recapitate the icosahedral geometry (**Figure 3.2**).[73]

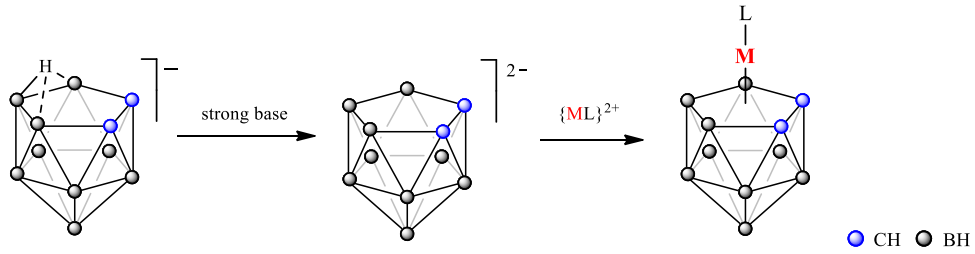

Figure 3.2 – Recapitation of the icosahedral geometry by insertion of a metal atom.

The literature based in the ruthenacarborane incorporating bipyridine ligands is not very vast. One good example of development of compounds of this type is the work developed by Jelliss *et al.*[74] In their work, Jelliss and co-workers demonstrated that the ruthenacarborane complex [3,3,3-$(CO)_3$-*closo*-3,1,2-$RuC_2B_9H_{11}$] previously presented by Hawthorne[75] can be a good starting material for the synthesis of the ruthenium-carboranyl complexes incorporating bipyridyl derivatives. However, the overall yields to obtain these compounds are very low. In this sense, and once the compounds are intended to be used in biomedical applications, a synthetic route with increased yield is of upmost importance. One of the main goals of this thesis was also improve the yield of this type of reaction and our strategies efforts are presented in the next segment.

3.2.1 Synthesis of the ruthenacarboranes complexes

A series of ruthenium-carboranyl complexes bearing bipyridyl derivatives as chelating agents was prepared and characterized for the first time. These three new neutral compounds (complexes **2a**, **2b** and **2c**) with general formula [3-CO-3,3-{k^2-4,4'-R_2-2,2'-bipy}-*closo*-3,1,2-$RuC_2B_9H_{11}$] were obtained by treatment of the parental complex [3,3,3-$(CO)_3$-*closo*-3,1,2-$RuC_2B_9H_{11}$] (complex **2**) with Me_3NO and the corresponding bipyridyl ligand (**2a**, R = $-CH_3$; **2b**, R = $-CH_2OH$; **2c**, R = $-CH_2OPLA$), as shown in **Scheme 3.1**. The synthetic method developed by Jelliss *et al.* was followed to prepare all complexes

and seemed to be the most appropriate way to get them although other synthetic routes were tried, as it will be described in section **3.2.1.1**.

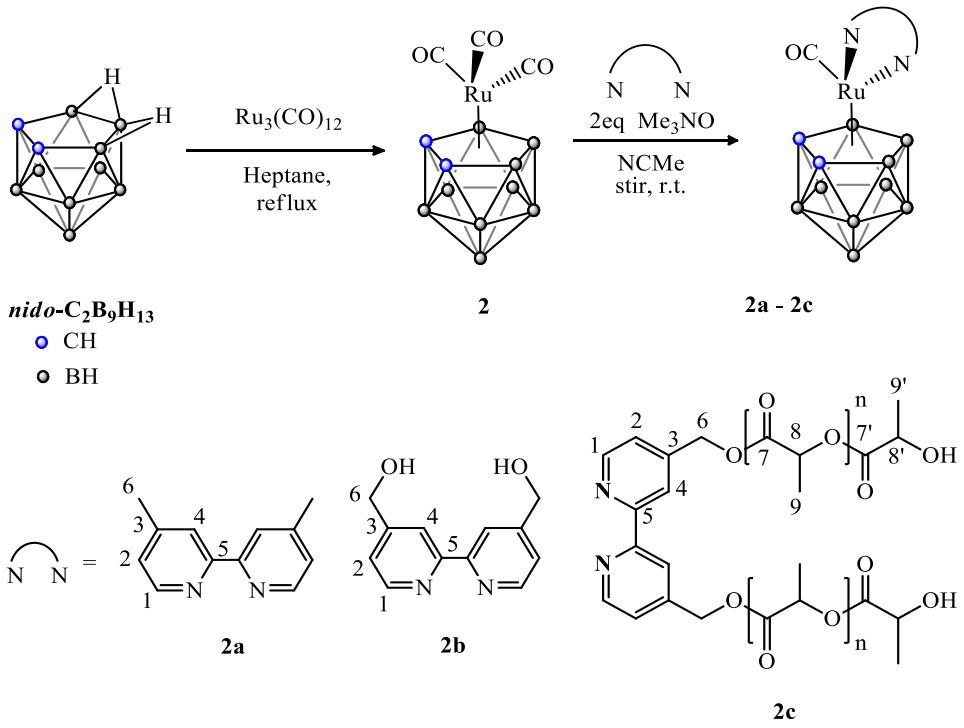

Scheme 3.1 – General reaction scheme for the synthesis of the ruthenacarborane family of compounds (**2a - 2c)**. Ligands are numbered for NMR spectral assignments. o and o represent CH and BH, respectively.

Mononuclear *closo*-ruthenacarborane complexes **2a, 2b** and **2c** were prepared by double carbonyl substitution of the starting tricarbonyl complex [3,3,3-$(CO)_3$-*closo*-3,1,2-$RuC_2B_9H_{11}$] (complex **2**) with 2 mol equivalent of the reagent Me_3NO, in the presence of a slight excess (1:1.1) of the respective 2,2'-bipyiridyl ligand (with exception for the **HMW** complex **2c**, where an excess of 1.1:1 of complex **2** was used). The bipyridyl derivatives chosen for the synthesis of the presented ruthenacarborane complexes comprise a methyl group (**2a**), a hydroxymethyl group (**2b**) or a polymeric chain obtained by ring opening polymerization reaction of the D,L-lactide (**2c**), in the *para* position of the aromatic ring, relatively to the nitrogen atoms of the *N*,*N*'-chelate.

Complexes were firstly purified by column chromatography on silica gel using as eluent a mixture of dichloromethane and hexane, and after that recrystallized by slow diffusion of *n*-hexane in acetone (**2a**) or tetrahydrofuran (**2b**) solutions, affording orange to yellow solids in 24 % (**2a**) and 15 % (**2b**). Successful attempts of single crystal growing allowed the structural determination for both compounds by X-ray diffraction analysis. Purification of complex **2c** followed a different approach. Since complex **2c** is a **HMW** compound, two forced precipitations with *n*-hexane in a dichloromethane solution, and two washes with diethyl ether were the steps followed to isolate the compound in 33 % yield.

This series of compounds was found to be fairly stable towards oxidation in air and moisture, both in the solid state and in solution, and was fully characterized by spectroscopic, analytical and electrochemical techniques.

3.2.1.1 Attempts to increase the overall yield of the ruthenacarborane compounds

The successful isolation of the complexes **2a**, **2b** and **2c** culminate from a series of several synthetic sequences. Many approaches were tested and, for one reason or another, they did not lead us to the expected results. **Scheme 3.2** present all attempts tried to increase the yield that did not led to the isolation of the intended complexes. Along with it, a brief explanation accompanies the strategy followed and the main reasons why the strategy was put aside.

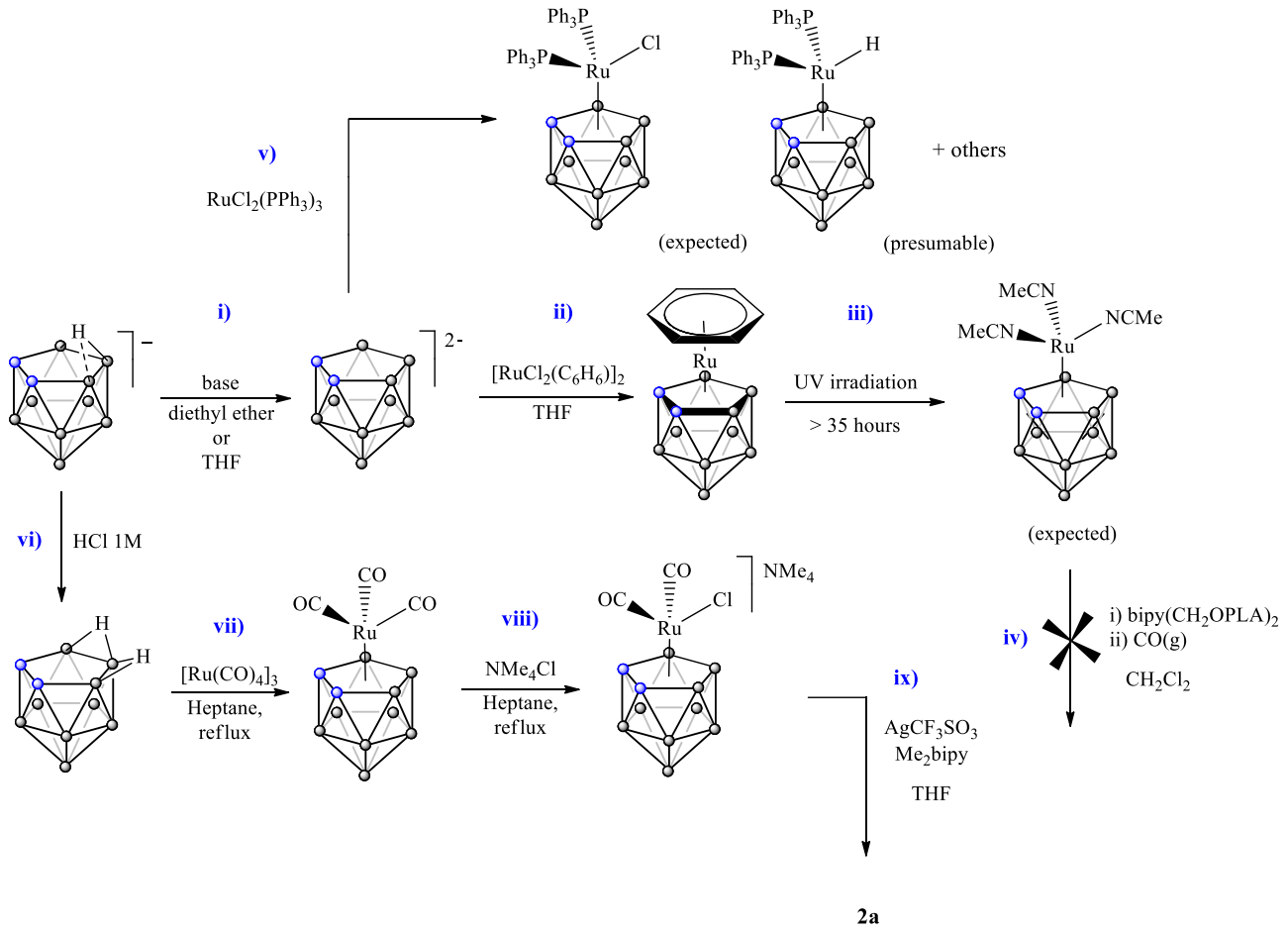

Scheme 3.2 – Attempted synthetic routes: i) deprotonation of the [*nido*-$C_2B_9H_{12}]^-$; ii) metalation of the [*nido*-$C_2B_9H_{11}]^{2-}$ dianion with the dimeric complex of ruthenium $[RuCl_2(C_6H_6)]_2$; iii) UV irradiation of the complex $[Ru(\eta^6\text{-}C_6H_6)(\eta^5\text{-}C_2B_9H_{11})]$; iv) attempt to coordinate the polymeric macroligand; v) attempt to coordinate the [*nido*-$C_2B_9H_{11}]^{2-}$ dianion to the inorganic complex of ruthenium $RuCl_2(PPh_3)_3$; vi) protonation of the [*nido*-$C_2B_9H_{12}]^-$ anionic ligand; vii) metalation of the neutral [*nido*-$C_2B_9H_{13}$] carboranyl ligand with the trimer $[Ru(CO)_4)_3]$ reagent; viii) introduction of a chlorine atom in neutral complex [3,3,3-$(CO)_3$-closo-3,1,2-$RuC_2B_9H_{11}$] to obtain the correspondent anionic complex ; ix) coordination reaction of the low molecular weight ligand Me_2bipy. CH BH

Figure 3.3 summarizes all the carboranyl forms used in the coordination to the different ruthenium reagents. They differ in charge (they turn from neutral to anionic or dianionic, from left to right, respectively) and have different characteristics that, in some way or another, can facilitate the coordination to the metal. The *nido*-$C_2B_9H_{13}$ has two bridged protons at the open face C_2B_3 whereas the [*nido*-$C_2B_9H_{12}]^-$ has only one, exemplifying the 3centre-2electrons type of bond. In its turn, the *nido*-$[C_2B_9H_{11}]^{2-}$ dianion has none hydrogen atoms. Elimination of the bridged proton can be achieved by the use of a strong base like *n*-BuLi or K[*t*-BuO] (step **i**) in **Scheme 3.1**).

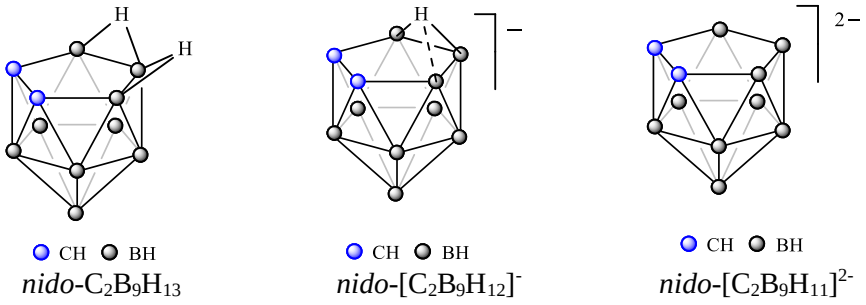

Figure 3.3 – Schematic representation of the three forms of the carboranyl used in work developed in this thesis (protonated at left, anionic at center an dianionic at right).

The first synthetic route used to get the ruthenacarborane complexes was the one published by Jelliss.[74] However, the yields obtained using this route are quite low (*ca*. 24% for the coordination of the no substituted bipyridine). Thus, we have decided to try other approaches based on our experience with other ruthenium-cyclopentadienyl precursors.

In our first approach we decided to mimic the synthesis of $[Ru(\eta^5\text{-}C_5H_5)(NCCH_3)_3]^+$ complex, using the *nido*-$[C_2B_9H_{11}]^{2-}$ instead of the η^5-$[C_5H_5]^-$. In this attempt, the synthesis of an intermediate compound $[Ru(\eta^6\text{-}C_6H_6)(\eta^5\text{-}C_2B_9H_{11})]$ was necessary and was achieved with success. The irradiation step (step **iii**) in **Scheme 3.1**) was performed twice, varying the concentration and the intensity of the lamp, for long periods (~35 hours). The total displacement of the arene ring was never achieved, however a new small peak increased with longer times of irradiation, making us believe that the expected [3,3,3-$(NCCH_3)_3$-*closo*-3,1,2-$RuC_2B_9H_{11}$)] neutral complex was formed, although in very low percentage (in annex). The results of the attempts to change the labile acetonitrile ligands in the presumable product with the bipyridyl macromolecular derivative (step **iv**) in **Scheme 3.1**) were not the expected. This approach proved to be very expensive since, when irradiated in the photochemical reactor, approximately 2 liters of acetonitrile are needed. Besides that, it seems that this type of replacement does not occur easily which make us conclude that the fragment Ru-arene-carboranyl is extremely stable. Possibly, other paths to irradiate the solution could be more effective.

The second approach (step **v**) in **Scheme 3.1**) was based in previously developed work in the catalysis field. Coordination of the dianionic [*nido*-$C_2B_9H_{11}]^{2-}$ to the ruthenium fragment $Ru(PPh_3)_3Cl_2$, occurred very fast and unfortunately the expected structure (see **Scheme 3.1**) was not isolated. A signal upfield appeared at the ^{1}H NMR showing that probably the chloride has been substituted by a hydride (as previously reported in the literature for rhodium complexes). Moreover, the complexity of the ^{1}H NMR and the ^{31}P NMR spectra gave us the information that multiple species could be present in solution. Due

to the difficult purification of the mixture obtained and the additional undesirable triphenylphosphane co-ligand presence in the structure, we moved away from this route also.

Formation of *nido*-$C_2B_9H_{13}$ and its complexation with the ruthenium reagent $[Ru(CO)_3]_4$ (steps **vi**) and **vii**) in **Scheme 3.1**) lead to the formation of (until the moment) the most adequate starting material, complex **1**. All previous attempts were not successful probably because of the nonappearance of the two protons at the open face of the carboranyl ligand or to the no adequate oxidation state of the ruthenium reagent. By this, we assume that the presence of the two protons at the coordination C_2B_3 face of the carboranyl ligand will allow the oxidation of the ruthenium center into Ru(II), as it happens in step **vii**) in **Scheme 3.1**.

The modification of the complex **1** into the correspondent anionic one (step **viii**) in **Scheme 3.1**) was achieved by reaction with a tetramethylammonium chloride salt, which allow the introduction of a chloride in the ruthenium coordination sphere. The successful coordination of the bipyridyl into this organometallic fragment (step **ix**) in **Scheme 3.1**) was successful, however the yield was also very low. This fact makes us conclude that the introduction of another step in the synthetic pathway to get the ruthenacarborane complex is not worthy since the double replacement of the carbonyl in complex **1** is simpler and does not lead (in so extended way) to other potential secondary products.

With no significant improvements obtained in the synthesis optimization process of the starting material we believed that, by the moment, the most adequate starting complex to proceed with the complexation synthesis is the [3,3,3-$(CO)_3$-*closo*-3,1,2-$RuC_2B_9H_{11}$] complex.

3.2.2 Characterization of the ruthenacarborane complexes

3.2.2.1 NMR spectroscopy

The full ^{1}H NMR and ^{11}B NMR spectral data for all complexes are given in **Table 3.1**. All resonances found were attributed using 1D and 2D NMR experiments (^{1}H, ^{13}C, COSY, HMQC and HMBC) and follows the atom labelling presented in **Scheme 3.1**.

Table 3.1 – Selected ^{1}H-NMR and ^{11}B-NMR data for the ligands and the complexes **2-2b**.

	^{1}H NMR δ / ppm [a]					**^{11}B NMR** δ / ppm [b]
Compound	**Cage CH**	**H_1**	**H_2**	**H_4**	**H_6**	
Me_2bipy	-	8.51	7.22	8.30	2.43	-
$(CH_2OH)_2$bipy [¥]	-	8.60	7.39	8.50	4.79	-
Complex 2	4.15	-	-	-	-	8.6 (1B), -4.2 (3B), -7.6 (2B), -16.7 (3B)
Complex 2a	3.26 (-0.89)	9.00 (0.49)	7.56 (0.34)	8.56 (0.26)	2.62 (0.19)	-0.9 (1B), -6.5 (3B), -8.2 (2B), -20.9 (3B)
Complex 2b[¥]	3.30 (-0.85)	9.09 (0.49)	7.70 (0.31)	8.64 (0.14)	4.96 (0.17)	-2.1 (1B), -7.8 (3B), -9.6 (2B), -22.3 (3B)

[a] In parenthesis the difference between the coordinated and free ligand resonances (δ_{coord} - δ_{free}).[b] ^{11}B{^{1}H} NMR data, performed at room temperature; in parenthesis the integration of each resonance. [¥] OH resonance for **$(CH_2OH)_2$bipy** is observed at 4.59 ppm, whereas for complex **2b** is observed at 5.05 ppm (0.46).

The two **LMW** ruthenacarborane complexes displayed resonances in their ^{1}H NMR spectra that were easily ascribed to the two CH cage protons due to their broad character. These signals appeared at δ 3.26

(**2a**) and δ 3.30 ppm (**2b**) and revealed, for both cases, an integration ratio of 1:1 between the carboranyl ligand and the respective 2,2'-bipyridyl derivative which is appropriate and coherent with the proposed structure for these two complexes. In both complexes, the bipyridyl aromatic protons resonate at higher chemical shift values when compared to the corresponding resonances of the free ligand (for complex **2b,** $\Delta H_1 \approx +0.49$ ppm, $\Delta H_2 \approx +0.34$ ppm and $\Delta H_4 \approx +0.31$ ppm, as **Figure 3.4** suggests) which agrees with a σ dative coordination to the ruthenium center. The protons of the substituent groups located at the *para* positions (relatively to the nitrogen) of the aromatic ring, also deshield upon coordination to the metal ($\Delta \approx +0.19$ ppm for the methyl group in **2a** and $\Delta \approx +0.17$ ppm for the geminal protons of the hydroxymethyl group in **2b**). Additionally, a resonance at δ 2.62 ppm appears in the ^{1}H NMR of complex **2a** and it is readily attributed to the equivalent protons of the methyl groups of the Me_2bipy, while the resonances for the two geminal protons of the hydroxymethyl groups of the 2,2'-bipyridyl ligand of complex **2b** resonate at δ 4.95 ppm, as a doublet. This general effect has already been observed for related compounds, where the bipyridyl is also substituted at the *para*-position (relatively to nitrogen). The results obtained are coherent with a σ-type of coordination for the bipyridyl ligand.

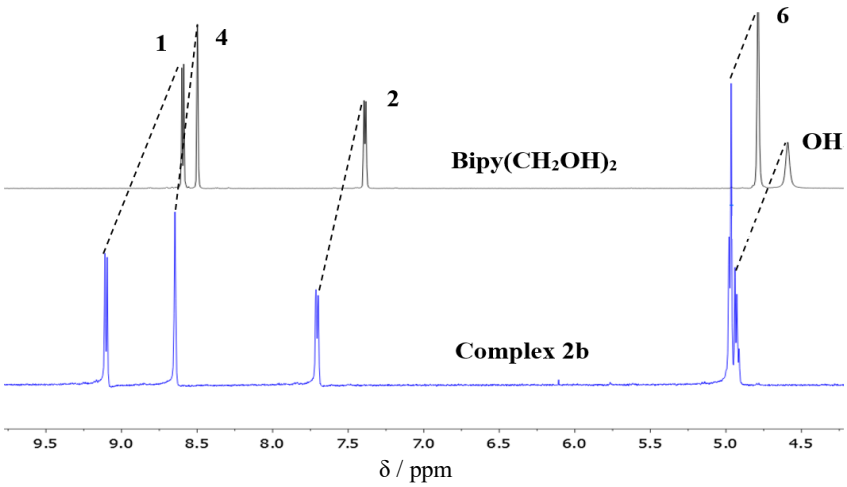

Figure 3.4 – Comparison between the ^{1}H NMR spectra of complex **2b** and its correspondent bipyridyl-based macroligand, in deuterated acetone. In the picture, only the aromatic resonances are presented.

Figure 3.5 appears as complementary information to the data presented at **Table 3.1**, as far as boron NMR spectroscopy is concerned. As we can see at the left of the figure, complex **2a** displayed at its $^{11}B\{^1H\}$ NMR spectrum, four peaks with an integration intensity ratio 1:3:2:3, being the second and fourth signals result of overlap of broad unresolved 1:2 resonances. The appearance of the aforementioned resonances agrees with the typical chemical shift range for the *closo*-3,1,2-$MC_2B_9H_{11}$ system (M = Rh, Ru) (-0.9 ppm < δ < -22.3 ppm).[76-79] In addition, the boron-proton coupling constants, $^1J_{HB}$, higher than 100 Hz were found in the ^{11}B NMR spectrum giving us a clear indication that all B-H protons of the $C_2B_9H_{11}$ cage remain intact. The same pattern was observed for the analogue **2b** and is in accordance with the expected structures for this type of complexes.

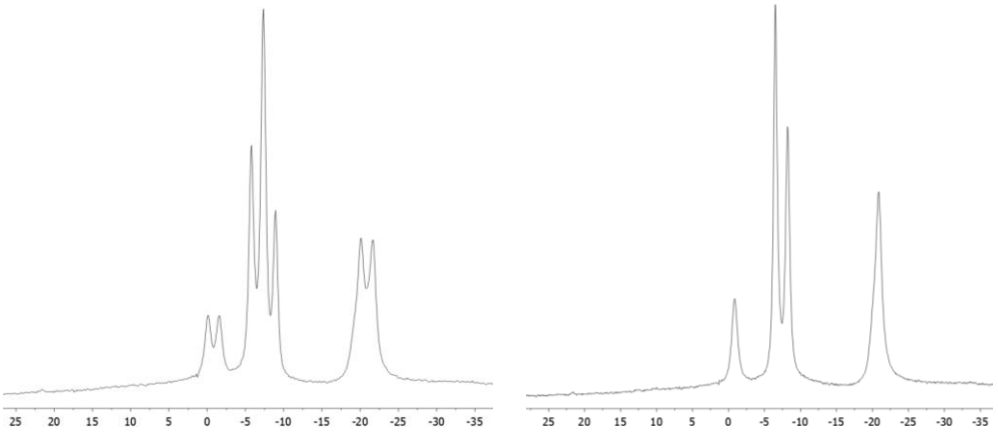

Figure 3.5 – ^{11}B NMR (left) and ^{11}B{^{1}H} NMR (right) spectra of complex **2a**, in deuterated acetone.

To complete the characterization of these complexes by NMR spectroscopy, ^{13}C-APT NMR experiments were ran and the results are in accordance with the previous discussed effects in the ^{1}H NMR analysis. All the detailed spectroscopic data concerning the ^{13}C{^{1}H} NMR experiments are in the experimental section (**Chapter 5**). In the ^{13}C{^{1}H} NMR spectra of complexes **2a** and **2b**, a broad singlet resonance appears at approximately 45 ppm and by their position and shape, were easily attributed to the two equivalent carbons present at the carboranyl structure. The resonances for the carbonyl co-ligand appear also in the spectra with the remaining carbons of the bipyridyl ligand (δ 198 ppm).

The general shielding effect observed for the cage and the carbonyl nuclei resonances combined with the confirmed deshielding of the bipyridyl protons, gives once again, a clear evidence of electron flow from the bipyridyl through the ruthenium center towards the boron cage and the carbonyl co-ligand. It is also very clear that the presence of a more donating groups at the bipyridine substituent improves the electronic flow to the carboranyl moiety.

Table 3.2 – Selected ^{13}C{^{1}H} -NMR data for complexes **2** – **2b**, in deuterated acetone.

	^{13}C{^{1}H} NMR δ / ppm [a]							
Compound	**Cage CH**	**CO**	**C_1**	**C_2**	**C_3**	**C_4**	**C_5**	**C_6**
Complex 2	47.9	201.9	-	-	-	-	-	-
Complex 2a	44.9	198.7	155.5	128.4	151.8	124.9	156.2	21.2
Complex 2b	44.9	198.5	155.7	124.6	156.1	121.0	156.2	62.7

Complex **2c** structure is very similar to complex **2b**, being the only difference the introduction of two polymeric chains obtained by ROP of the D,L-lactide.

Although the introduction of the polymeric macroligand into the ruthenacarborane complex promotes lower resolution in the ^{1}H NMR essentially, there are clear evidences that it is coordinated to the ruthenium center, as it will be seen furthermore. **Table 3.3** shows the overall resonances attributions for all protons in complex **2c** and compare them with the free ligand and the correspondent precursor.

Table 3.3 – ^{1}H NMR data for the **HMW** ligand and complexes **2** and **2c**, in deuterated acetone.

Compound	^{1}H NMR δ / ppm [a]						
	Cage CH	**H_1**	**H_2**	**H_4**	**H_6**	**H_a / $H_{a'}$**	**H_b / $H_{b'}$**
$(CH_2OPLA)_2$bipy	-	8.71	7.45	8.49	5.39	5.21 / 4.30	1.55 / 1.39
Complex 2	4.15	-	-	-	-	-	-
Complex 2c	3.35 (-0.80)	9.20 (0.49)	7.76 (0.31)	8.68 (0.19)	5.54 (0.15)	5.21 / 4.30 (0.0 / 0.0)	1.55 / 1.39 (0.0 / 0.0)

[a] In parenthesis the difference between the coordinated and free ligand resonances (δ_{coord} - δ_{free}). [¥] OH resonance for **$(CH_2OH)_2$bipy** is observed at 4.59 ppm.

As previously observed for the **LMW** analogues, upon coordination of the macroligand, it can be observed an upfield shift of the CH cage resonance (to 3.35 ppm, $\Delta \approx$ -0.80 ppm) and a shift to lower field of the aromatic hydrogen atoms of the bipyridyl ring ($\Delta H_1 \approx$ +0.49 ppm, $\Delta H_2 \approx$ +0.31 ppm and $\Delta H_4 \approx$ +0.19 ppm, as **Figure 3.6** suggests). The resonances of the polymeric chains (CH and CH_3 groups) macroligand does not change after reaction with the parental complex **2**, giving us the confirmation that, as expected, this fragment remains intact in the methodology used.

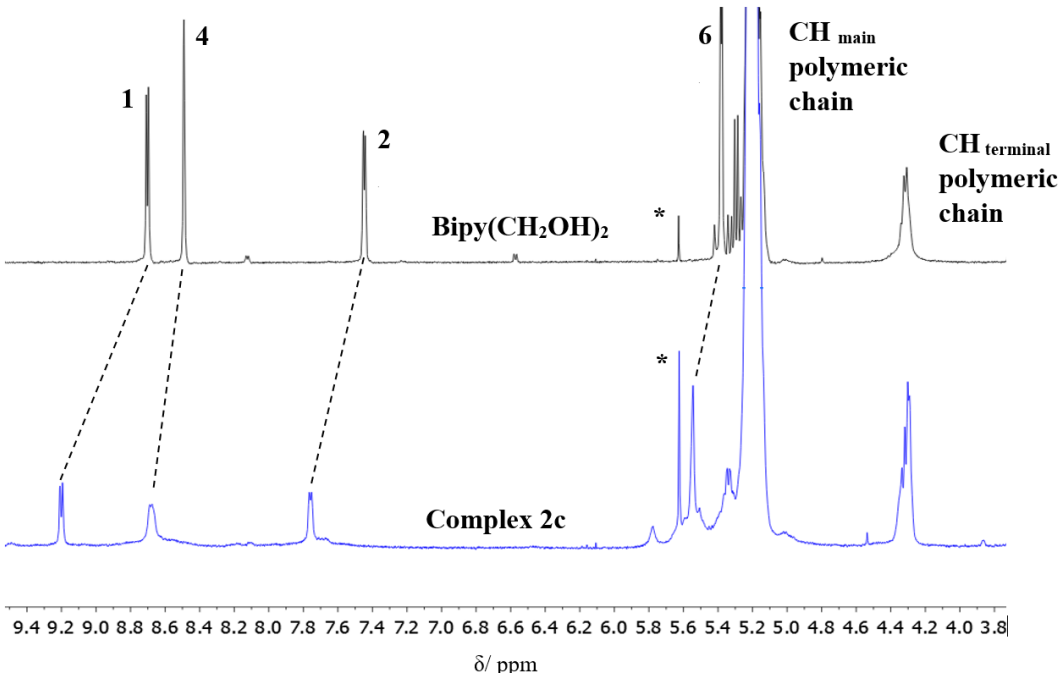

Figure 3.6 – Comparison between the ^{1}H NMR spectra of complex **2c** and its correspondent bipyridyl-based macroligand, in deuterated acetone. In the picture, only the aromatic resonances are presented. * Dichloromethane residual peak.

Like for its **LMW** analogues, the ^{11}B NMR studies revealed a similar pattern, although not so well resolved. The proton decoupled boron NMR experiment, ^{11}B{^{1}H} NMR, shown four peaks that appear in the regular chemical shift range of this type of complexes. The four peaks show an integration ratio of 1:2:3:3 (with also two signals resulting from unresolved resonances) and are in agreement with the previous results obtained. J_{BH} coupling constants were also calculated, analogously as for **2a** and **2b**, and the values obtained are indicative that all BH remain in the carboranyl motif.

The sensitivity of the electron distribution in *closo* icosahedral carborane/metallacarborane derivatives to the presence of substituents at the vertexes has long been apparent.[80] It is observed that the chemical shifts of the cluster boron atoms of the *closo* ruthenacarboranes in the ^{11}B NMR spectra vary with the nature of bipyridyl ligand. The averaged chemical shift values, $<\delta>$, move upfield (**Table 3.4**) when the ligand is bipyridyl indicating shielding of the cluster in the *closo* ruthenacarboranes **2a-2c** with respect to **2**. The largest effect is produced by the 4,4'-disubstituted bipyridyl ligands. This result goes in parallel with the CH_{cage} resonances in the ^{1}H NMR that are shifted upfield in the *closo* ruthenacarboranes **2a-2c** with respect to **2.**

As for the $^{13}C\{^{1}H\}$ NMR spectroscopic data obtained, it is also in agreement with the previously observed for the **LMW** relatives. The peak corresponding to the carboranyl cage appears as a broad signal at 45.2 ppm and is more shielded than its precursor. The shielding effect has been also observed in the carbon signal of the carbonyl co-ligand, showing that, upon coordination of the macroligand, a prominent electronic compensation is generated towards the carbonyl and carboranyl ligands.

Table 3.4 along with **Table 3.5** show, respectively, the results obtained for the $^{11}B\{^{1}H\}$ NMR and $^{13}C\{^{1}H\}$ NMR experiments and compare them with the respective values for the parental complex **2**.

Table 3.4 – $^{11}B\{^{1}H\}$ NMR data collected for complex **2** and **2a-2c**, in deuterated acetone.

Compound	**^{11}B NMR** δ / ppm [a]	**$<\delta>$ / ppm**
Complex **2**	8.6 (1B), -4.2 (3B), -7.6 (2B), -16.7 (3B)	-7.70
Complex **2a**	-0.9 (1B), -6.5 (3B), -8.2 (2B), -20.9 (3B)	-11.06
Complex **2b**	-2.1 (1B), -7.8 (3B), -9.6 (2B), -22.3 (3B)	-12.40
Complex **2c**	-0.8 (1B), -7.6 (3B), -9.4 (2B), -22.3(3B)	-12.14

Table 3.5 – $^{13}C\{^{1}H\}$ NMR data for complexes **2** and **2c**, in deuterated acetone.

	^{13}C NMR δ / ppm [a]										
Compound	**Cage CH**	**CO**	**C_1**	**C_2**	**C_3**	**C_4**	**C_5**	**C_6**	**C_7 / $C_{7'}$**	**C_8 / $C_{8'}$**	**C_9 / $C_{9'}$**
Complex **2**	47.9	201.9	-	-	-	-	-	-	-	-	-
Complex **2c**	45.2	198.2	156.2	125.5	156.3	122.1	149.1	65.1	170.2 / 170.6	69.8 / 67.1	17.1 / 20.8

The global effect of the acceptor/donor abilities of the bipyridyl and carbonyl co-ligands over the carboranyl moiety can now be discussed and the dependence of each ligand into the metallic core evaluated. As it can be seen from the previous tables (**Table 3.1-3.5)** there is a noticeable shift in the CH carboranyl resonance that must be related with the co-ligands bounded to the ruthenium center. For complex **2**, [3,3,3-$(CO)_3$-$RuC_2B_9H_{11}$], the correspondent resonance for the carboranyl moiety appears at considerable higher chemical shift (δ 4.15), result from the presence of strong π-acceptor ligand, leading to a decreased level of electronic density in the metal center. So, to equilibrate the lack of electrons on the metal, the carboranyl moiety can donate some electrons to the metal, and this is probably what lead to a more deshielded resonance for the CH protons. The di-substitution of CO ligands by a chelating agent as the bipyridyl, a strong σ donor, will allow a stronger π-backdonation to the carbonyl ligand since the bipyridyl can introduce electron density to the metal. The more efficient electron donation

capacity of the bipyridyl co-ligand will allow a weaker compensation of the electronic density in the ruthenium center by the carboranyl ligand, leading to a less intense electronic compensation from the part of the carboranyl ligand which justify the less deshielded resonance on the complexes **2a-2c**.

3.2.2.2 UV-vis spectroscopy

The optical absorption spectra of all ruthenacarborane complexes were recorded using $1.0x10^{-4}$ to $1.0x10^{-5}$ M solutions in dichloromethane and dimethylsulfoxide.

Table 3.6 presents all the values obtained for the molar absorptivity coefficient and the correspondent wavelengths, whereas **Figure 3.7** and **Figure 3.8** show the behavior of the **LMW** and **HMW** complexes **2a** and **2c**, respectively, in both solvents.

The trend observed in the electronic absorption spectra for complexes **2a-2c** follows the same pattern and the presented figures are representative of their behavior. Despite the strong absorption bands characteristic of each bipyridyl derivative and the {Ru(CO)($C_2B_9H_{11}$)} organometallic fragment (appearing below 300 nm), typical electronic spectra of this series of compounds are characterized by two broad, medium-strength absorption bands appearing in the range of 330 to 530 nm (**Table 3.6**).

Table 3.6 – Optical spectral data for complexes **2** – **2c** in different solvents. Measurements were performed at room temperature using 10^{-4}-10^{-5} M solutions. (Sh = Shoulder).

	λ_{max}/nm (ε x 10^3 / $M^{-1}cm^{-1}$)	
Compound	**Dichloromethane**	**Dimethylsulfoxide**
Complex **2**	277 (4.81), 346 (1.86)	-
Complex **2a**	246 (11.28), 287 (10.25), 311 (*Sh*), 362 (2.74), 451 (0.60)	283 (18.71), 311 (13,01), 350 (5.80), 438 (1.35)
Complex **2b**	245 (18.92), 289 (16.84), 314 (*Sh*), 368 (4.33), 453 (1.07)	284 (16.06), 313 (10.45), 347 (4.32), 434 (1.08)
Complex **2c**	244 (17.13), 296 (16.14), 314 (*Sh*), 380 (3.60), 506 (0.95)	290 (18.26), 318 (*Sh*), 363 (4.51), 493 (*Sh*)

The solvatochromic behavior of all compounds was studied in order to clarify and facilitate the band attribution. Previous studies with similar compounds,[74] attributed the bands near the 350 nm as charge transfer transitions involving the metal and the ligand(s), due to the fact that they have similar intensity and due to the fact they do vary in position when the solvent's polarity change.

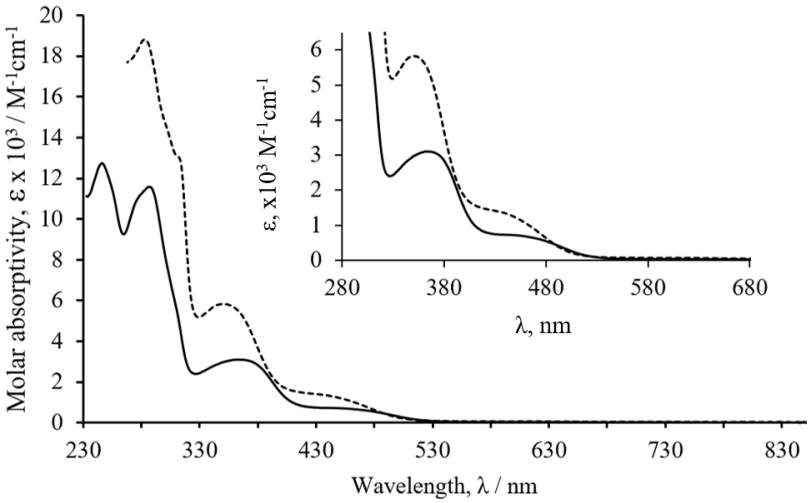

Figure 3.7 – Electronic spectra of complex **2b** in dichloromethane (——) and dimethylsulfoxide (- - - -). Expansion of the spectra to better seeing the identified CT and d–d transitions.

As it was said before and as it can be seen in **Figure 3.8** for example, below 300 nm, there can be found two absorptions transitions with high intensity and energy: the first one (246 nm) is attributed to the electronic transitions that occur in the organometallic fragment by resemblance with the precursor complex [3,3,3-$(CO)_3$-*closo*-3,1,2-$RuC_2B_9H_{11}$], and the second one is attributed to the $\pi \rightarrow \pi^*$ transitions that takes place in the coordinated chromophores.

The other two low energy transitions of intermediate-strength (362 nm; 2.74 x 10^4 $M^{-1}cm^{-1}$ and 451 nm; 0.66 x 10^4 $M^{-1}cm^{-1}$, for complex **2a**, for example) are clearly blue-shifted with the increase of the polarity of the solvent (362 nm in CH_2Cl_2 *vs.* 350 nm in DMSO for the stronger absorption; 451 nm in CH_2Cl_2 *vs.* 438 nm in DMSO for the weaker absorption) and based in their position, intensity and similar behavior in related compounds, we can affirm that they are indicative of charge transfer (possibly LMCT) and d–d transitions, respectively.[74] This solvatochromic response effect is more noticeable in the presumable charge transfer band of complexes **2b** and **2c**, where differences of -21 nm and -17 nm can be observed, respectively.

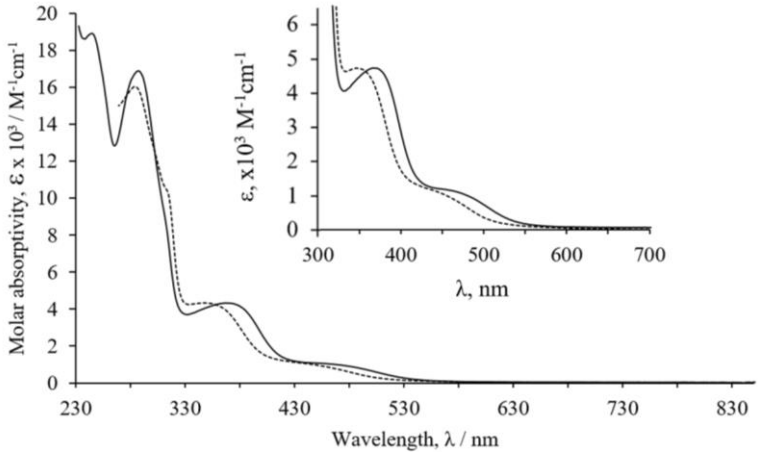

Figure 3.8 – Electronic spectra of complex **2c** in dichloromethane (——) and dimethylsulfoxide (- - - -). Expansion of the spectra to better seeing the identified CT and d–d transitions.

3.2.2.3 IR spectroscopy

The information obtained from the solid state FTIR spectra provided important information for the structural analysis, not only about the coordination modes of the ligands to the metal center but also about the electronic effects between them. Once again, based on a qualitative analysis of the vibrational spectra, is possible to identify the presence of specific functional groups that are expected to be found at the molecular structure of each compound of this ruthenium-carboranyl series. **Table 3.7** shows selected FTIR data for the synthesized complexes along with the correspondent information for its precursor.

In general, the FTIR spectra of the ruthenacarborane complexes presented the characteristic bands of the carboranyl moiety ($\nu_{C\text{-}H,\ stretching}$ ~ 3040 cm^{-1} and $\nu_{B\text{-}H,\ stretching}$ ~ 2550 cm^{-1}) and the bipyridyl derivatives ligands (*ca.* 1520-1400 cm^{-1} and at ~ 2960 cm^{-1} for $\nu_{C\text{-}H,\ stretching}$). It is also noticeable the presence of the stretching frequency of the primary and secondary alcohol groups, respectively, in the complexes **2b** and **2c** spectra ($\nu_{O\text{-}H,\ stretching}$ ~ 3310 and 3540 cm^{-1}). In the latter, typical $\nu_{C=O}$ stretching mode correspondent to the carbonyl group of the polymeric chains was also found in the FTIR spectra, at approximately 1755 cm^{-1}.

Table 3.7 – FTIR data collected for complexes **2**-**2c**, in KBr pellets.

	IR (cm^{-1})				
Compound	**υ (C-H)**	**υ (B-H)**	**υ (CO)**	**υ (CO-O)**	**υ (OH)**
Complex **2**	3040, 2924	2555	2114, 2054	-	-
Complex **2a**	2963, 2924, 2854	2549	1967	-	-
Complex **2b**	2922, 2852	2520	1950	-	3310
Complex **2c**	2997, 2947, 2681	2551	1965	1755	3540

When compared to the relative precursor, complex **2**, complexes **2a**-**2c** displayed only a band that was attributed to vibrational frequency of metallic carbonyl at approximately 1960 cm^{-1}. The clear disappearance of the double band characteristic of the $\nu_{C\equiv O}$ stretching mode of the tricarbonyl complex, gives us once more, the belief that the substitution of two carbonyl co-ligands by the bipyridyl derivate occurred successfully. Altogether, the results analysed in this section are very concordant with the previously discussed data for the NMR and UV-Vis spectroscopies.

The carbonyl bound to the metal center, presented in all complexes as co-ligand, is coordinated in a linear fashion and its bonding to the ruthenium ion can be explained by two synergetic contributions: σ-donation from the ligand to the metal and π-backdonation from the metal to the ligand. This type of interaction between the orbitals of the metal and the ligand lead, in all cases, to a negative shift of the $\nu_{C\equiv O}$ (*av.* 93 cm^{-1}). The high displacement to lower frequencies is therefore a consequence of the strong magnitude of the σ-donation/π-backdonation effects, once the bigger these effects get, the weaker will be the bond between the carbon and oxygen atoms leading to a less energetic vibration between these two atoms. The fact that the signal of the carbon from the CO shields in the ^{13}C NMR spectra is also a good indicative of this effect and correlates very well with the FTIR data.

3.2.2.4 Elemental analysis

Elemental analysis was performed to conclude about the level of purity of the compounds prepared and the obtained results are shown in **Table 3.8**. The purity level of complex **2c** was not assessed by elemental analysis due to the high molecular weight of this compound. In this case, gel permeation chromatography and Maldi-ToF mass spectrometry analysis was preferred and are undergoing.

Table 3.8 – Analytical data for complex **2a** and **2b**.

Compound	**Analysis [a] / %**		
	C	H	**N**
Complex **2a**•¼ CH_2Cl_2	39.1 (39.2)	5.2 (5.1)	5.5 (6.0)
Complex **2b**•¼ THF	38.8 (38.8)	5.1 (5.1)	5.1 (5.7)

[a]Calculated values are given in parenthesis

A good correlation between the calculated and experimental values was obtained by adding some percentage of remaining solvent molecules. Despite the possible contamination by residual solvent, the results obtained this technique indicate good level of purity for compound **2a** and **2b**. These results agree well with the information given by the NMR spectroscopy results.

3.2.2.5 Electrochemical studies

The electrochemical behavior of organometallic ruthenium-carboranyl complexes was followed by cyclic voltammetry in acetonitrile and dichloromethane solutions. The potentials were measured using a platinum disk as working electrode and a silver wire pseudo-reference electrode, ferrocene as internal reference and ammonium hexafluorophosphate as supporting electrolyte.

Table 3.9 summarizes all the electrochemical data for complexes bearing bipyridyl derivatives in acetonitrile and dichloromethane, at room temperature.

Table 3.9 – Electrochemical data for complexes **2-2c** (all values *vs.* SCE, v = 100 mVs^{-1}).

Compound	Acetonitrile					Dichloromethane				
	E_{pa} (V)	E_{pc} (V)	$E_{1/2}$ (V)	$E_{pa} - E_{pc}$ (mV)	I_{pc}/I_{pc}	E_{pa} (V)	E_{pc} (V)	$E_{1/2}$ (V)	$E_{pa} - E_{pc}$ (mV)	I_{pc}/I_{pc}
Complex **2**	--	-1.36	--	--	--	--	--	--	--	--
Complex **2a**	1.12	--	--	--	--	1.12	1.00	1.06	120	0.5
	--	-1.45	--	--	--	--	-1.60	--	--	--
	-1.50	-1.58	-1.54	80	0.9	--	-1.69	--	--	--
Complex **2b**	1.16	--	--	--	--	1.17	--	--	--	--
	--	-1.50	--	--	--	--	-1.60	--	--	--
	--	-1.59	--	--	--					
Complex **2c**	1.17	--	--	--	--					
	1.33	--	--	--	--	1.25	--	--	--	--
	--	-1.62	--	--	--					

Complex **2** showed a weak redox activity in acetonitrile and complete redox inactivity in dichloromethane. However, after coordination of the bipyridyl derivatives, the electrochemical behaviour of the compounds completely changes.

Complex **2a** (**Figure 3.9**), for instance, showed a consistent ruthenium centred irreversible oxidative process at positive potentials (E_{pa} = 1.12 V in acetonitrile and dichloromethane) that does keep its irreversibility when isolated and studied at different scan rates. Probably, after oxidation, the resultant species decomposes and the correspondent reductive process is not able to be observed. Along with this oxidative process, follows two other irreversible reductive processes at negative potentials (in acetonitrile at E_{pc} = -1.45 V and E_{pc} = -1.58 V) that are consistent with redox processes addressed to the bipyridyl ligand as previously studied in related ruthenium-cyclopentadienyl complexes.

In general, the typical electrochemical response of all complexes in dichloromethane is consistent with the behaviour observed in acetonitrile, with irreversible redox processes in approximate potentials values. In some cases, the cyclic voltammogram (complex **2b** and **2c)** presented the same behaviour but with less defined redox processes.

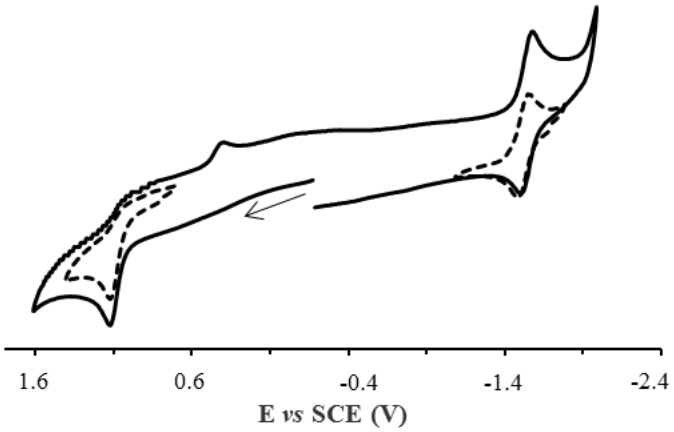

Figure 3.9 – Cyclic voltammogram of complex **2a** in acetonitrile, at 100 mV/s, showing the reversibility and irreversibility of the isolated oxidative processes (dashed lines).

The oxidation potential found for the Ru^{II}/Ru^{III} redox pair in this series of compounds are indeed lower than the related in the $[Ru(\eta^5\text{-}C_5H_5)(CO)(bipy)][CF_3SO_3]$ cyclopentadienyl analogue, which in the same experimental conditions, has not shown any oxidation band in the range of potential used.[81] With these results, we can surely say that the presence of the carboranyl ligand facilitates the oxidation of the metal center, as it was expected by the ability of higher oxidation states stabilization characteristic of the [*nido*-7,8-$C_2B_9H_{11}]^{2-}$ ligand.[82]

3.2.2.6 Single-crystal X-ray diffraction of complexes 2a and 2b

Structural determination of complexes **2a** and **2b** (**Figure 3.10**) was performed and the information collected about some of the interatomic distances of these complexes are presented in **Table 3.10**. Single yellow crystals of **2a** were obtained, under air and at room temperature, by slow evaporation of an acetone solution whereas the orange crystals for **2b** were grown also at room temperature but by slow recrystallization from *n*-hexane in tetrahydrofuran under nitrogen atmosphere. Complex **2a** crystallizes in monoclinic system, space group P21/c whereas complex **2b** crystallizes in monoclinic system, space group P21/n.

In the crystallographic studies, it was possible to see that the basic structural skeleton of this type of complexes is the expected three-legged piano stool structure. Each correspondent crystallographic data revealed that the presence of the 2,2'-bipyridyl derivatives does not affect the full engagement of the C_2B_3 face of the carboranyl ligand towards the ruthenium center, once it remains coordinated in its pentahapto fashion. No evidence of cage slippage or distortion between the carbon atoms of the carboranyl was noticed for any of the complexes. In addition to the fully coordinated planar 2,2'-bipyridyl ligand (C(1)-C(2) 1.658 Å, Ru-C_{cage} (average) 2.196 Å, Ru-B (average) 2.240 Å for complex **2a,** and C(1)-C(2) 1.642 Å, Ru-C_{cage} (average) 2.200 Å, Ru-B (average) 2.456 Å for complex **2b**) there is the lone carbonyl co-ligand, bounded in the expected linear form.

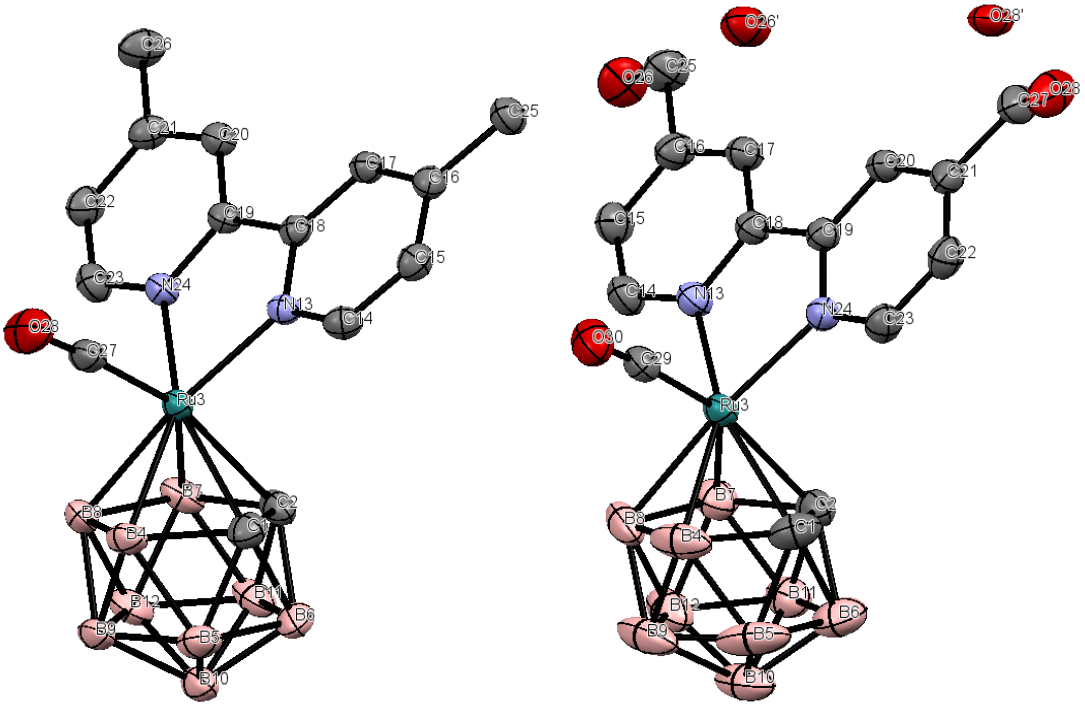

Figure 3.10 – Molecular structure of complex **2a** (left) and **2b** (right). All the non-hydrogen atoms are presented by their 50 % probability ellipsoids. Hydrogen atoms are omitted for clarity.

The crystal structure of complex **2b** reveals two orientations of molecules (head-to-tail) arranged in infinite double zig-zag chains running parallel to the *c* crystallographic axis (**Figure 3.11**). The two carborane B─H vertices located at the B_5 plane that are *trans* to the two carbon cluster atoms and participate in the B─H···O interactions. These intermolecular B─H···O interactions are clearly strong, since the sum of the van der Waals radii of H and O is 2.72 Å and B-H···O distances between neutral molecules as small as 2.54 Å.

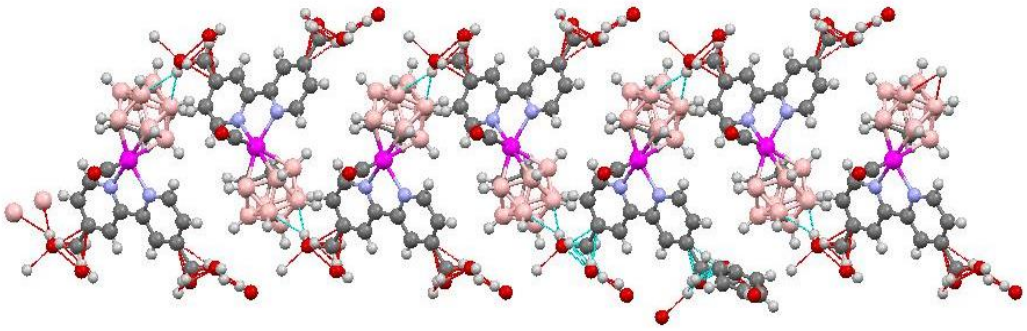

Figure 3.11 – Crystal structure of complex **2b** showing the B–H···O hydrogen bonding which results in a head to tail arrangement of molecules forming an infinite double zig-zag chains running parallel to the *c* crystallographic axis.

Table 3.10 – Selected distances and angles from molecular structures of complex **2a** and **2b**, obtained by single crystal X-ray diffraction analysis.

Distances (Å)	Complex 2a	Complex 2b
Ru(3)–C(27)	1.863(2)	1.865(3)
Ru(3)–N(24)	2.1018(18)	2.104(2)
Ru(3)–N(13)	2.1317(17)	2.125(2)
Ru(3)–C(1)	2.174(2)	2.179(3)
Ru(3)–C(2)	2.218(2)	2.220(3)
Ru(3)–B(4)	2.214(3)	2.210(4)
Ru(3)–B(7)	2.247(3)	2.239(4)
Ru(3)–B(8)	2.266(3)	2.272(4)
O(28)–C(27)	1.143(3)	1.134(4)
C(1)–C(2)	1.658(3)	1.642(5)
Angles (Degree)		
C(27)–Ru(3)–N(24)	91.04(9)	91.61(12)
C(27)-Ru(3)-N(13)	94.12(9)	91.17(11)
N(24)–Ru(3)–N(13)	75.85(8)	76.40(9)
N(24)–Ru(3)–C(1)	114.93(10)	153.72(12)
C(27)–Ru(3)–B(4)	81.96(10)	82.26(15)
N(13)–Ru(3)–B(4)	132.30(10)	131.22(17)
C(2)-Ru(3)-C(27)	158.44(10)	157.52(13)
N(13)-Ru(3)-C(2)	94.32(8)	95.56(11)
C(1)-Ru(3)-C(2)	44.34(9)	43.83(13)
N(13)-Ru(3)-B(8)	171.28(8)	173.04(12)
N(24)-Ru(3)-B(7)	87.32(9)	87.47(13)

3.2.3 Stability and biological studies

3.2.3.1 Stability studies in aqueous media

The possibility of interactions between the drug and biological species could interfere with the medicinal potential of the intended compounds. With this idea in mind, we decided to follow the behavior of the compounds in cellular media and evaluate their stability in order to have an idea if the species synthesized are always the same one during the biological assays. The study was followed by UV-Vis spectroscopy and the results are presented in **Figure 3.12**.

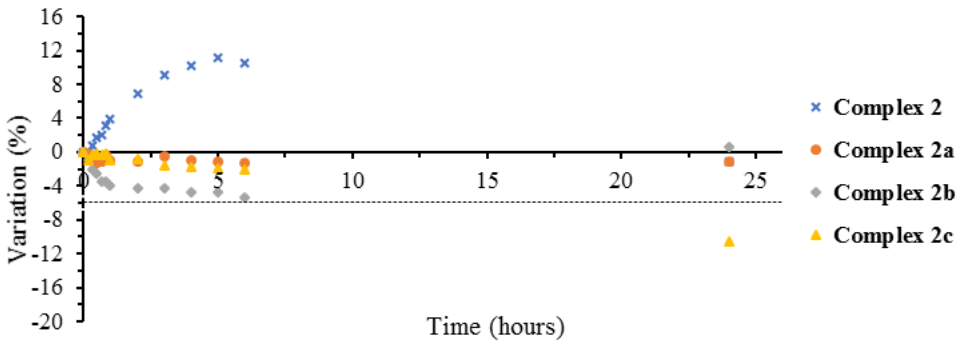

Figure 3.12 – Stability studies in cellular media, DMEM/DMSO (98 % / 2 %).

The UV-Vis absorption spectra of complexes **2**, **2a**, **2** and **2c** exhibit one strong absorption band in the UV range and two broad absorptions in the visible range, similarly to the correspondent behavior observed in the electronic absorption studies presented in section **3.2.2.2**. The samples used in the measurements were protected from light sources and were stored at room temperature between measurements.

Only small variations (lower than 6 % over the first 6 hours) were observed for all complexes with the bipyridyl derivatives, which support that the complexes are quite stable over the 24 h challenge.

3.2.3.2 *n*-Octanol/Water partition coefficient determination

As early described in the previous chapter, the evaluation of the lipophilic/hydrophobic character of new species have a relevant importance. Therefore, in order to evaluate the level of lipophilicity of the compounds, the determination of the partition coefficient was performed, when possible, by using the flask shake method. This method, also used previously for the methylcyclopentadienyl family of compounds (**Chapter 2**), measures the affinity of the compound between an organic and aqueous phase and evaluate their distribution among them. Unfortunately, the synthesized ruthenacarboranes **2b** and **2c** have poor (or none) solubility in the system chosen so the determination of this property could not be assessed using this system of mimetic solvents.

The methodology used to determine the partition coefficient for the ruthenacarborane family of compounds was the same as described in the previous chapter (section **2.2.3.2**). As earlier defined, triplicate experiments have been performed for each complex and the concentration for each sample was determined using the respective calibration curve (**Figure 2.9** e.g., for complex **2a** the calibration curve is shown in **Figure 3.13)**. The correspondent values obtained for this series of compounds are then summarized in **Table 3.11**.

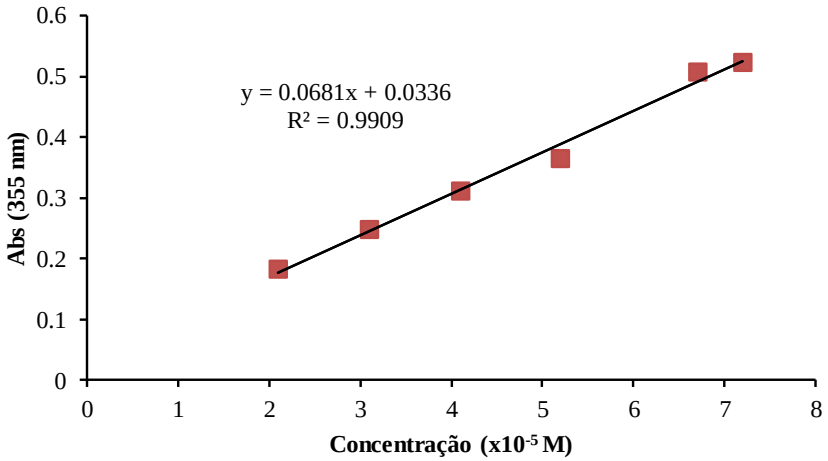

Figure 3.13 – Calibration curve obtained for complex **2a**.

Table 3.11 – Partition coefficients obtained by the shake flask method for complexes **2-2c**.

Compound	$logP_{ow}$
Complex **2**	1.16
Complex **2a**	2.04
Complex **2b**	*
Complex **2c**	*

*It was not possible to calculate an exact value for this compound due to low solubility in the system used.

The presented experiments performed for compound **2** and **2**a was performed in the same conditions as for complexes **1-1d** and the overall results shown that they also possess a more lipophilic character once the compounds mostly remained in the *n*-octanol fraction. Once again is important to underline that, in drug development, this is an important property once the transport to (at least) the cell membranes must be accomplish.

3.2.3.3 Cell viability assay

The cytotoxic outline of the ruthenacarborane complexes **2-2c** was studied on the A375 human cancer cell line, using the MTT assay as colorimetric method. As previously described, low IC_{50} values are indicative of cytotoxicity or antiproliferative activity at low drug concentrations.

Human cutaneous malignant melanoma remains as one of the most deadly form of skin cancer, having a poor prognosis and still no effective therapy.[83,84] Its resistance towards the conventional chemotherapeutic DNA-damaging agents, makes this cancer resistant to cisplatin,[84] being one of the most difficult cancers to treat. Hence, we have used the human melanoma A375 cells, derived from a metastatic melanoma to perform the cytotoxic assay.

Cells were incubated with each compound, in a concentration range of 1 µM to 200 µM, for a period of 24 hours. After the incubation period, the (anti)proliferative cell rate was assayed. **Table 3.12** summarizes the IC_{50} values obtained in the biological assays and can be compared with the IC_{50} value for metallodrug used as reference, cisplatin (CDDP).

Table 3.12 – IC_{50} values (µM) found for the **LMW 2**, **2a** and **2b** and **HMW 2c** complexes, along with the metallodrug reference cisplatin in human A375 human melanoma cancer cell line at 37 ºC, for a period of incubation of 24 h.

	IC_{50} (µM) [a]
Compound	**A375**
Complex **2**	51.4 ± 15
Complex **2a**	> 100
Complex **2b**	55.7 ± 30
Complex **2c**	> 100
CDDP	> 200 [b]

[a] Measured after 24 h of incubation. [b] Measured after 48 h of incubation

All compounds exhibited a low cytotoxic profile against the tested cell line, as it was expected by the introduction of the carbonyl co-ligand. Among these four ruthenacarborane complexes, the most promising ones to pursue in the BNCT preliminary assays are the complexes **2a** and **2c**, since contrarily to the previous family of compounds (**1-1d**) this type of anticancer agents, must not be cytotoxicity to the application of BNCT. Complex **2c** might be advantageous relatively to complex **2a** once the high molecular weight can increase selectivity towards cancerous cells.

3.3 Conclusions

In this chapter we presented the synthesis, characterization and preliminary cytotoxic evaluation of new Ru^{II}-η^5-carboranyl complexes containing 2,2'-bipyridine derivatives as ligands. Three new complexes with general formula [3-CO-3,3-{k^2-4,4'-R_2-2,2'-bipy}-*closo*-3,1,2-$RuC_2B_9H_{11}$], where R = -CH_3 (**2a**), R = -CH_2OH (**2b**), R = -CH_2OPLA (**2c**), have been isolated. They were fully characterized by spectroscopic, electrochemical and analytical techniques. Their anticancer properties were also accessed by preliminary studies *in vitro*.

The spectroscopic data supports the successful formulation of all ruthenacarboranes herein described. Coordination of the carboranyl ligand in all complexes and of a unique carbonyl (in complexes **2a**, **2b** and **2c)** to the metallic center was easily confirmed by FTIR and NMR spectroscopies, whereas the presence of the derivatized 2,2'-bipyridyl scaffold was confirmed by FTIR, NMR, UV-Vis measurements and structural resolution.

The overall NMR data collected from the ^1H, ^{13}C and ^{11}B measurements confirms the π-backdonation from the metal towards the carbonyl and the carboranyl ligands, which is also coherent with the results of the FTIR spectra. The presence of the four resonances in the ^{11}B NMR spectrum coming from the boron cluster in the typical chemical shift range of the *closo*-3,1,2-MC_2B_9 (M = Rh, Ru) framework also confirms the successful formulation of these complexes. The downfield shift on the protons of the aromatic bidentate ligand also confirm the σ-dative contribution to the metal.

UV-Vis spectroscopic data confirmed the coordination of the aromatic derivatives into organometallic fragment used as starting material (complex **2**). Additionally to the transitions observed for the coordinated ligands (π→π*) and the transitions observed in the organometallic fragment, a transition with medium-strength intensity and broad character located in the 360-389 nm region could be addressed to charge transfer, MLCT or LMCT processes.

The electrochemical behavior of the ruthenacarborane complexes **2**-**2c** was studied by cyclic voltammetry in acetonitrile and dichloromethane. All compounds, with exception of the parental tricarbonyl complex used as starting material (complex **2**), showed to be electroactive and their behavior was characterized by one irreversible oxidation process at positive potentials ascribe to the ruthenium metal followed by other two irreversible reductive processes at negative potentials that were assigned to the to the bipyridyl ligand.

Taking advantage of the good single crystals obtained for complexes **2a** and **2b**, we could confirm that the typical structural architecture of the family of compounds is the expected three-legged piano stool geometry comprising the carboranyl ligand fully engaged to the metal core along with the planar bipyridyl derivative and the almost linear carbonyl occupying the three remaining positions. All the distances obtained between the atoms and the angles measured from the structure resolution of the compounds are consistent with previously reported ruthenacarborane incorporating N-donor ligands.

Preliminaries biological assays were performed to evaluate the cytotoxicity of the all complexes synthesized. These experiments were determined *in vitro* in a carefully selected cancer cell line, the human melanoma A375 cell line which is derived from a human cutaneous malignant melanoma. At the 24 h challenge, complexes **2** and **2b** showed moderate cytotoxicity against this cell line whereas complexes **2a** and **2c** showed to be less cytotoxic than its analogues (IC_{50} values higher than 100 μM). These results are very promising envisaging the applications of these compounds in BNCT.

Chapter 4

Experimental

Experimental

General considerations

All polymerization and organometallic synthesis were carried out under nitrogen atmosphere using standard *Schlenk* techniques.[85,86] Methylcyclopentadiene was obtained by thermal cracking of its dimer and used immediately. *Nido*-$C_2B_9H_{13}$ was obtained by protonation of the correspondent anionic form, [*nido*-$C_2B_9H_{12}$]$^-$, and used *in situ* for the synthesis of the starting material of the organometallic ruthenacarborane complexes.

The solvents used were previously dried from Na/benzophenone (THF, diethyl-ether and *n*-heptane (without benzophenone)) and/or CaH_2 or $CaCl_2$ (dichloromethane, *n*-hexane and acetonitrile) and were freshly distilled under nitrogen atmosphere before use, according to common literature methods,[87] and stored in glass flasks (with J. Young valves).

All commercial reagents used (with exception of D,L-Lactide) were used without further purification and were purchased mainly from Sigma-Aldrich or Acrös Organics. D,L-lactide purification was performed by recrystallization in toluene three times and dried overnight in the vacuum line.

The deuterated solvents used in the sample preparation of the NMR measurements ($(CD_3)_2CO$-d_6 (99 %), DMSO-d_6 (99 %), CD_3CN-d_3 (99 %)) were used as received from Aldrich mainly.

The starting materials used in the preparation of the organometallic complexes were prepared following the methods described in the literature: [Ru(η^5-MeCp)$(PPh_3)_2$Cl][88] and [3,3,3-$(CO)_3$-*closo*-$RuC_2B_9H_{11}$][75].

Characterization techniques

Nuclear Magnetic Resonance spectroscopy (NMR)

NMR spectra were recorded on a *Brucker Avance 400* spectrometer (^{1}H, 400 MHz; ^{13}C, 100.62 MHz; ^{19}F, 282 MHz; ^{31}P, 161.97 MHz) or on a *Brucker Avance 300* spectrometer (^{11}B, 96.29 MHz) at probe temperature. ^{1}H and ^{13}C chemical shifts were reported downfield from the residual solvent peak, whereas the ^{11}B, ^{19}F and the ^{31}P NMR chemical shifts were reported downfield from the external standard, $BF_3{\cdot}OEt_2$, 85 % H_3PO_4 and $CFCl_3$, respectively.

All resonances were characterized for their chemical shifts (δ) given in parts-per-million (ppm), and for their coupling constants (*J*) expressed in hertz (Hz). Resonance multiplicity is expressed as follows: singlet (s), doublet (d), doublet of doublets (dd), triplet (t), multiplet (m) and broad (*br*). All assignments were attributed using HMBC, HMQC and COSY 2D-RMN techniques.Each sample was prepared under air and at room temperature, using the most adequate deuterated solvent.

Electronic spectroscopy (UV-vis)

The electronic UV-Vis spectra and the solvatochromic behavior of all compounds were recorded in dichloromethane and dimethylsulfoxide solutions (10^{-4}-10^{-5} M), under air, using 1 cm optical path quartz cells on a *Jasco V-560* spectrometer in the range of 200-900 nm.

Infrared spectroscopy (FTIR)

The infrared spectra were recorded in a *Shimadzu IRAffinity-1 FTIR* spectrophotometer in dry KBr pellets, under air and at room temperature. Bands intensity was defined as follows: broad (*br)*, strong (s), medium (m) and weak (w).

Elemental analysis (EA)

Elemental analyses were obtained at *Laboratório de Análises*, *Instituto Superior Técnico*, using a *Fisons Instruments EA1108* system. Data acquisition, integration and handling was performed using a PC with the software package EAGER-200 (Carlo Erba Instruments).

Single-crystal X-ray diffraction

The structural determination of complexes were performed by Doctor Fernando Avecilla (complex **1a** at Departamento de Química Fundamental, Universidade da Coruña, Spain) and by Doctor Xavier Fontrodona Gubau (complexes **2a** and **2b**, at Parc Científic i Tecnològic de la Universitat de Girona, Spain), according to established procedures.

Three-dimensional X-ray data for complex **1a**, **2a** and **2b** were collected on a *Bruker SMART Apex CCD* diffractometer at 100(2) K or 193(2) K, using a graphite monochromator and Mo-K_α radiation (λ = 0.71073 Å) by the ϕ-ω scan method. Reflections were measured from a hemisphere of data collected of frames each covering 0.3 degrees in ω. After data collection, in each case a multi-scan absorption correction (SADABS) was applied, and the structure was solved by direct methods and refined by full matrix least-squares on F^2 data using SHELXT - SHELXL suite of programs.[89]

The structures were solved by direct methods and refined by full-matrix least-squares methods on F^2. The non-hydrogen atoms were refined with anisotropic thermal parameters in all cases. Hydrogen atoms were included in calculation positions and refined in the riding mode, except the carborane B-H and C-H which were located in the difference Fourier map and refined freely. The C atoms in the carborane were located using the VCD and BHD methods.[90] All graphic representations were performed using the Mercury1.1.2 program.[91]

Cyclic voltammetry (CV)

Electrochemical measurements were performed on an *EG&G Princeton Applied Research* (PAR) Potentiostat/Galvanostat Model 273A equipped with *Electrochemical Powersuite* v2.51 software for electrochemical analysis, in dried acetonitrile or dichloromethane with tetrabutylammonium hexafluorophosphate (0.1 M or 0.2 M, respectively) as supporting electrolyte. The electrochemical cell was a home made three electrode configuration cell with a platinum-disc working electrode (1.0 mm diameter) probed by a Luggin capillary connected to a silver-wire pseudo-reference electrode and a platinum wire auxiliary electrode. All experiments were performed under nitrogen atmosphere and at room temperature. All the potentials reported were measured against the ferrocene/ferrocenium redox couple as internal standard and normally quoted relative to SCE (using the ferrocenium/ferrocene redox couple $E_p1/2$ = 0.46 or 0.40 V *versus* SCE for dichloromethane or acetonitrile, respectively).[92] The electrochemical grade electrolyte was purchased from Aldrich. All solvents used, dichloromethane and acetonitrile, were dried and distilled by standard procedures before use.

Chromatography

For the thin layer chromatography (TLC) analytical assays, silica gel 60 F_{254} pates of several appropriate dimensions was used. The elution of these plates was performed using different mixtures of solvents. Upon elution, the TLC plates were observed under UV light at 254 and 366 nm.

Cell viability assay in human cancer cell lines

The biological studies were performed by Doctor Fernanda Marques (Unidade de Ciências Químicas e Radiofarmacêuticas, Campus Tecnológico e Nuclear – IST, Portugal) and by the Master student Ana Rita Brás (member of Professor's Ana Preto research group – Centro de Biologia Molecular e Ambiental, at Universidade do Minho, Portugal), according to established procedures.

Four human cancer cell lines and one noncancerous human cell line were used in this study: A2780 (human ovarian adenocarcinoma), A375 (human malignant melanoma), SW480 (human colon adenocarcinoma), RKO (human colorectal carcinoma) and NCM460 (normal colon epithelial mucosa). The cells were maintained in DMEM (Dulbecco's Modified Eagle's Medium, Invitrogen) containing Glutamax 1 (A2780, A375 and RKO) or RPMI medium (SW480 and NCM460), supplemented with 10 % (v/v) heat inactivated fetal bovine serum (FBS) and 1 % penicillin/streptomycin (Invitrogen). All cell lines were kept in a CO_2 incubator with 5 % CO_2 at 37 ºC in a humidified atmosphere.

The cytotoxicity activity of the compounds was evaluated in the aforementioned cell lines within the concentration range of 10^{-10}-10^{-4} M using the one of the following colorimetric assays: MTT or SRB assays. MTT (3-(4,5-dimethylthiazol-2-yl)-2,5-diphenyltetrazolium bromide) is reduced to purple formazan in living cells, whereas SRB (sulforhodamine B) is a bright-pink aminoxanthene dye with two sulfonic groups that bind to basic amino-acids residues under mild acid conditions and dissociate under basic conditions.[93,94] The MTT assay, measures the amount of MTT reduction by mitochondrial dehydrogenase and assumes that cell viability (corresponding to the reductive activity) is proportional to the production of formazan that is measured spectrophotometrically usually between 500-600 nm.[93] The SRB assay, relies on the ability of SRB to bind to protein components of cells that have been fixed to tissue-culture plates by trichloroacetic acid and since the bind of SRB is stoichiometric, the amount of dye extracted from stained cells is directly proportional to the cell mass.[94] In both cases, cells were seeded in 200 μL of complete medium in 96-well (MTT) or 24-well plates (SRB) which were incubated

at 37 ºC for 24 h prior to complex testing to allow cell adhesion. The stock solution in DMSO of each compound was freshly prepared and used for sequential dilutions in complete medium. Analysis of cell survival was carried out at the end of 24 hours (A2780 and A375) or 48 hours (RKO, SW480 and NCM460) cell exposure by each colorimetric method. After appropriate treatment, specific of each colorimetric method, cellular viability was evaluated by measurement of the absorbance at 570 nm (or 540 nm) by using a plate spectrophotometer (PowerWave Xs, Bio-Tek or SpectraMax 340PC Molecular Devices). Each experiment was repeated at least two times, and each concentration tested in at least four replicates. Results are expressed as a percentage of survival with respect to control cells in the absence of the compound. The IC_{50} value (i.e. drug concentration that induces 50 % of cell death) was calculated from plots for cell survival (%) *versus* compound concentration with the *GraphPad Prism* software (version 4.0).

Procedures

Polymerization synthesis

In a typical polymerization, purified D,L-lactide (ca. 1 g), bipy$(CH_2OH)_2$ (ca. 0.08 g) and DMAP (ca. 0.06 g) were weighted and placed together in a polymerization *Schlenk* vessel, along with a magnetic stirrer bar. The reactional vessel was then submersed in an oil bath at 135 ºC for 15 minutes, with constant magnetic stirring. After that, *quenching* of the reaction was performed with some drops of a biphasic solution of water and methanol [50/50 (% v/v), 40 mL]. Then, dichloromethane was added to completely dissolve the solid obtained and each soluble fraction was transferred to the remaining biphasic mixture. After complete addition in the water/methanol mixture, the polymeric compound was totally precipitated, under reduced pressure, until the solution become translucent. The solution was decanted and the residue was washed with diethyl ether (2x10 mL) and dried under vacuum yielding a pure off-white foamy polymer. ^{1}H-NMR spectra was recorded at the end of each synthesis to confirm purity and to determine the degree of polymerization of the batch synthesized.

Yield: 95 %.

^{1}H NMR [$(CD_3)_2CO$, Me_4Si, δ / ppm]: 8.71 (d, 2H, H_1), 8.49 (s, 2H, H_4), 7.45 (d, 2H, H_2), 5.39 (s, 4H, H_6), 5.21 (m, H, H_a), 4.30 (m, 44H, $H_{a'}$), 1.55 (m, 2H, H_b), 1.39 (m, H, $H_{b'}$).

Organometallic synthesis described in Chapter 2

Synthesis of [Ru(η^5-MeCp)(PPh_3)$_2$Cl] (1)

To a stirred and degassed solution of hydrated ruthenium trichloride (0.5 g, 2.4 mmol) in ethanol (50 mL) was added triphenylphosphane (2.89 g, 11 mmol) and freshly distilled methylcyclopentadiene (5-6 mL). The dark brown mixture obtained was refluxed, with vigorously stirring, for 8 hours until no more precipitation of the orange complex **[Ru(η^5-MeCp)(PPh_3)$_2$Cl]** was observed. After refluxing, the mixture was cooled to room temperature overnight. The precipitate was filtered, washed with water (2x20 mL), cold ethanol (2x20 mL) and a mixture of ethanol and light petroleum ether (50:50 (% v/v), 2x20 mL). The orange powder obtained was dried under vacuum originating **1**, **[Ru(η^5-MeCp)(PPh_3)$_2$Cl].** Single crystals were isolated by recrystallization from dichloromethane/*n*-hexane.

Yield: 48 %.

EA found (calculated): C, 67.8 (68.1); H 5.0 (5.0).

^{1}H NMR [$(CD_3)_2CO$, Me_4Si, δ / ppm]: 7.41 (t, 12H, $^3J_{HH}$ = 8, H_o-PPh_3), 7.28 (t, 6H, $^3J_{HH}$ = 7.2, H_p-PPh_3), 7.17 (t, 12H, $^3J_{HH}$ = 7.2, H_m-PPh_3), 3.88 (s, 2H, H_3), 3.33 (s, 2H, H_4), 1.87 (s, 3H, H_1).

^{31}P NMR [$(CD_3)_2CO$, δ / ppm]: 40.01 [s, PPh_3].

^{1}H NMR [($CDCl_3$, Me_4Si, δ / ppm]: 7.37 (t, 12H, $^3J_{HH}$ = 8.2, H_{meta}-PPh_3), 7.21 (t, 6H, $^3J_{HH}$ = 7.2, H_{para},PPh_3), 7.11 (t, 12H, $^3J_{HH}$ = 7.4, H_{orto},PPh_3), 3.96 (s, 2H, H_3), 3.26 (s, 2H, H_4), 1.92 (s, 3H, H_1).

^{13}C NMR [($CDCl_3$, Me_4Si, δ / ppm]: 138.7 ($C_q$$PPh_3$, $^1J_{CP}$ = 19.1), 133.9 ($CH_o$$PPh_3$, $^2J_{CP}$ = 5.1), 128.7 ($CH_p$$PPh_3$), 127.5 ($CH_m$$PPh_3$, $^3J_{CP}$ = 4.5), 104.9 (C_2), 81.0 (C_3), 76.7 (C_4), 12.0 (C_1).

^{31}P NMR [$CDCl_3$, δ / ppm]: 40.11 [s, PPh_3].

FTIR [KBr pellets, cm^{-1}]: 3100-2850 cm^{-1} ($\upsilon_{C-H,}$ MeCp and phenyl rings), 1440 ($\upsilon_{C=C,}$ phenyl rings).

UV-Vis in CH_2Cl_2 [λ_{max} / nm (ε x10^3 / $M^{-1}cm^{-1}$)]: 289 (*Sh*), 336 (*Sh*), 386 (*Sh*), 448 (*Sh*).

UV-Vis in DMSO [λ_{max} / nm (ε x10^3 / $M^{-1}cm^{-1}$)]: 289 (*Sh*), 336 (*Sh*), 386 (*Sh*), 448 (*Sh*).

Synthesis of [Ru(η^5-MeCp)(PPh_3)(Me_2bipy)][CF_3SO_3] (1a)

To a stirred solution of [Ru(η^5-MeCp)(PPh_3)$_2$Cl] (0.250 g, 0.34 mmol) in dichloromethane (40 mL), $AgCF_3SO_3$ (0.09 g, 0.37 mmol) was added. The resulting solution was stirred for 1 hour at room temperature followed by addition of Me_2bipy (0.07 g, 0.36 mmol). After refluxing for 5 hours the solution turned from orange to deep red. AgCl precipitate was separated from the solution by cannula-filtration and the solvent was evaporated under vacuum. The remaining solid was recrystallized from dichloromethane/*n*-hexane and then washed twice (10 mL) with *n*-hexane affording **1a**, **[Ru(η^5-MeCp)(PPh_3)(Me_2bipy)][CF_3SO_3]**, as an bright orange powder. Single crystals were grown from slow diffusion of *n*-hexane on a dichloromethane solution.

Yield: 67 %.

EA [calculated for complex **1a** • ⅓ CH_2Cl_2] found (calculated): C 55.5 (55.7), H 4.2 (4.3), N 3.4 (3.4), S 4.2 (4.0).

^{1}H NMR [$(CD_3)_2CO$, Me_4Si, δ / ppm]: 9.24 (d, 2H, $^3J_{HH}$ = 6, H_5), 8.04 (s, 2H, H_8), 7.43 (t, 6H, $^3J_{HH}$ = 6, H_pPPh_3), 7.22 (d, 2H, $^3J_{HH}$ = 6.8, H_6), 7.33 (t, 6H, $^3J_{HH}$ = 7.2, H_mPPh_3), 7.12 (t, 6H, $^3J_{HH}$ = 8, H_oPPh_3), 4.68 (s, 2H, H_4), 4.57 (m, 2H, H_3), 2.46 (s, 6H, H_{10}), 1.65 (s, 3H, H_1).

^{13}C NMR [$(CD_3)_2CO$, Me_4Si, δ / ppm]: 156.3 (C_9), 155.9 (C_5), 149.2 (C_7), 133.8 ($^2J_{PC}$ = 11, CH_oPPH_3), 133.0 ($^1J_{PC}$ = 40, C_qPPH_3), 130.8 ($^4J_{PC}$ = 2, CH_pPPH_3), 129.3 ($^3J_{PC}$ = 10, CH_mPPH_3), 127.3 (C_6), 124.6 (C_8), 103.0 (C_2), 76.5 (C_4), 76.4 (C_3), 20.8 (C_{10}), 11.7 (C_1).

^{31}P NMR [$(CD_3)_2CO$, δ / ppm]: 51.83 [s, PPh_3].

FTIR [KBr pellets, cm^{-1}]: 3100-2850 cm^{-1} ($\upsilon_{C-H,}$ MeCp and phenyl rings), 1440 ($\upsilon_{C=C,}$ phenyl rings), 1260 cm^{-1} ($\upsilon(CF_3SO_3^-)$).

UV-Vis [CH_2Cl_2, λ_{max} / nm (ε x10^3 / $M^{-1}cm^{-1}$)]: 288 (24.8), 323 (7.7), 423 (4.6), 478 (*Sh*).

UV-Vis [DMSO, λ_{max} / nm (ε x10^3 / $M^{-1}cm^{-1}$)]: 291 (26.7), 333 (*Sh*), 418 (4.8), 479 (*Sh*).

Synthesis of [Ru(η^5-MeCp)(PPh_3)(bipy(CH_2OH)$_2$))][CF_3SO_3] (1b)

To a stirred solution of [Ru(η^5-MeCp)(PPh_3)$_2$Cl] (0.250 g, 0.34 mmol) in dichloromethane (50 mL), $AgCF_3SO_3$ (0.09 g, 0.37 mmol) was added. The resulting solution was stirred for 1 hour at room temperature followed by addition of bipy(CH_2OH)$_2$ (0.08 g, 0.36 mmol). After refluxing for 5 hours the solution turned from orange to deep red. AgCl precipitate was separated from the solution by cannula-filtration and the solvent was evaporated under vacuum. The remaining solid was recrystallized from tetrahydrofuran/*n*-hexane and then washed (2x10 mL) with n-hexane affording **1b**, **[Ru(MeCp)(PPh_3)(bipy(CH_2OH)$_2$)][CF_3SO_3]**, as an bright orange powder.

Yield: 58 %.

EA [calculated for complex **1b** • ½ CH_2Cl_2] found (calculated): C 53.0 (53.0), H 4.0 (4.2), N 3.3 (3.3), S 4.0 (3.8).

^{1}H NMR [$(CD_3)_2CO$, Me_4Si, δ / ppm]: 9.34 (d, 2H, $^3J_{HH}$ = 5.6, H_5), 8.10 (s, 2H, H_8), 7.40 (t, 3H, $^3J_{HH}$ = 6.8, H_pPPh_3), 7.36 (d, 2H, $^3J_{HH}$ = 6, H_6), 7.31(t, 6H, $^3J_{HH}$ = 7.2, H_mPPh_3), 7.11 (t, 6H, $^3J_{HH}$ = 8.8, H_oPPh_3), 4.79 (m, 4H, H_{10}), 4.71 (s, 2H, H_4), 4.60 (s, 2H, H_3), 1.66 (s, 3H, H_1).

^{13}C NMR [$(CD_3)_2CO$, Me_4Si, δ / ppm]: 156.3 (C_9), 156.1 (C_5), 153.7 (C_7), 133.8 ($^2J_{PC}$ = 11, CH_oPPH_3), 132.9 ($^1J_{PC}$ = 40, C_qPPH_3), 130.8 ($^4J_{PC}$ = 2, CH_pPPH_3), 129.3 ($^3J_{PC}$ = 9, CH_mPPH_3), 123.6 (C_6), 120.8 (C_8), 103.0 (C_2), 76.7 (C_4), 76.6 (C_3), 62.5 (C_{10}), 11.7 (C_1).

^{31}P NMR [$(CD_3)_2CO$, δ /ppm]: 51.85 [s, PPh_3].

FTIR [KBr pellets, cm^{-1}]: 3450-3410 cm^{-1} (υ_{O-H}), 3100-2850 cm^{-1} ($\upsilon_{C-H,}$ MeCp and phenyl rings), 1440 ($\upsilon_{C=C,}$ phenyl rings), 1256 cm^{-1} ($\upsilon(CF_3SO_3^-)$), 1225 cm^{-1} (υ_{C-O}).

UV-Vis [CH_2Cl_2, λ_{max} / nm (ε x10^3 / $M^{-1}cm^{-1}$)]: 292 (20.8), 354 (*Sh*), 424 (3.6), 472 (*Sh*).

UV-Vis [DMSO, λ_{max} / nm (ε x10^3 / $M^{-1}cm^{-1}$)]: 290 (54.0), 350 (*Sh*), 422 (6.8), 480 (*Sh*).

Synthesis of [Ru(η^5-MeCp)(PPh_3)(*per*Fluoro-bipy)][CF_3SO_3] (1c)

To a stirred solution of [Ru(η^5-MeCp)(PPh_3)$_2$Cl] (0.26 g, 0.36 mmol) in dichloromethane (50 mL), $AgCF_3SO_3$ (0.10 g, 0.40 mmol) was added. The resulting solution was stirred for 1 hour at room temperature followed by addition of *perFluoro*-bipy (0.390 g, 0.35 mmol). After refluxing for 6 hours the solution turned from orange to brown. AgCl precipitate was separated from the solution by cannula-filtration and the solvent was evaporated under vacuum. The remaining solid was recrystallized once from slow diffusion of *n*-hexane in dichloromethane and then precipitated twice, abruptly, with the same solvent pair affording **1c**, **[Ru(η^5-MeCp)(PPh_3)(*perFluoro*-bipy)][CF_3SO_3]**, as an dark orange to brown powder.

Yield: 31 %.

EA [calculated for complex **1c** •½ C_6H_{14}], found (calculated): C, 41.3 (41.3); H, 2.5 (2.7); N, 1.2 (1.6); S, 2.0 (1.8).

^{1}H NMR [$(CD_3)_2CO$, Me_4Si, δ / ppm]: 9.16 (d, 2H, $^3J_{HH}$ = 8, H_5), 7.82 (d, 2H, $^3J_{HH}$ = 2.4, H_8), 7.41 (t, 3H, $^3J_{HH}$ = 8, H_pPPh_3), 7.33 (t, 6H, $^3J_{HH}$ = 8, H-PPh_3), 7.14 (t, 6H, , $^3J_{HH}$ = 8 H-PPh_3), 7.03 (dd, 2H, $^3J_{HH}$ = 6.5, 2.6, H_6), 4.63 (s, 2H, H_4), 4.51 (m, 2H, H_3), 4.39 (m, 4H, H_{10}), 2.47 (m, 4H, H_{12}), 2.15 (m, 4H, H_{11}) 1.66 (s, 3H, H_1).

^{13}C NMR [$(CD_3)_2CO$, Me_4Si, δ / ppm]: 166.3 (C_7), 158.1 (C_9), 157.2 (C_5), 133.9 (d, J_{PC} = 11, CH-PPh_3), 133.4 (d, $^1J_{PC}$ = 40, C_qPPh_3), 130.7 (d, J_{CP} = 2, CH-PPh_3), 129.3 (d, J_{PC} = 10, CH-PPh_3), 114.3 (C_6), 110.2 (C_8), 102.5 (C_2), 76.0 (C_4), 75.8 (C_3), 68.6 (C_{10}), 28.0 (C_{12}), 20.9 (C_{11}), 11.8 (C_1), 133.6+133.2+123.9+120.7 (C_{13}-C_{20}).

^{19}F NMR [$(CD_3)_2CO$, δ/ppm]: -78.88, -81.65, -114.72, -122.23, -122.46, -123.29, -123.94, -126.78.

^{31}P NMR [$(CD_3)_2CO$, δ/ppm]: 51.50 [s, PPh_3].

FTIR [KBr pellets, cm^{-1}]: 3100-2880 cm^{-1} (υ_{C-H} aromatic), 1250 cm^{-1} ($\upsilon CF_3SO_3^-$), 1342 cm^{-1} (υ_{C-F}), 1220 cm^{-1} (υ_{C-O}).

UV-Vis [CH_2Cl_2, λ_{max} / nm (ε x10^3 / $M^{-1}cm^{-1}$)]: 270 (22.6), 294 (*Sh*), 348 (*Sh*), 419 (4.2), 476 (*Sh*).

UV-Vis [DMSO, λ_{max} / nm (ε x10^3 / $M^{-1}cm^{-1}$)]: 273 (27.1), 297 (*Sh*), 355 (*Sh*), 414 (4.6), 473 (*Sh*).

Synthesis of [Ru(η^5-MeCp)(PPh_3)(bipy($CH_2OPLA)_2$)][CF_3SO_3] (1d)

To a stirred solution of [Ru(η^5-MeCp)(PPh_3)$_2$Cl] (0.11 g, 0.15 mmol) in dichloromethane (50 mL), $AgCF_3SO_3$ (0.05 g, 0.15 mmol) was added. The resulting solution was stirred for 1 hour at room temperature followed by addition of bipy-polylactide (0.300 g, 0.1 mmol). After refluxing for 4 h 30 min, AgCl precipitate was separated from the solution by cannula-filtration and the solvent was evaporated under vacuum. The residue obtained was recrystallized from dichloromethane/*n*-hexane twice and then the remaining oil was washed (2x10 mL) with diethyl ether affording **1d**, **[Ru(η^5-MeCp)(PPh_3)(bipy($CH_2OPLA)_2$][CF_3SO_3]**, as an orange foamy product.

Yield: 62 %

^{1}H NMR [$(CD_3)_2CO$, Me_4Si, δ / ppm]: 9.47 (d, 2H, $^{3}J_{HH}$ = 5.2, H_5), 8.11 (s, 2H, H_8), 7.55 (d, 2H, $^{3}J_{HH}$ = 6, H_6), 7.43 (t, 3H, J_{HH} = 6.8, H_pPPh_3), 7.33 (t, 6H, $^{3}J_{HH}$ = 6.8, H_mPPh_3), 7.11 (t, 6H, $^{3}J_{HH}$ = 8.8, H_oPPh_3), 5.36 (s, 4H, H_{10}), 5.20 (m, 42H, CH_{PLA}), 4.77 (s, 2H, H_4), 4.67 (s, 2H, H_3), 4.31 (m, 3H, $CH_{PLA,\ terminal}$), 1.68 (s, 3H, H_1), 1.55 (m, 134H, $CH_{3\ PLA}$), 1.39 (m, 7H, $CH_{3\ PLA,\ terminal}$).

^{13}C NMR [$(CD_3)_2CO$, Me_4Si, δ / ppm]: 175.0 ($C_{11'}$), 170.2 (C_{11}), 156.5 (C_9), 156.3 (C_5), 146.5 (C_7), 133.8 ($^{2}J_{PC}$ = 11, CH_oPPH_3), 132.3 ($^{1}J_{PC}$ = 40, C_qPPH_3), 131.0 (CH_pPPH_3), 129.4 ($^{3}J_{PC}$ = 9, CH_mPPH_3), 124.4 (C_6), 121.9 (C_8), 103.4 (C_2), 77.0 (C_3+C_4), 69.8 (C_{12}), 67.1 ($C_{12'}$), 65.0 (C_{10}), 20.8 ($C_{13'}$), 17.1 (C_{13}), 11.7 (C_1).

^{31}P-NMR [$(CD_3)_2CO$, δ /ppm]: 51.63 [s, PPh_3].

FTIR [KBr pellets, cm^{-1}]: 3450-3410 cm^{-1} (υ_{O-H}), 3100-2880 cm^{-1} (υ_{C-H} aromatic and υ_{CH3} PLA), 1757 cm^{-1} ($\upsilon_{C=O}$), 1400-1350 cm^{-1} ($\upsilon_{C=C}$ MeCp and phenyl rings), 1273 cm^{-1} ($\upsilon(CF_3SO_3^-)$).

UV-Vis [CH_2Cl_2, λ_{max} / nm (ε x10^3 / $M^{-1}cm^{-1}$)]: 294 (29.7), 329 (*Sh*), 438 (4.8), 507 (*Sh*).

UV-Vis [DMSO, λ_{max} / nm (ε x10^3 / $M^{-1}cm^{-1}$)]: 295 (23.5), 332 (*Sh*), 430 (4.2), 503 (*Sh*).

Organometallic synthesis described in Chapter 3

Transformation of [$NHMe_3$][*nido*-$C_2B_9H_{12}$] into [*nido*-$C_2B_9H_{13}$]

The method used to obtain the protonated species of [*nido*-$C_2B_9H_{12}$]$^-$ was very well stablished at Professor's Clara Viñas research group. The method used was adapted from their previous work.

[$NHMe_3$][*nido*-$C_2B_9H_{12}$] (0.2 g, 1 mmol) was dissolved in diethyl ether (15 mL) and extracted with a solution of HCl 1M (3x15 mL). After that, the organic phase was collected and dried with magnesium sulfate. Finally, the solvent was removed under reduced pressure and the obtained residue was dried in vacuo for a couple of hours. The compound [*nido*-$C_2B_9H_{13}$] was generated *in situ* and was used with no further purification.

Synthesis of [3,3,3-$(CO)_3$-closo-3,1,2-$RuC_2B_9H_{11}$] (2)

[$Ru(CO)_4]_3$ (0.19 g, 0.29 mmol) and *nido*-7,8-$C_2B_9H_{13}$ (0.12 g, 0.09 mmol) were heated in heptane (40 mL) during 4 hours, at reflux temperatures, changing from bright orange to dark red. After that time, the solution was cooled down to room temperature and about half of the solvent was remove by vacuum and the remaining decanted from the residue. The residue was extracted with a mixture of dichloromethane-petroleum ether (2:1, 15 mL) and then Celite® was added. After filtration, solvent was removed once again under vacuum and the obtained residue was washed twice with n-hexane (5 mL) yielding a dark red precipitate of **2**.

Yield: 73 %.

^{1}H NMR [$(CD_3)_2CO$, Me_4Si, δ / ppm]: 4.15 (s, CH_{cage}).

^{13}C NMR [$(CD_3)_2CO$, Me_4Si, δ / ppm]: 201.94 (CO), 47.86 (C_{cage}).

^{11}B NMR [$(CD_3)_2CO$, δ / ppm(integration)]: 8.6 (1B), -4.2 (3B), -7.6 (2B), -16.7 (3B).

FTIR [KBr pellets, cm^{-1}]: 3050-2920 cm^{-1} (υ_{C-H}), 2550 (υ_{B-H}), 2114 ($\upsilon_{C\equiv O}$), 2058 ($\upsilon_{C\equiv O}$).

UV-Vis in CH_2Cl_2 [λ_{max} / nm (ε x10^3 / $M^{-1}cm^{-1}$)]: 277 (4.81), 346 (1.86).

Synthesis of [3-CO-3,3-{k^2-4,4'-$(CH_3)_2$-2,2′-bipy}-closo-3,1,2-$RuC_2B_9H_{11}$] (2a)

Complex **2** [3,3,3-$(CO)_3$-*closo*-3,1,2-$RuC_2B_9H_{11}$] (0.20 g, 0.63 mmol) was combined with 1 equivalent of Me_2bipy (0.10 g, 0.63 mmol) and 2 equivalents of Me_3NO (0.10 g, 1.26 mmol) in a *Schlenk* and MeCN (40 mL) was added to the reactants. The reaction mixture was stirred for 24 hours. After that period, solvent was removed in vacuo and the residue obtained was chromatographed in silica gel using as eluent a mixture of dichloromethane and *n*-hexane (4:1). Extraction yielded a bright canary yellow band that was removed from the column with increased proportion of the *n*-hexane phase. After removing all the yellow fraction, solvent was removed in vacuo. The residue obtained was recrystallized by slow diffusion of *n*-hexane in dichloromethane. Yellow needle shaped single crystals of **2a** were obtained from slow evaporation of an acetone solution, under air.

Yield: 24 %.

EA [calculated for **2a** • ¼ CH_2Cl_2 (MW = $gmol^{-1}$)] found (calculated): C 39.1 (39.2), H 5.2 (5.1), N 5.5 (6.0).

^{1}H NMR [$(CD_3)_2CO$, Me_4Si, δ / ppm]: 9.00 (d, 2H, $^3J_{HH}$ = 5.6, H_1), 8.56 (s, 2H, H_4), 7.56 (d, 2H, $^3J_{HH}$ = 5.2, H_2), 3.26 (s, 2H, CH_{cage}), 2.62 (s, 6H, H_6).

^{13}C{^{1}H} NMR [$(CD_3)_2CO$, Me_4Si, δ /ppm]: 198.7 (CO), 156.2 (C_5), 155.5 (C_1), 151.8 (C_3), 128.4 (C_2), 124.9 (C_4), 44.9 (*br*, C_{cage}), 21.2 (C_6).

^{11}B{^{1}H} NMR [$(CD_3)_2CO$, δ / ppm(integration)]: -0.9 (1B), -6.5 (3B), -8.21 (2B), -20.9 (3B).

FTIR [KBr pellets, cm^{-1}]: 2960-2850 cm^{-1} (υ_{C-H}), 2549 cm^{-1} (υ_{B-H}), 1967 cm^{-1} ($\upsilon_{C\equiv O}$).

UV-Vis in CH_2Cl_2 [λ_{max} / nm (ε x10^3 / $M^{-1}cm^{-1}$)]: 246 (11.28), 287 (10.25), 311 (*Sh*), 362 (2.74), 451 (0.60).

UV-Vis in DMSO [λ_{max} / nm (ε x10^3 / $M^{-1}cm^{-1}$)]: 283 (18.71), 311 (13,01), 350 (5.80), 438 (1.35).

Synthesis of [3-CO-3,3-{k^2-4,4'-$(CH_2OH)_2$-bipy}-closo-3,1,2-$RuC_2B_9H_{11}$] (2b)

Complex **2** [3,3,3-$(CO)_3$-*closo*-3,1,2-$RuC_2B_9H_{11}$] (0.20 g, 0.63 mmol) was combined with 1.1 equivalents of bipy$(CH_2OH)_2$ (0.14 g, 0.64 mmol) and 2 equivalents of Me_3NO (0.10 g, 1.26 mmol) in a *Schlenk* and MeCN (40 mL) was added to the reactants. The reaction mixture was stirred for 24 hours. After that period, solvent was removed in vacuo and the residue obtained was chromatographed in silica gel using as eluent a mixture of dichloromethane and methanol (2:0.2). Extraction yielded a dark orange band that was removed from the column. Then all the pure fractions were collected and solvent was removed in vacuo. The residue obtained was recrystallized by slow diffusion of *n*-hexane in tetrahydrofuran affording light orange needle shaped single crystals of **2b**.

Yield: 15 %.

EA [calculated for Complex **2b** • ¼THF found (calculated)]: C 38.8 (38.8), H 5.1 (5.1), N 5.1 (5.7).

^{1}H NMR [$(CD_3)_2CO$, Me_4Si, δ /ppm]: 9.09 (d, 2H, $^{3}J_{HH}$ = 5.6, H_1), 8.64 (s, 2H, H_4), 7.70 (d, 2H, $^{3}J_{HH}$ = 5.6, H_2), 5.05 (t, 2H, J_{HH} = 5.6, O<u>H</u>), 4.96 (d, 4H, J_{HH} = 4.8, H_6), 3.30 (s, 2H, CH_{cage}).

^{13}C{^{1}H} NMR [$(CD_3)_2CO$, Me_4Si, δ /ppm]: 198.5 (CO), 156.2 (C_5), 156.1 (C_3), 155.7 (C_1), 124.6 (C_2), 121.0 (C_4), 62.7 (C_6), 44.9 (*br*, C_{cage}).

^{11}B{^{1}H} NMR [$(CD_3)_2CO$, δ /ppm]: -2.1 (1B), -7.8 (3B), -9.6 (2B), -22.3 (3B).

FTIR [KBr pellets, cm^{-1}]: 3310 cm^{-1} (υ_{O-H}), 2920-2850 cm^{-1} (υ_{C-H}), 2520 cm^{-1} (υ_{B-H}), 1950 cm^{-1} ($\upsilon_{C\equiv O}$).

UV-Vis in CH_2Cl_2 [λ_{max} / nm (ε x10^3/$M^{-1}cm^{-1}$)]: 245 (18.92), 289 (16.84), 314 (*Sh*), 368 (4.33), 453 (1.07).

UV-Vis in DMSO [λ_{max} / nm (ε x10^3/$M^{-1}cm^{-1}$)]: 284 (16.06), 313 (10.45), 347 (4.32), 434 (1.08).

Synthesis of [3-CO-3,3-{k^2-4,4'-$(CH_2OPLA)_2$-2,2′-bipy}-closo-3,1,2-$RuC_2B_9H_{11}$] (2c)

Complex **2** [3,3,3-$(CO)_3$-*closo*-3,1,2-$RuC_2B_9H_{11}$] (0.09 g, 0.27 mmol) was combined with 0.98 equivalents of bipy$(CH_2OPLA)_2$ (0.7 g, 0.26 mmol) and 2 equivalents of Me_3NO (0.04 g, 0.54 mmol) in a *Schlenk* and MeCN (50 mL) was added to the reactants. The reaction mixture was stirred for 24 hours. After that period, solvent was removed in vacuo and the residue obtained was dissolved in dichloromethane. Forced precipitation caused by the addition of *n*-hexane yielded a dark brown oil that was washed two times with diethyl ether and dried overnight. After dried the product has a brownish foamy look, similarly to polymeric analogues like complex **1d.**

Yield: 33 %.

^{1}H NMR [$(CD_3)_2CO$, Me_4Si, δ / ppm]: 9.20 (d, 2H, H_1, $^{3}J_{HH}$ = 5.6), 8.68 (s, 2H, H_4), 7.76 (d, H_2, $^{3}J_{HH}$ = 5.2), 5.54 (s, 4H, H_6), 5.21 (m, H, CH_{PLA}), 4.30 (s, 2H, CH_{cage}), 3.35 (*br*, 2H, CH_{cage}) 1.55 (, H, $CH_{3,\ PLA}$), 1.39 ($CH_{3,\ PLA}$).

^{13}C{^{1}H} NMR [$(CD_3)_2CO$, Me_4Si, δ / ppm]: 198.2 (CO), 170.2-170.6 (C_7+$C_{7'}$), 156.3(C_3), 156.2 (C_1), 149.1 (C_5), 125.5 (C_2), 122.1 (C_4), 69.8-67.1 (C_8+$C_{8'}$), 65.1 (C_6), 45.2 (*br*, C_{cage}), 20.8-17.1 (C_9+$C_{9'}$).

^{11}B{^{1}H} NMR [$(CD_3)_2CO$, δ / ppm]: -0.8 (s, 1B), -7.6 (3B), -9.4 (2B), -22.3 (3B).

FTIR [KBr pellets, cm^{-1}]: 3540 cm^{-1} (υ_{O-H}), 3000-2860 cm^{-1} (υ_{C-H}), 2551 cm^{-1} (υ_{B-H}), 1965 cm^{-1} ($\upsilon_{C\equiv O}$), 1755 cm^{-1} ($\upsilon_{C=O}$).

UV-Vis in CH_2Cl_2 [λ_{max} / nm (ε x10^3 / $M^{-1}cm^{-1}$)]: 244 (17.13), 296 (16.14), 314 (*Sh*), 380 (3.60), 506 (0.95).

UV-Vis in DMSO [λ_{max}/nm (ε x10^3/$M^{-1}cm^{-1}$)]: 290 (18.26), 318 (*Sh*), 363 (4.51), 493 (*Sh*).

Chapter 5

Conclusions and future perspectives

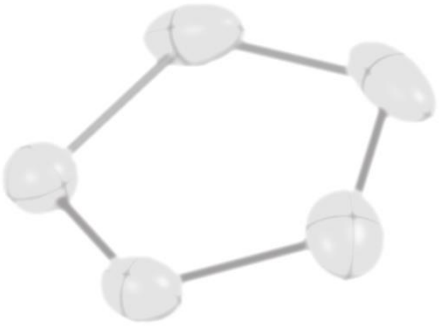

Conclusions and future perspectives

Since cancer is one of the leading causes of death worldwide improved ways to defeat this condition are crucial and urgent. This thesis reported the successful synthesis and characterization of new potential anticancer agents based on two different main scaffolds: the ruthenium-methylcyclopentadienyl and the ruthenium-carboranyl fragments.

A first generation of compounds was synthesized by conjugation of two 2,2'-bipyridyl derivatives to each pentahapto coordination motifs (**1a**, **1b**, **2a** and **2b**). To circumvent the low selectivity observed for some low molecular weight drugs, the development of one macromolecular ruthenium-methylcyclopentadienyl based complex (**1c**) and two new RuPMCs (**1d** and **2c**) complexes bearing the two pentahapto coordination fashion motifs was proposed and successfully achieved in this work. The material used to create the nanovector in the RuPMCs was the polylactide (PLA), one of the most promising bio-based polymers, which possess as advantage the fact of being biodegradable and biodegradable and is approved by FDA.

The synthetic routes developed and optimized within this thesis allowed, in total, the isolation of seven new organometallic complexes. All compounds were characterized spectroscopically, electrochemically, analytically and when possible, structurally by single crystal X-ray diffraction. The compounds were also screened *in vitro* for their cytotoxicity against a range of human cancer cell lines (A2780 ovarian adenocarcinoma, A375 melanoma, RKO and SW480 colon carcinoma) and showed high potential as anticancer chemotherapeutics.

Finally, the present project allowed the beginning of an exploratory investigation line in two different areas with clearly two different final goals: one of them is the classical chemotherapy, where the ruthenium-methylcyclopentadienyl family of compounds can successfully be applied due to their high cytotoxicity character; and the second one is the alternative Boron Neutron Capture Therapy (BNCT), where the ruthenium-carboranyl family of compounds can be inserted since they are an efficient source of ^{10}B atoms able to be irradiated by the intended technique. Future work could include:

- Incorporation of specific biomolecules at the end of the polymer chains, creating by this way a third generation of compounds, hopefully with increased selectivity and cell uptake;
- Keep on the development of new precursors alternatives to complex **2**, to increase yield of the reaction for the ruthenacarborane complexes;
- Incorporation of another *N,N'*-type and *N,X'*-type (X = O, S) donors into the ruthenium fragments;
- Enlarge the screening *in vitro* in a larger panel of cells;
- Internalization studies and studies on the mechanism of action of these drugs;
- And among others, the optimization of the conditions to operate the first BNCT assays.

Altogether, the proposed aims for this work were completely fulfilled with the synthesis and characterization of seven new organometallic compounds that show promising features as traditional chemotherapeutic agents (Ru-MeCp) or to be used in BNCT (Ru-carboranyl), as explained above. Also,

the new ‘Ru-MeCp’ family of compounds, analogous to the ‘Ru-Cp’ family already studied by our Group, will allow a complete structure-activity study, in order to assess the role of the $–CH_3$ donating group on the overall activity of these compounds.

References

1. National Cancer Institute at https://www.cancer.gov/about-cancer (accessed at June 12, 2017).
2. Cancer research UK at http://www.cancerresearchuk.org/health-professional/cancer-statistics/worldwide-cancer#heading-Zero (accessed at June 12, 2017).
3. WHO| Cancer at http://www.who.int/mediacentre/factsheets/fs297/en/ (accessed at June 12, 2017).
4. M. E. Fox, F. C. Szoka, and J. M. J. Fréchet, *Acc. Chem. Res.*, 42, 8, 1141–1151, 2009.
5. Y. Matsumura, Y. Maeda, H., *Cancer Res*., 46, 6387–92, 1986.
6. Rosenberg *et al*., *Cancer*, 55, 2303-2316, 1985.
7. G. Giaccone, *Drugs*, 59, 4, 9-17, 2000.
8. M. S. Robillard, J. Reedijk, *Platinum-based Anticancer Drugs*, in Encyclopedia of Inorganic Chemistry, 1-11, 2006.
9. M. J. Hannon, *Pure Appl. Chem.*, 79, 12, 2243-2261, 2007.
10. Ott I., Gust R., *Arch. Pharm.*, 340, 117–126, 2007.
11. G. Sava, A. Bergamo A., in Bonetti A. *et al*., Platinum and other heavy metal compounds in cancer chemotherapy. Humana Press; New York, 57–66, 2009.
12. Kostova I., *Curr. Med. Chem.*, 13, 1085–1107, 2006.
13. P. Heffeter, U. Jungwirth, M. Jakupec, C. Hartinger, *Drug Resist. Updat.*, 11, 1–16, 2008.
14. P. Schluga, C. G. Hartinger, A. Egger, E. Reisner, *Dalton Trans.*, 14, 1796–1802, 2006.
15. S. Rockwell, I. T. Dobrucki, E. Y. Kim, S.T. Marrison,, *Curr. Mol. Med.*, 9, 442–458, 2009.
16. R. Gagliardi, G. Sava, S. Pacor, *Clin. Exp. Metastasis.*, 12, 93–100, 1994.
17. A. Bergamo *et al.*, *Int. J. Oncol.*, 33, 1281–1289, 2008.
18. G. Sava, E. Alessio, A. Bergamo, *Top. Biol. Inorg. Chem.*, 1, 143–169, 1999.
19. T. Pieper, K. Borsky, B. K. Keppler, *Top. Biol. Inorg. Chem.*, 1, 171–199, 1999.
20. Y. K. Yan, M. Melchart, P. J. Sadler, *Chem. Commun*., 38, 4764-4776, 2005.
21. V. Brabec, O. Novakova, *Drug Resist. Updates*, 9, 111-122, 2006.
22. W. H. Ang, P. J. Dyson, *Eur. J. Inorg. Chem.*, 20, 4003-4018, 2006.
23. V. Moreno *et al*., *J. Inorg. Biochem.*, 105, 241–249, 2011.

24. Moreno, V. *et al*., *Bioinorg. Chem. Appl.*, 1-11, 2010.

25. Morais, T. S. *et al*., *J. Organomet. Chem.*, 713, 112–122, 2012.

26. Garcia, M. H. *et al*., *J. Inorg. Biochem.*, 103, 354–361, 2009.

27. Garcia, M. H. *et al*., *Future Med. Chem*., 8, 5, 527-544, 2016.

28. Tomaz, A. I. *et al*., *J. Inorg. Biochem.*, 117, 261–269, 2012.

29. Morais, T. S. *et al*., *J. Inorg. Biochem.*, 122, 8–17, 2013.

30. Morais, T. S. *et al*., *J. Inorg. Biochem.* 114, 65–74, 2012.

31a. T. S. Morais, *et al*., *J. Inorg. Biochem*., 129, 94-101, 2013.

31b. N. Mendes *et al*., *Anti-Cancer Agents in Medicinal Chemistry*, 17, 1, 126-136, 2017.

32. Y. Matsumura, H. Maeda , *Cancer Res.*, 46, 6387–6392, 1986.

33. I. Chau, D. Cunningham, *J. Clin. Oncol.*, 21, 2049–51, 2003.

34. V. P. Torchilin, *Drug Delivery*, 197, 3–53 (Springer Berlin Heidelberg), 2010.

35. N. Bertrand, J. Wu, X. Xu, N. Kamaly, O. C. Farokhzad, *Adv. Drug Deliv. Rev*., 66, 2–25, 2014.

36. D.P. Nowotnik, E. Cvitkovic, *Advanced Drug Delivery Reviews*, 61, 1214–1219, 2009.

37. A. Valente *et al*., *J. Inorg. Biochem*., 127, 79–81, 2013.

38. R. B. King, *Chem. Rev.*, 101, 1119-1152, 2001.

39. W. H. Eberhardt, B. Crawford, Jr., W. N. Lipscomb, *J. Chem. Phys*., 22, 989-1001, 1954.

40. B. Štíbr, *Chem. Rev*., 92, 225-250, 1992.

41. V. I. Bregadze, *Chem. Rev*., 92, 209-223, 1992.

42. R. W. Rudolph, *Acc. Chem. Res*., 9, 446-452, 1976.

43. M. F. Hawthorne *et al*., *Inorg. Chem*., 35, 5417-5426, 1996.

44. M. F. Hawthorne, *J. Organomet. Chem*., 100, 97-110, 1975.

45. R. A. Wiesboek, M. F. Hawthorne, *J. Am. Chem. Soc.*, 86, 1642-1643, 1964.

46. L. I. Zakharkin, V. N. Kalinin, *Tetrahedron Lett*., 6, 407-409, 1965,

47. M. A. Fox *et al*., *Polyhedron*, 15, 565-571, 1996.

48. F. Teixidor *et al*., *Organometallics*, 16, 1278-1283, 1997.

49. R. Sillanpää, C. Viñas, F. Teixidor, *Acta Cryst*., C57, 900-901, 2001.

50. M. G. Davidson *et al*., *Chem. Commun.*, 17, 1649-1650, 1999.

51. a) M.F. Hawthorne, A. Maderna, *Chem. Rev*., 99, 3421-3434, 1999. b) V. Bregadze, I. Sivaev, S. Glazun, *Anticancer Agents in Medicinal Chemistry*, 6, 2, 75-109, 2006.

52. G. L. Lochner, *Am. J. Roentgenol*., 36, 1-13, 1936.

53. J. A. Coderre, G. M. Morris, *Radiat. Res.*, 151,1-18, 1999.

54. Y. Nakagawa, H. Hatanaka, *J. Neurooncol.*, 33, 105-115, 1997.

55. Y. Mishima, M. Ichihashi, K. Yamamura, *Cell Res.*, 2, 226-234, 1989.

56. a) T. Aihata *et al.*, *Head Neck*, 28, 850, 2006; b) I. Kato, *et al*., *Appl. Radiat. Isto.*, 51, 1069, 2004.

57. a) J. Cai *et al.*, *J. Med. Chem.*, 40, 3887, 1997; b) L. Gedda, *et al*., *Anticancer Drug Chem*., 12, 671, 1997; c) D. P. Kelly, *et al*., *Aust. J. Chem*., 47, 247 ,1994; d) H. Nakamura, M. Sekido, Y. Yamamoto, *J. Med. Chem.*, 40, 2825, 1997.

58. A. M. Cioran, *Synthesis of high boron content polyanionic multicluster macromolecules for their potential use in medicine*, PhD thesis, ICMAB-CSIC, 2013.

59. E. Heber *et al*., *Arch Oral Biol*., 49, 313-324, 2004.

60. G. Calbrese *et al.*, *Drug Disc. Today*, 17, 314, 2012.

61. H. Nakamura, *Methods Enzymol*. 465, 179–208, 2009.

62. D. A. Feakes *et al*., *Tetrahedron*, 55, 11177–11186, 1999.

63. G. Wu *et al.*, *Bioconjug. Chem*., 15, 185–194, 2004.

64. M.W. Renner, M. Miura, M. G. Vicente, *Anticancer Agents Med. Chem*., 6, 145–157, 2006.

65. V. Olshevskaya *et al*., *Bull Korean Chem. Soc.*, 28, 1910–1916, 2007.

66. S. Kahl, M. Koo in: *Progress Neutron Capture Therapy*. Allen B, Moore D, Harrington B, editor. Plenium Press, New York, 223–226, 1992.

67. X. Pan, *et al.*, *Bioconjug Chem.*, 18, 101–108, 2007.

68. H. Nakamura in: *Boron Science: New Technologies and Applications*. Hosmane N, editor. CRC Press; Liposomal boron delivery system for neutron capture therapy of cancer, 165–179, 2012.

69. T. S. Morais *et al.*, *J. Inorg Biochem.*, 122, 8-17, 2013.

70. G. Nogueira *et al*., *J. Organ. Chem.*, 820, 20-29, 2016.

71. M. F. Martins, *Aplicação de SARS e QSARS à concepção de novos fármacos*, (digital support as pdf files), 2016.

72. R. A. Wiesboeck, M. F. Hawthorne, *J. Am. Chem. Soc*., 86, 1642-1643, 1964.

73. (a) J. S. Roscoe, S. Kongpricha, S. Papetti, *Inorg. Chem.*, 9, 1561, 1970; (b) M. F. Hawthorne, P. A. Wegner, *J. Am. Chem. Soc.*, 90, 896, 1968.

74. P. A. Jelliss, *et al., Inorg. Chem.*, 45, 1, 370–385, 2006.

75. P. E. Behnken, M. F. Hawthorne, *Inorg. Chem.*, 23, 3420, 1984.

76. O. Tutusaus *et al*., *J. Am. Chem. Soc.*, 125, 11830-11831, 2003.

77. O. Tutusaus, C. Viñas, F. Teixidor, *Chem. Commun*., 2458-2459, 2003.

78. O. Tutusaus, R. Núñez, F. Teixidor, *Inorg. Chem.*, 43, 6067-6074, 2004.

79. R. Núñez *et al.*, *Organometallics*, 23, 2273-2280, 2004.

80. R. J. Wilson, L. F. Warren, Jr., M. F. Hawthorne, *J. Am. Chem. Soc.*, 91, 16, 758, 1969.

81. Internal data from the *Group of Bioinorganic Chemistry and Drug Development*, FCUL, 2017.

82. R. J. Wilson, L. F. Warren Jr., M. F. Hawthorne, *J. Am. Chem. Soc.*, 91, 758, 1969.

83. D. M. Su *et al.*, *Mol. Cancer Ther.*, 8, 1292–1304, 2009.

84. W. Li, D. W. Melton, *Oncogene*, 31, 2412–2422, 2012.

85. D. F. Shriver, *The Manipulation of Air Sensitive Compounds*; McGraw-Hill, 1969.

86. D. F. Shriver, *Experimental Organometallic Chemistry*. A practicum in synthesis and characterization, ACS symposium series 357; Washington DC, 1987.

87. D. D. Perrin, W. L. F. Amarego, D.R. Perrin, *Purification of laboratory chemical*; 2nd Edition, Pergamon Press, New York, 1980.

88. R. G. Teixeira *et al.*, 2017 (submitted).

89. G. M. Sheldrick, *SADABS, version 2.10*, University of Göttingen, Germany, 2004.

90. G. M. Sheldrick, *A short Hist. SHELX*, 112–122, 2008.

91. F. Macrae *et al.*, *Mercury: visualization and analysis of crystal structures, J. Appl. Cryst*., 39, 453, 2006.

92. N. G. Connelly, W.E. Geiger, *Chem. Rev*., 96, 877-910, 1996.

93. T. Mosmann, *J. Immunol. Methods*, 65, 55-63, 1983

94. F. Capone *et al.*, *The Scientific World Journal*, article ID 450390, 2014.

Annexes

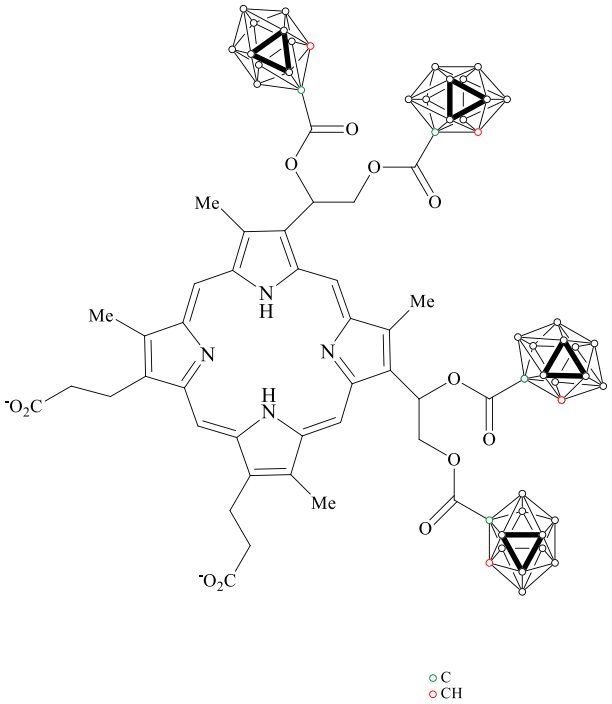

Annex A1.1 – Molecular structure of BOPP (2,4-bis(alpha,beta-dihydroxyethyl)-deutero-porphyrin IX).

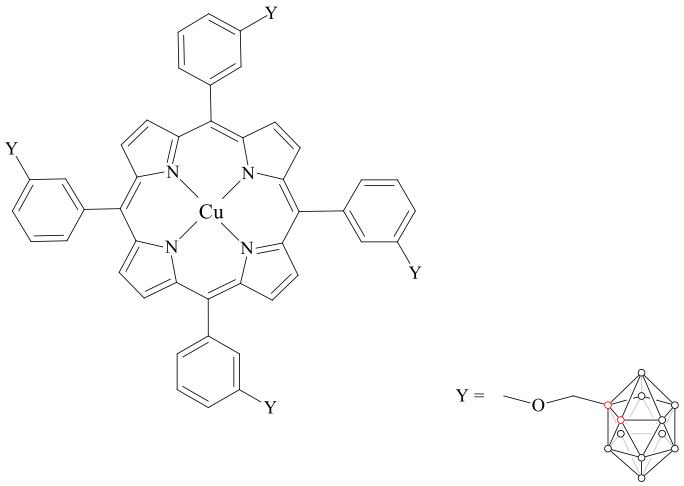

Annex A2 – Molecular structure of CuTCPH (Copper tetracarboranyltetraphenylporphyrin).

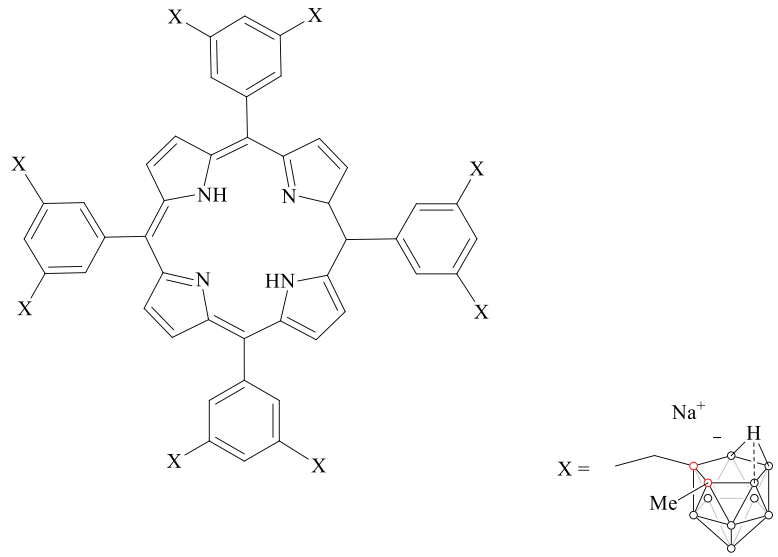

Annex A3 – Molecular structure of H_2OCP (5,10,15,20-tetra[3,5-(nido-carboranylmethyl)phenyl]porphyrin).

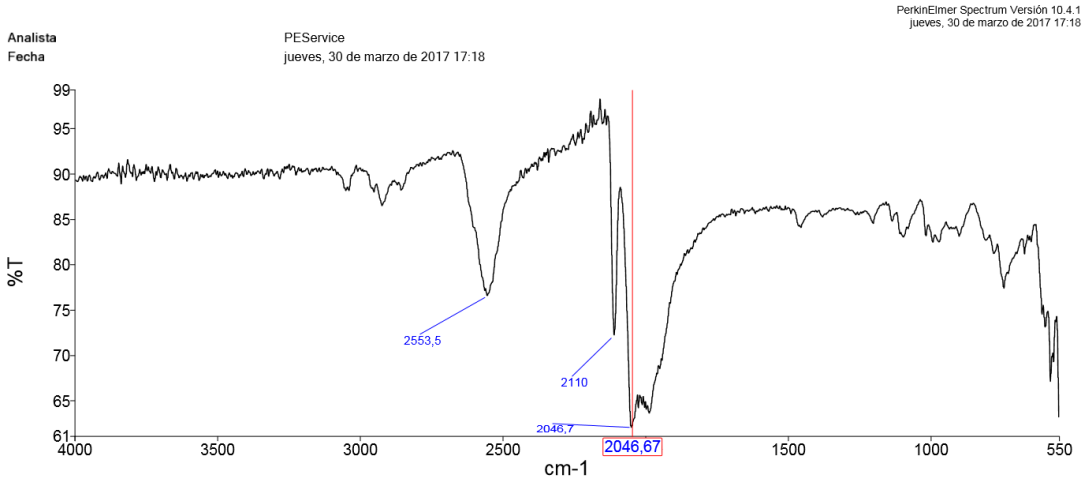

Nombre de la muestra	Descripción
RT11_ICMAB only	Muestra 006 Por PEService Fecha jueves, marzo 30 2017

Annex A4 – Solid state FTIR spectra of complex **2**.

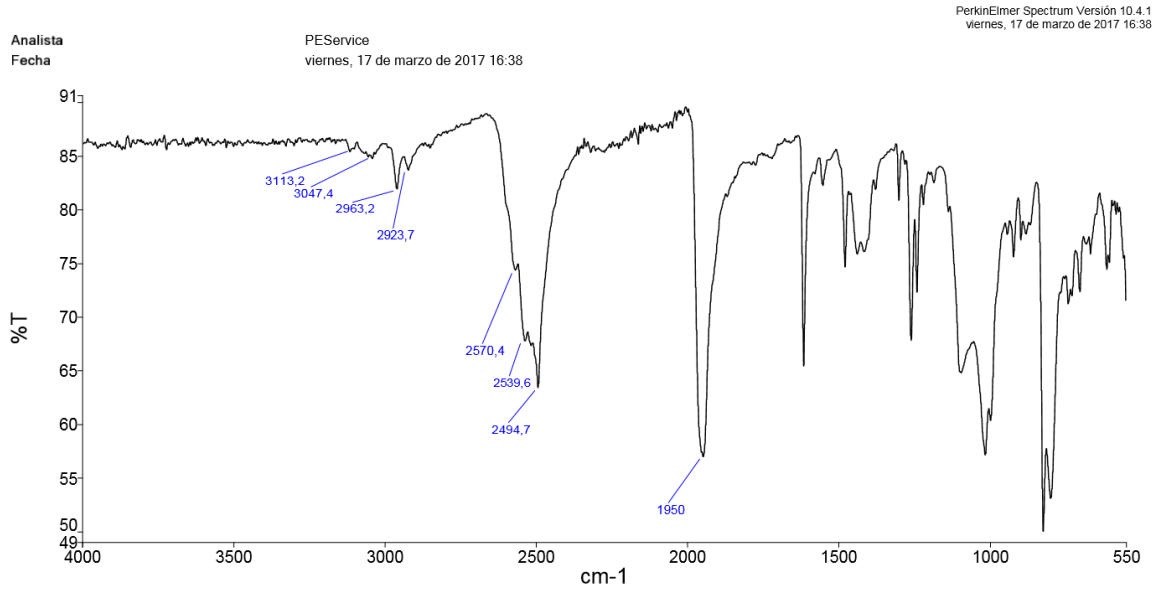

Annex A5 – Solid state FTIR spectra of complex **2a**.

Annex A6 – Crystal data and structure refinement for complexes **1a**, **2a** and **2b.**

Identification	Complex **1a**	Complex **2a**	Complex **2b**
Empirical formula	C38 H36 Cl2 F3 N2 O3 P Ru S	C15 H23 B9 N2 O Ru	C18 H26 B9 N2 O3 Ru
Formula weight	860.69	445.71	516.77
Temperature	100(2) K	193(2) K	193(2) K
Wavelength	0.71073 Å	0.71073 Å	0.71073 Å
Crystal system, space group	Triclinic, P-1	Monoclinic, P 21/n	Monoclinic, P 21/c
Unit cell dimensions	a = 13.4977(7) Å alpha 92.801(3) deg. b = 15.8956(9) Å beta = 92.794(3) deg. c =17.7658(10) Å gamma = 106. 502(3) deg.	a = 12.589(2) Å alpha = 90 deg. b = 11.463(2) Å beta = 111.301(2) deg. c = 14.575(2) A gamma = 90 deg.	a = 6.8160(14) Å alpha = 90 deg. b = 25.702(5) Å beta = 92.384(4) deg. c = 12.914(3) A gamma = 90 deg.
Volume	3642.5(3) $Å^3$	1959.7(6) $Å^3$	2260.4(8) $Å^3$
Z, Calculated density	4, 1.569 Mg/m^3	4, 1.511 Mg/m^3	4, 1.518 Mg/m^3
Absorption coefficient	0.735 mm^{-1}	0.808 mm^{-1}	0.718 mm^{-1}
F(000)	1752	896	1044
Crystal size	0.28 x 0.17 x 0.08 mm^3	0.35 x 0.35 x 0.12 mm^3	? x ? x ? mm
Theta range for data collection	1.15 to 26.43 deg.	1.836 to 28.363 deg.	2.237 to 28.386 deg.
Limiting indices	-16<=h<=16, -19<=k<=19, -22<=l<=22	-15<=h<=16, -9<=k<=15, -17<=l<=19	-9<=h<=9, -33<=k<=33, -17<=l<=17
Reflections collected / unique	14898 [R(int) = 0.0496]	13262 / 4534 [R(int) = 0.0272]	35439 / 5582 [R(int) = 0.0317]
Completeness to theta	= 26.43 99.5 %	= 25.242 100.0 %	= 25.242 99.9 %
Refinement method	Full-matrix least-squares on F^2	Full-matrix least-squares on F^2	Full-matrix least-squares on F^2
Data / restraints / parameters	14898 / 0 / 925	4534 / 0 / 299	5582 / 0 / 359
Goodness-of-fit on F^2	1.055	1.031	1.064
Final R indices [I>2sigma(I)]	R1 = 0.0403, wR2 = 0.1086	R1 = 0.0308, wR2 = 0.0745	R1 = 0.0391, wR2 = 0.1149
R indices (all data)	R1 = 0.0463, wR2 = 0.1125	R1 = 0.0389, wR2 = 0.0802	R1 = 0.0445, wR2 = 0.1190

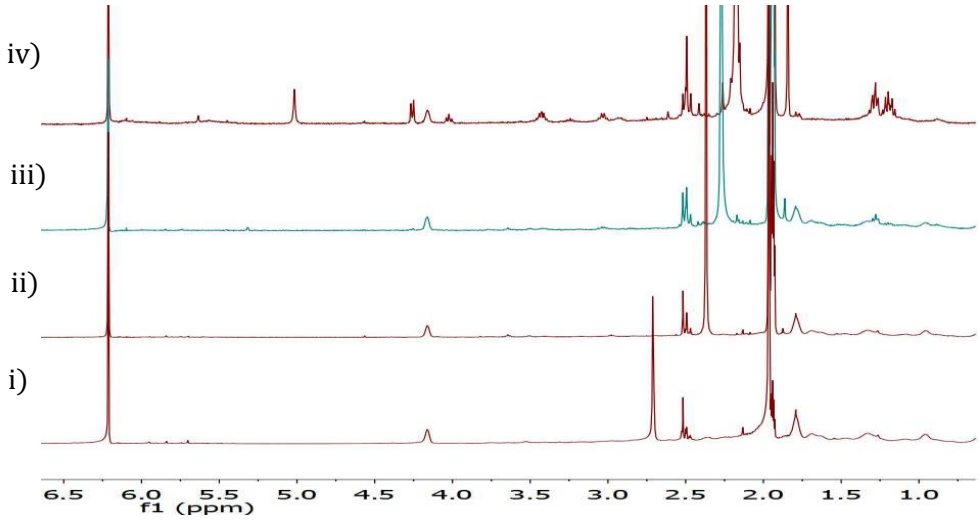

Annex A7 – Evolution of the irradiation reactional step described in section **3.2.1.1**. All experiments were measured in CD_3CN after i) 0h, ii)5h, iii) 13h, iv) 35h.

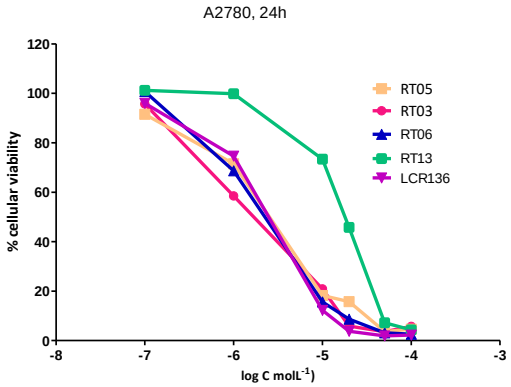

Annex A8 – Dose-response curve obtained in the *in vitro* screening of complexes 1-1b and 1d in the A2780 cell line after 24 h of incubation. (RT13 = complex 1, RT03 = complex 1a, RT06 = complex 1b and RT05 = complex 1d)